New Analytical and Numerical Methods in Structural Analysis of Nonlinear Two-Dimensional Curved Membranes

by

Sara Jabbarizadeh

A Dissertation submitted in partial fulfillment
of the requirements for the degree of
Doctor of Philosophy
(Naval Architecture and Marine Engineering)
in The University of Michigan
2012

Doctoral Committee:

Associate Professor Dale G. Karr, Chair
Professor Michael M. Bernitsas
Assistant Professor Ann E. Jeffers
Research Investigator and Lecturer, Steven F. Zalek

To My Family

My most valuable treasure

Acknowledgments

I would like to thank my advisor, Professor Dale G. Karr, for his great help throughout my graduate studies at the University of Michigan. His continuous guidance and complete support has been the key to my developed skills during this period. I also want to extend my appreciation to the members of my Ph.D. committee, Professor Michael Bernitsas, Professor Ann Jeffers and Dr. Steven Zalek for their support and interest in providing me with invaluable advice and deep insight and suggestions to improve the quality of my work.

Most of all, I would like to express my greatest appreciations to my parents, Behdokht Salehi and Mohammad Hossein Jabbarizadeh, for their unconditional love and support that gave me the strength to continue in the most difficult days and to my brother, Roozbeh Jabbarizadeh, who is my first teacher and has always been a great inspiration for me to never stop learning. And my special thanks to my husband, Amir Behzadan, who shared with me his valuable knowledge and experience and has walked with me every step of the way through my graduate studies experience. In the end, I would also like to thank all my friends for their priceless support.

Sara Jabbarizadeh

Table of Contents

List of Figures

List of Tables

List of Abbreviations

ACV: Air Cushion Vehicles

CAD: Computer Aided Design

CFD: Computational Fluid Dynamics

DOF: Degree of Freedom

ETFE: Ethylene Tetra Fluoro Ethylene

FE: Finite Element

FSI: Fluid Structure Interaction

GA: Genetic Algorithms

PTFE: Poly Tetra Fluoro Ethylene

PVC: Poly Vinyl Chloride

SES: Surface Effect Ship

Abstract

Membranes have many engineering applications due to their light weight and low construction cost, as well as their flexibility. As a specific example, optimal design of seal and skirt system in Air Cushion Vehicles (ACVs) is essential to achieve higher speed and stability, and lower fuel consumption. Previously developed methods have considered elastic and hyperelastic membranes, as well as membranes with flexural rigidity. However, some membranes are inextensible, and have no or negligible bending stiffness. This dissertation proposes a number of methods to analyze structural behavior of membranes which can be effectively applied to membranes with complex geometries, those that are extensible or inextensible, as well as membranes with or without resistance to bending.

In particular, this dissertation presents:

- An **analytical method** to investigate the deformation and internal forces in circular semi-submerged inextensible massless membranes,
- A **numerical method** to predict the hydrodynamic pressure applied to bow seal membranes based upon their mechanical properties and forces involved,
- A **Finite Element (FE) method** to model both weightless and weighted inextensible curved membranes under a variety of forces, and

- A numerical method based on **Isogeometric Analysis** capable of analyzing a wide range of membranes.

The analytical method is a powerful, easy and precise method for a weightless membrane with specific geometry subjected to varying normal pressure. The first FE method considers weighted and weightless membranes under shear and normal pressure. Although there are some limitations in the range of applied forces this method can analyze, constant radius arc elements provide a good representation for curved membranes and very accurate results ideal for simple geometries by relatively faster analysis. The method based on the Isogeometric Analysis overcomes the limitations in the FE method; nonetheless it has potential for improvement in cases such as modeling low curvature membranes, by choosing higher degree Bezier curves or B-Spline base functions. This method, especially if improved, provides more accurate result for more complex geometries. The methods presented in this dissertation set the stage for Fluid Structure Interaction (FSI) problems that involve membranes. Large displacements are assumed in all analyses.

Chapter 1

Introduction

Membranes belong to a class of structures that ideally can carry tension but no compression or bending. A membrane structure can be air supported, frame supported, or tensile structures (supported only by the tension generated in them). Due to their light weight and low construction cost, as well as their flexibility which leads to their ability to offer a large variety of configurations and a wide range of free form aesthetic shapes, they are frequently considered as the ultimate solution for special applications such as large roof construction, and temporary, light weight, or mobile structures. Combined with supporting elements such as ropes, cables, and columns they can span large areas while satisfying aesthetic aspects of the design by offering a variety of complex shapes [1].

In air supported structures, as the name implies, internal gas is used to define the shape of the structure. To sustain the structural integrity, the internal pressure is needed to be maintained at a larger or equal level than external pressures applied to the structure. For very dynamic external pressures, the information from the sensors mounted on the structure is used to adjust the internal pressure accordingly. These structures need to be

anchored to the base. The air supported structures offer all the advantages of membrane structures, including low construction cost, easy and fast assembly, disassembly, and relocation, and the option of using translucent material which eliminates the need for interior lighting. In addition, by eliminating the need for a supporting structure, air supported membranes provide open interiors. On the other hand, due to their structural characteristics, they have shorter life span and lower load carrying capacity. Hence, it is necessary that the internal pressure as well as external applied loads be continuously monitored. Also, due to insulation issues, ventilation and air conditioning will not be as effective as in conventional structures. One of the first large-scale air-supported membrane structures is the United States pavilion at Expo 70, designed by David H. Geiger [2].

Frame supported membrane structures often can be assembled and disassembled very fast to accommodate temporary events or even be transported to another place. When not in service, they can be easily compacted and stored in small storage areas. Also, thanks to their flexible framing, they can be used to build temporary, semi-permanent, or even permanent structures [3]. Gridshells are one of the structures that are typically used as frame for membrane structures. They can easily be made to have a specific profile to span a large area. In addition, the fact that minimum material is used makes gridshells a lightweight option. One disadvantage of frame supported membrane structures in comparison with air supported structures is that the interior space is usually divided by columns or other support elements that transfer the structural loads. The optimal design that minimizes the cost of construction is very critical especially in case of large

structures. One of the latest examples of the frame supported membrane structures is the temporary basketball arena for the London 2012 Olympic Games which is supported by steel frames [4].

A tensile membrane, as the name implies, supports its structural integrity by means of its internal tension. This tension is created in the membrane through supporting elements such as masts or cables. Applying corrosion protection and paying special attention to load transfer mechanisms where the membrane material meets such supporting elements or is connected to another piece of membrane material, are two issues of critical importance. An example of large scale lightweight tensile membrane structures is the Munich Olympic stadium which is supported by steel cables [5].

1.1. Material Used in Membrane Structures

Depending on the intended application, different types of synthetic fabrics may be used in construction of membranes. Polyester fabrics are used for their wrinkle and environmental resistance as well as their durability [6]. Another type of synthetic fabrics is Polyethylene-based which is lightweight and durable and hence, a suitable choice for membrane material [7]. Heat resistance, low moisture absorption, high strength, and dimensional stability are the advantages of fiberglass fabrics as suitable materials for membrane structures. These fabrics are coated with Polyvinyl Chloride (PVC) and Poly Tetra Fluoro Ethylene (PTFE) for additional flexibility, environmental, corrosion and wear resistance, and reduced friction [8]. Foils made of PVC and Ethylene Tetra Fluoro

Ethylene (EFTE) make an attractive option for a membrane structure material due to their high strength, corrosion, and weather durability. Beijing National Aquatics Center is the world largest structure made of ETFE film, benefiting from more penetrated light and heat [9]. Materials should be selected carefully for each type of membrane structure and specific characteristic of each design, as a material that might be ideal for one specific design may not be a good option for the others.

Membrane structures are generally used when a small weight-to-applied load ratio is required. Large load carrying capacity is possible in flexible membranes due to their internal tension induced by methods such as pre-tensioning. To achieve this capacity, optimization methods are often employed to determine the optimal structural shape [10]. Consequently, the design process is very different from that of conventional structures, due to the specific characteristics of the membrane structures. The shape and form of a membrane, determined during an essential design step called form finding, play a big role in the strength and integrity of the structure of which the membrane is a part. As a result of high flexibility, the internal tension in membranes governs the shape and stability of the structure. Inevitably, load analysis is another major step in the design process during which, the necessity and importance of nonlinear analyses is significant considering the large deflection membrane structures are subjected to.

1.2. Applications in Naval and Marine Design

In light of the characteristics described earlier, membranes are frequently used in special naval applications such as pontoon bridges, amphibious helicopters, and Air Cushion Vehicles (ACVs). Their light weight is ideal for high speed vehicles. In addition, a vehicle that has to move on a non-smooth surface needs a flexible contact area. Flexibility of membranes is another distinctive property that makes the design of a high speed transformable craft possible.

An ACV is a major example of naval applications of membranes. An air cushion, contained by a convex profiled flexible skirt reduces the friction on the vehicle surface and allows ACVs to hover above any surface. The primary application of these vehicles is in amphibious operations and shallow waters. Considering their specific application, the environments ACVs operate in, and the wave impact, the tear strength of the membrane (i.e. skirt system) should be accordingly designed.

Initial development of ACVs started in 1920s and the full scale models were built by the end of 1950s, but the developments of ACVs even continue to this date [11, 12]. Experimental studies have analyzed the mechanical properties of the material used to manufacture the skirt of ACVs [13]. Based on these experimental results, in the same study, Finite Element (FE) analysis was conducted, and despite an agreement between experimental and analytical results in many properties, some disagreement on ultimate bearing capacity was reported. The linear and non-linear dynamics of the ACVs have also been previously studied [14]. The results of the linear analysis with a simplified

geometric model and the assumption of air flow incompressibility were found to be in agreement with experimental analysis. Also, the bag-to-cushion pressure ratio was determined as the controlling factor of the vehicle stability [15]. Moreover, the depth of transverse stability skirt was found to be a determinant factor in coupled heave and pitch motion of air cushion vehicles, and the nature of motion was described to be nonlinear in response to sinusoidal waves due to skirt structure and material. Finally, large fluctuations of the membrane's internal pressure were observed [16]. In a different study, air compressibility due to the accumulation of air in the vehicle compartments was determined to be a significant factor in increasing the coupled heave and pitch motion [17]. Other types of motion of the ACVs have been studied experimentally and numerically [18]. In a linear study based on a more complex realistic (bag and finger) skirt system and compressible air flow, the undesirable heave motion was found to be a function of skirt geometry and mass [19]. Although the possible changes in geometry did not significantly affect the heave motion, the results of this study suggested that the possible changes in skirt mass would lead to a more desirable heave response. In order to improve the shortcomings of the current skirt system and its undesirable effects on the vehicle's heave motion, it is optimized by studying two-dimensional (2D) sections using Genetic Algorithms (GAs) that consider vehicle structure and weight [20]. Also, the influence of the platform shape, canal sides, and bottom and distribution of the pressure were studied in an effort to improve the skirt system design and methods to estimate the resistance and other important quantities with good accuracy were presented [21].

The concept of ACVs has attracted many scientists and researchers through the years. Despite this, its development has suffered many disruptions and several of its applications were discontinued or replaced by other types of marine vehicles such as Surface Effect Ships (SES) and catamarans. Yet, none of these vehicles are comparable with ACVs in some specific aspects, the most important of which is amphibiousness. This is extremely important in cases when there is a need for a vehicle that can easily move between land, mud, water, and ice. Another characteristic that is specific to ACVs is their high speed. Considering their type, weight, and structure they can reach speeds as high as 80 knots (kn). Their light weight can contribute to the efficiency of the vehicle and its speed. These characteristics are extremely important in military and rescue mission applications.

1.3. Research Objectives

Efficient design of flexible ACV seals has been an inspiration for a major impact on Navy operations that use amphibious crafts with higher tonnage, stability, and speed, and can easily travel from a sea base to shore and vice versa while transporting cargo without the need to a port. Studies have shown that the design of the seal and skirt systems plays an important role in the performance of the ACVs as it controls the pressure distribution and therefore the motion of the vehicle in waves, as well as the weight, efficiency, and environmental and tear resistance. To this end, there is a need for a methodology to model and study the skirt system under different loading conditions and to calculate the deformed shape and resulting reaction forces.

Hence, the objective of this research was to develop new methods to analyze curved membranes that can be easily used to model complex shapes with applications in marine (e.g. ACV skirt system) as well as other engineering desciplines. The material used in manufacturing the skirt of ACVs, with a base of fabric and rubber like coatings, shows no or negligible extensibility. Yet, they have very small to none bending stiffness. Previously developed numerical methods that consider different ranges of elasticity do not account for such material. The existing commercial codes offer analysis based on elastic membranes. To impose inextensibility one should choose a very large modulus of elasticity. This in turn results in high bending stiffness which does not represent membranes that are very flexible to bending. Therefore, it is essential to develop a method to simultaneously consider both inextensibility and flexibility in bending as these two characteristics are intrinsic features of a group of membranes such as the seal system of ACVs.

Another important issue concerns the degrees of freedom (DOFs) and boundary conditions, which are usually selected based upon the available information about the design problem. In many cases, the boundary conditions in the real system are in terms of displacement. Therefore, in this research, the developed methods were sought to be able to accommodate for displacement boundary conditions and DOFs. These methods were then validated by comparing the results with analytical methods. It should be noted that specific loading conditions may result in large deformations in membranes due to their extremely flexible nature. These deformations are highly nonlinear and require geometrically nonlinear analysis. In some cases, such analyses result in multiple

solutions, which require further analysis, physical interpretation, and selecting the most appropriate solution.

The main question this dissertation aimed to address was how a curved membrane deforms in contact with fluids. This was achieved through careful consideration of several approaches. In particular, first, an ideal massless circular membrane was considered in an analytical solution. Then, an FE method was developed that allowed for the weight of the membrane to be also included in the calculations. The analysis indicated a few limitations in the application of this method. Consequently, an alternative method was designed and implemented to address these limitations for ideal as well as non-ideal membranes of general shape based on a relatively new and advanced method called Isogoemetric Analysis.

The findings of this research are expected to set the stage for dynamic Fluid Structure Interaction (FSI) analysis of membranes. FSI occurs when a structure is deformed in contact with a fluid, as a result of its pressure and viscous forces [22]. This in turn can produce new boundary conditions for the fluid. Under these circumstances, the response of the structure is updated and this process continues recursively. These phenomena result in highly non-linear equations. A large body of problems in naval architecture and marine engineering involves the interaction of fluid with a structure. To alleviate this, inclusion of the Isogeometric Analysis in the developed numerical methods provides the opportunity for the analysis of complicated and computationally massive objects with a better precision. The methodology presented in this dissertation is based on Bezier

quadratic curve and is the first step towards the Isogeometric Analysis of dynamic fluid membrane interaction problems.

1.4. Dissertation Outline

Each Chapter in this dissertation serves as a stand-alone document that discusses the details of a new method to analyze curved membranes, describes the challenges involved and the assumptions considered in the established method, algorithms and methodologies, examples, and presents case studies to address a particular research objective.

The presented work focuses on the structural aspect of the FSI problem. Others have conducted considerable amount of work on the fluid aspect (e.g. wave resistance, drag forces, powering, scaling models, friction resistance [23-26]) of this problem. There is also direct application of this work to inflatable cylindrical pontoons. Although the skirt and seal system of the ACVs has been a motivation for this research, the developed FE method and Isogeometric Analysis can be applied to any curved membrane.

In Chapter 2, a specific case of a circular membrane being partially submerged is considered. The equilibrium equations are established based on a 2D model of a cylindrical membrane with ¾ of a circle profile. The membrane is pin connected at the top to a rigid plate, and is assumed to be inextensible, perfectly flexible, and with negligible weight. Fundamental to the analysis is that the density of the surrounding fluid is assumed to be larger than the fluid within the membrane. Also, the variation of the

pressure in the fluid-filled membrane and the tangential friction were both assumed to be negligible. Equilibrium equations defined the deformed geometry of the membrane as a function of its internal tension. The Newton-Raphson iterative method and displacement boundary condition at the point where the membrane is connected to the rigid plane are used to solve the equilibrium equations for tension and deformed geometry.

In Chapter 3, a mathematical model has been established as a part of a study to model a 2D SES vessel seal based on experimental results. Beam bending theory was used to derive the required pressure to achieve the geometry indicated by experiment. The results from this Chapter were compared with those of a Computational Fluid Dynamics (CFD) model developed by Zalek et al. [27].

Chapter 4 introduces a new FE method to model inextensible membranes with negligible flexural rigidity, which is the definition of an ideal membrane. To facilitate the modeling of curved membranes, each element was assumed to be an arc with two nodes (one at each end), two DOFs, displacements in x and y directions per node, and a radius defined as a function of the applied pressure. The stiffness influence coefficient method was used to determine the local stiffness of the elements, which was then transferred to a global coordinate system and assembled to form the global stiffness matrix of the model. The elements of the force vector were found by counteracting the imbalance of forces applied to nodes. Again, the Newton-Raphson iterative method was used to solve for the displacement. In addition to the normal pressure, the deflection of the membrane under shear pressure and its own weight was considered. After finding the deflected

configuration of the model, tension at each element was easily found using the radius of the element. The results from this method were then compared with the results from the analytical method presented in Chapter 1 and other methods developed by Yu and Karr [28].

Chapter 5 introduces a new numerical method, inspired by Isogeometric Analysis that takes advantage of the benefits of this method over the FE method, the most important of which is the ability to present conical profiles and complex shapes with a more exact geometric representation. The quadratic Bezier curve was selected as the basis function of each element and therefore, each element has three control points and two displacement DOFs at each node. The principle of virtual work is employed to formulate the problem. It should be noted that pressures applied to the membrane are non-conservative forces and thus, the principle of minimum total potential energy cannot be applied. The elements of the force vector were found by expressing the total virtual work in terms of DOFs using the quadratic Bezier curve definition. In turn, the elements of stiffness matrix can be calculated by expressing the force vector elements in terms of DOFs. In this Chapter, the Newton-Raphson iterative method was employed to solve for displacements. Also, the case of a non-ideal membrane with axial and bending stiffness was considered. In addition, supporting examples and case studies were developed for validation.

In the previously developed methods, the interaction of membranes with fluids has been studied mostly through analytical methods. Using these methods, all types of membranes,

with different material characteristics in multiple configurations have been studied. Despite these efforts, only a limited number of FE methods have been developed thus far to study membranes, although shells and plates have been comprehensively studied [29-32]. Given the fact that the Isogeometric Analysis is a relatively new method, there are still many aspects of it (e.g. application of this method in membrane analysis) that have not been fully developed.

1.5. References

[1] Armijos, S.J. (2008), Fabric Arhitecture: Creative Resources for Shade, signage, and Shelter, W.W. Norton & Company Inc., New York, New York, United States, 20-23, Introduction.

[2] Geiger, D. H. (1975), "Low-profile air structures in the USA", Batiment International, Building Research and Practice, 3(2), pp. 80.

[3] American Society of Civil Engineers (2010), Tensile Membrane Structures, American Society of Civil Engineers, Virginia, United States, 1, Chap. 1

[4] Riddle, M. (2011, December). Temporary basketball arena for the London 2012 Olympics is a winner. Retrieved from http://specialtyfabricsreview.com/articles/1211_wv_basketball_arena.html

[5] Argyris, J. H. et al. (1974), "A general method for the shape finding of lightweight tension structures", Computer Methods in Applied Mechanics and Engineering, 3(1), pp. 135-149.

[6] Nireki, T. et al. (1990), "Durability of PVC-coated Fabrics for Membrane Structures", Durability of Building Materials and Components Proceedings of the Fifth International Conference, Brighton, U.K.

[7] Wang, J. T., Johnson, A. R. (2002), "Deployment Simulation of Ultra-Lightweight Inflatable Structures", 43rd AIAA/ASME/ASCE/ AHS/ASC Structures, Structural Dynamics, and Materials Conference and Exhibit, Denver, Colorado, U.S.A.

[8] Razak, H. A. et al. (2004), "Weatherability of coated fabrics as roofing material in tropical environment", Building and Environment, 39(1), pp. 87-92.

[9] Lan, T. T. (2009), "A Retrospective View of Olympic Structures in China", International Journal of Space Structures, 24(2), pp. 79-86.

[10] Ding, Y. (1986), " Shape optimization of structures: a literature survey", Computers and Structures, 24(6), pp. 985-1004.

[11] Cummings, D. et al. (1975), "Mathematical Model of an Air Cushion Vehicle", Charles Stark Draper Laboratory Incorporated, AD-A015 699.

[12] Yun, L. and Bliault A. (2005), Theory and Design of Air Cushion Craft, Elsevier Butterworth-Heinemann, Oxford, United Kingdom, 9-36, Chap. 1.2-1.5

[13] Zhou, J. et al. (2009), "Nonlinear FEM Simulation of Air Cushion Vehicle (ACV) Skirt Joint Under Tension Loading", Naval Engineers Journal, 121(2), pp. 91-97.

[14] Sullivan, P.A. et al. (1985), "Non-linear oscillations of a simple flexible skirt aircushion", Journal of Sound and Vibration, 102(2), pp. 269-283.

[15] Ma, T. and P.A. Sullivan (1986), "Linear analysis of the heave dynamics of a bag and finger air cushion vehicle skirt", AIAA 8th Advanced Marine Systems Conference, U.S.A.

[16] Doctors, L.J. (1975), "Nonlinear Motion of an Air Cushion Vehicle over Waves", Journal of Hydronautics, 9(2), pp. 49-57.

[17] Doctors, L.J. (1976), "The Effect of Air Compressibility on the Nonlinear Motion of an Air Cushion Vehicle Over the Waves", Eleventh Symposium on Naval Hydrodynamics, London, U. K.

[18] Carrier, R. et al. (1978), "Seakeeping Dynamics of a Single Cushion, Peripheral Cell-Stabilized Air Cushion Vehicle", Journal of Hydronautics, 12(2), pp. 49-54.

[19] Chung, J. and Sullivan, P.A. (2000), "Linear Heave Dynamics of an Air-Cushion Vehicle Bag-and-Finger Skirt", Transactions of the Japan Society for Aeronautical and Space Sciences, 43(140), pp. 39-45.

[20] Chung, J. and Jung, T.C. (2004), "Optimization of an Air Cushion Vehicle bag and finger skirt using genetic algorithms", Aerospace Science and Technology, 8(3), pp. 219-229.

[21] Doctors, L.J. (1993), "On the Use of Pressure Distributions to Model the Hydrodynamics of Air-Cushion Vehicles and Surface-Effect Ships", Naval Engineers Journal, 105(2), pp. 69-89.

[22] Paidoussis P.M. (1998), Fluid-Structure Interactions: Slender Structures and Axial Flow, Volume 1, Academic Press, San Diego, California, U.S.A., 23-25, Chap. 2.2.1.

[23] Doctors, L. J. and McKesson, C. B. (2006), "The resistance components of a surface-effect ship", Proceedings of the Twenty-Sixth Symposium on Naval Hydrodynamics, Rome, Italy.

[24] Graham, T.A., P.A. Sullivan, and M.J. Hinchey (1985), “Skirt material effects on air cushion dynamic stability.” Journal of Aircraft, 22(2), pp. 101-108.

[25] Wilson, R. A., Wells, S. M., and Heber, C. E. (1979), "Powering predictions for surface effect ships based on model results", Journal of Hydronautics, 13(4), pp. 113-119.

[26] Doctors, L. J. (1992), "On the use of pressure distributions to model the hydrodynamics of air-cushion vehicles and surface-effect ships", High Performance Marine Vehicle Conference and Exhibit, Washington, D.C., U.S.A.

[27] Zalek, S.F. et al. (2011), "Modeling of air cushion vehicle's flexible seals under steady state conditions", Ocean Systems Engineering, 1(1), 17-29.

[28] Yu, B. and Karr D.G., "Analytical Solutions of 2D Membrane Shapes within Different Inflation and Deflation Regimes", The Quarterly Journal of Mechanics and Applied Mathematics,(In preparation).

[29] Cirak, F. et al. (2000), "Subdivision surfaces: a new paradigm for thin-shell finite-element analysis", International Journal for Numerical Methods in Engineering, 47(12), 2039-2072.

[30] Kiendl, J. et al. (2010), "The bending strip method for isogeometric analysis of Kirchhoff–Love shell structures comprised of multiple patches", Computer Methods in Applied Mechanics and Engineering, 199(37-40), 2403-2416.

[31] Hughes, T.J.R. et al. (1977), “A simple and efficient finite element for plate bending”, International Journal for Numerical Methods in Engineering, 11(10), 1529-1543.

[32] Beirao de Veiga, L. et al. (2012), “An isogeometric method for the Reissner–Mindlin plate bending problem”, Computer Methods in Applied Mechanics and Engineering, 209-212, 45-53.

Chapter 2

Analytical Approach of Two-Dimensional Inextensible Membranes

In this Chapter, the structural behavior of partially submerged two-dimensional inextensible membranes is studied using an analytical method. In particular the deformation and tension of the membrane is sought under constant internal pressure and hydrostatic external pressure. The effect of friction forces is neglected. As an example, the membrane is considered to be ¾ of a circle before deformation, pinned at the top to a solid plate, and assumed to be weightless.

2.1. Prior Work in Analytical Investigation of Membranes

The defining equations of the deformed profile of inflated cylindrical membranes in floating and submerged conditions, pushed down by a flat plate on the top have been developed based on the equilibrium equations [1]. Bearing in mind that one of the usual applications of membranes is to store large masses of liquids, the profile of long cylindrical membranes to be used as large scale flexible floating containers has been

analyzed under static conditions [2]. Neglecting the weight of the container and friction, equilibrium equations were found for the shape of the container to be a function of circumferential stress, internal pressure, and the position of the container with respect to the waterline. Simpson's rule was used to approximate the integral calculations and the equations are solved by a modified Newton-Raphson method procedure. The success of the procedure is a function of the initial choice values.

Plaut and Suherman [3] established closed form and approximate solutions for the shape and tension in geosynthetic tubes when laid on a horizontal solid foundation and also presented a number of numerical examples. The analyses presented shape and tension as a function of top and bottom pressure. Numerical results were obtained using a shooting method. The presented solution is an exact solution in which equations of tension and geometry can simply be solved using the Newton-Raphson method and boundary conditions. Other cases of a tube being partially or fully submerged, laid on deformable foundation, and exposed to non-symmetric pressure were also studied. The tubes were assumed to be weightless and incompressible. A linear study of a two-dimensional liquid-filled floating membrane was conducted by Zhao [4] to predict dynamic tension and motion in waves. Neglecting the elastic deformation, he first solved the static case by using the equilibrium equation and then a numerical scheme was developed to predict the shape and tension. Ghavanloo and Daneshmand [5] applied nonlinear analysis to reach a closed form solution to the profile of air-filled membranes laid on different inclined surfaces. Numerical results were developed for different conditions and confirmed by comparison with previously published works.

2.2. Two-Dimensional Partially Submerged Membranes

Consider the profile of a circular membrane with a rigid cover with uniform internal pressure as shown in Figure 2.1. The shape of the membrane changes under the water line due to varying pressure, while it remains circular above the waterline.

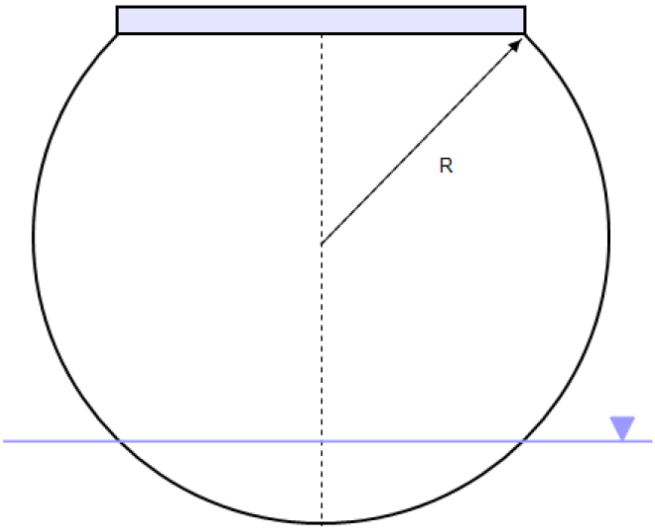

Figure 2.1. Profile of the membrane

Figures 2.2a and 2.2b show a section of this membrane in three and two dimensions, respectively, where N is the tension force per unit length, T is the tension force, P is the internal pressure and q is the internal force per unit length. In Figure 2.2b, the membrane is of unit width perpendicular to the page. Also, as depicted in Figure 2.2b, the angle θ is measured from the horizontal to the tangential plane.

It is assumed that the membrane is inextensible and has negligible weight. Tangential friction is also neglected. Force equilibrium then requires

$$\frac{d\theta}{ds} = \frac{q}{T} \tag{2.1}$$

and

$$\frac{dT}{ds} = 0 \tag{2.2}$$

The difficulties of solving Equation (2.1) when density of the external fluid is less than twice the density of the internal fluid are described by Hawthorne [6].

The horizontal coordinate is *x* and the vertical coordinate is *y* as shown in Figure 2.2b. Considering the geometrical configuration in Figure 2.2b, we note also

$$\frac{dy}{ds} = \sin\theta \ , \quad \frac{dx}{ds} = \cos\theta \tag{2.3a,b}$$

From geometric considerations we denote the curvature, ρ, and radius of curvature, R, which are related by:

$$\rho = \frac{1}{R} = \frac{d\theta}{ds} \tag{2.4}$$

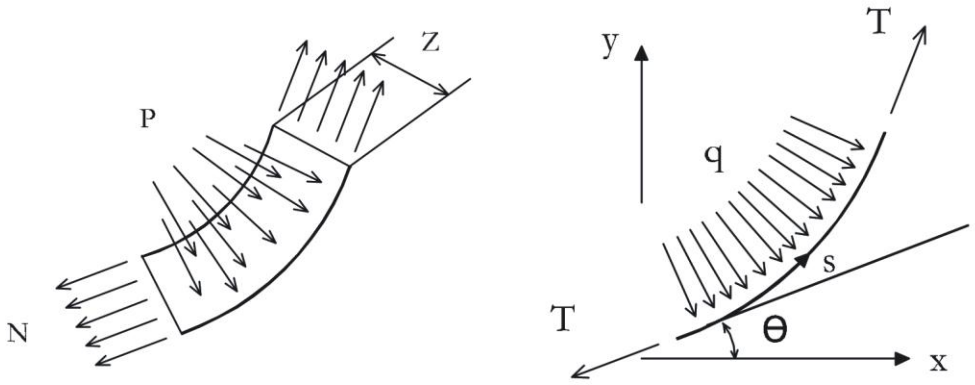

Figure 2.2. Representative membrane segment (a) Three-dimensional depiction (b) Two-dimensional depiction

The radius, R, can be written in terms of the tension and pressure in familiar fashion by substituting Equation (2.1) into Equation (2.4):

$$R = \frac{T}{q} \tag{2.5}$$

2.3. Parametric Analysis

The relationships for position x and y are sought as functions of arc length, s. The equilibrium configuration, $x(s)$ and $y(s)$ are thus established by solving the governing differential equations. These relationships are later compared to the developed finite element solutions presented in Chapters 4 and 5.

The portion of a partially submerged membrane above the waterline has constant pressure and constant radius, while the pressure under the waterline is variable with depth and

therefore the solution to the governing equations are different for these two parts (Figure 2.3). For compatibility, the values for pressure, tension, angle and position should be the same at the waterline. Consider point O being the lowest point on the membrane and O_1 being the point where the membrane meets the waterline. The *y*-axis is thus a plane of symmetry. Solutions above and below the waterline are established in the following Sections.

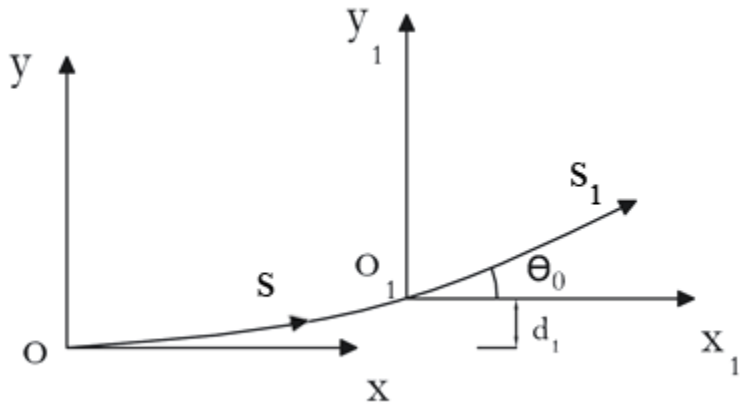

Figure 2.3. Above the waterline and general case coordinate systems

2.4. Constant Pressure – Above the Waterline

From Equation (2.1) with constant pressure q_0 we find the inclination angle above the waterline

$$\theta_1 = \frac{q_0}{T} s_1 + \theta_0 \qquad (2.6)$$

or,

$$s_1 = \frac{T}{q_0}(\theta_1 - \theta_0) \tag{2.7}$$

Here we note the boundary condition at point "O_1" is $\theta(s_1 = 0) = \theta_0$. The rectangular coordinate, x and y, above the waterline are then found from Equations (2.3) and (2.7)

$$y_1 = \frac{T}{q_0}(\cos\theta_0 - \cos\theta_1) \tag{2.8}$$

$$x_1 = \frac{T}{q_0}(\sin\theta_1 - \sin\theta_0) \tag{2.9}$$

2.5. Varying Pressure – Below the Waterline

Consider a membrane in which the deformed submerged depth is d_1. As it is depicted in Figure 2.4, the origin of s is set to be the lowest point of the membrane. For a given d_1, the following equations describe the exact solution to the profile of the submerged portion of the membrane.

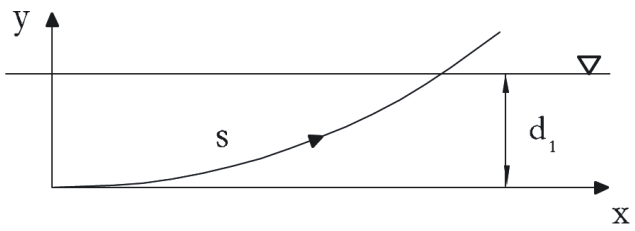

Figure 2.4. Coordinate system below the waterline

The pressure below the waterline follows from hydrostatics

$$q_1 = q_0 + \gamma_f (y - d_1) \tag{2.10}$$

where γ_f is the weight density of water times the unit membrane width. Also from Equations (2.1) and (2.10)

$$\frac{d\theta}{ds} = K_1 + K_2 y \tag{2.11}$$

in which,

$$K_1 \equiv \frac{q_0 - \gamma_f d_1}{T} \tag{2.12}$$

and

$$K_2 \equiv \frac{\gamma_f}{T} \tag{2.13}$$

Differentiating Equation (2.11) with respect to s and applying Equation (2.3a),

$$\frac{d^2\theta}{ds^2} = K_2 \sin\theta \tag{2.14}$$

We now let

$$p \equiv \frac{d\theta}{ds} = K_1 + K_2 y \tag{2.15}$$

and hence:

$$\frac{dp}{ds} = p\frac{dp}{d\theta} \tag{2.16}$$

Combining Equations (2.14) , (2.15) and (2.16),

$$p\ dp = K_2 \sin\theta\ d\theta \tag{2.17}$$

and upon integration,

$$p = \sqrt{C_1 - 2K_2 \cos\theta} \tag{2.18}$$

In Equation (2.18), C_1 is constant of integration. From Equation (2.15), we also find,

$$ds = \frac{d\theta}{\sqrt{C_1 - 2K_2 \cos\theta}} \tag{2.19}$$

and

$$s = \int \frac{d\theta}{\sqrt{C_1 - 2K_2 \cos\theta}} \tag{2.20}$$

From Equations (2.3) and (2.19),

$$dy = \frac{\sin\theta \; d\theta}{\sqrt{C_1 - 2K_2 \cos\theta}} \tag{2.21}$$

Integration of Equation (2.21) yields

$$y = \frac{1}{K_2}(\sqrt{C_1 - 2K_2 \cos\theta} - \sqrt{C_1 - 2K_2}) \tag{2.22}$$

Recall that from Equations (2.15) and (2.18),

$$p = \sqrt{C_1 - 2K_2 \cos\theta} = K_1 + K_2 y$$

Solving for C_1 by applying the symmetry conditions of the origin yields

$$C_1 = K_1^2 + 2K_2 \tag{2.23}$$

By substituting Equation (2.23) into Equations (2.20) and (2.22),

$$y = \frac{1}{K_2}(\sqrt{C_1 - 2K_2 \cos\theta} - K_1) \tag{2.24}$$

By repeating the process in the same manner for x, we also find

$$x = \int \frac{\cos\theta \, d\theta}{\sqrt{C_1 - 2K_2 \cos\theta}} \tag{2.25}$$

The value of the integrals in Equations (2.20) and (2.25) can be evaluated using the trapezoid method or using the Taylor series of the integrand.

For any particular depth (d_1), the angle between the waterline and membrane can be calculated from Equation (2.24):

$$\theta_w = \cos^{-1}[\frac{C_1}{2K_2} - \frac{K_2}{2}(d_1 + \frac{K_1}{K_2})^2] \qquad (2.26)$$

We note that x, y and s are all expressed as functions of the parameter θ. Our approach is to first solve for s as a function of θ from Equation (2.20). Equations (2.24) and (2.25) then provide $x = x(\theta)$ and $y = y(\theta)$. Expression for $x = x(s)$ and $y = y(s)$ can then implicitly be found through Equation (2.20). The iterative method to find the tension is described in detail in the following Section.

2.6. Iterative Solution on the Tensile Force

The correct answer for T, the tension in the membrane, results in a deformed shape in which the top of the membrane meets the corner of the cover (Figure 2.5). Starting with an initial value (the tension in the membrane above the waterline is used) the Newton-Raphson method [6] is applied to reach the correct answer. Figure 2.5 shows the correct deformed shape versus the shape resulted from an initial estimate for the tension value.

Figure 2.6 shows an algorithm of the process adopted from the Newton-Raphson method.The slope of the line connecting any two solution points in the (x_{Total} - x_{Top}) vs. T plane, is found by

$$m = \frac{[x_{total} - x_{top}]_1 - [x_{total} - x_{top}]_2}{T_1 - T_2} \qquad (2.27)$$

and the new tension is calculated using:

$$T_{new} = T_{old} - \frac{[x_{total} - x_{top}]_{old}}{m} \tag{2.28}$$

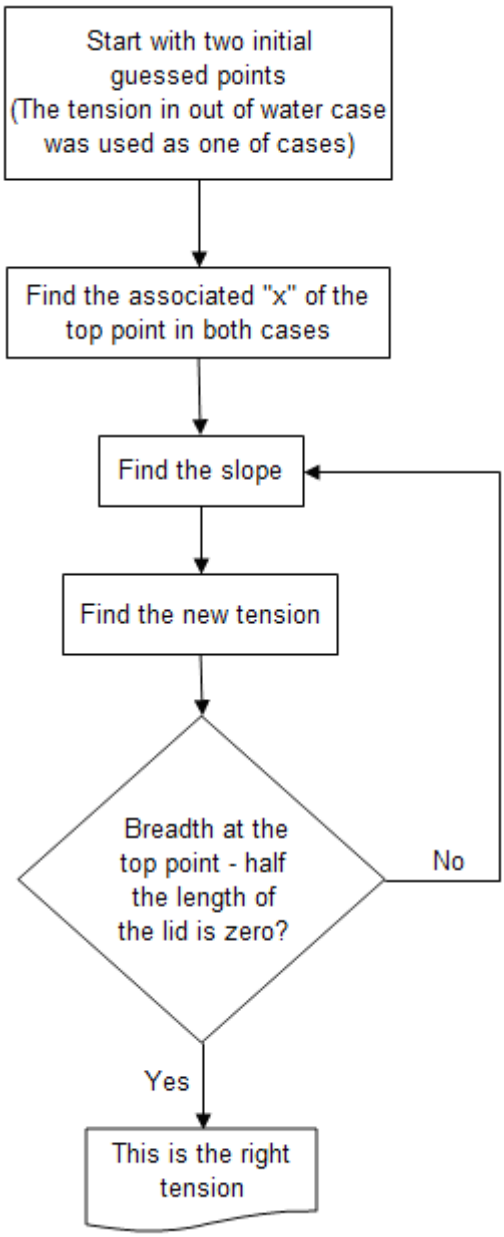

Figure 2.6. The Algorithm of the Newton-Raphson iteration process

The iteration convergence rate is very good. The process is explained in more detail in the following Section.

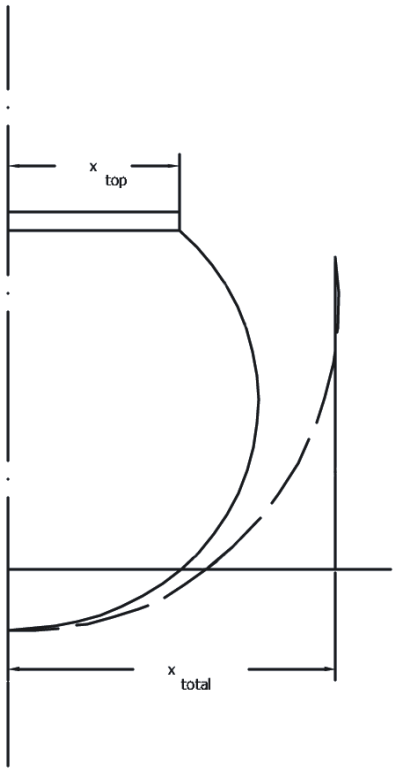

Figure 2.5. Resulted shape in an iteration step (dashed line) and correct deformed shape of the membrane (solid line)

2.7. Example Analyses and Results

As an example, consider a membrane with an initial radius of 1.000 m. The length of the membrane is 4.712 m and it is positioned symmetrically with respect to the vertical radius (y axis). The membrane is connected to a rigid plate at the top. The width of the lid is 1.414 m (Figure 2.1).The internal pressure is 10.14 kPa and weight density of water is

10.12 kN/m^3. The undeformed shape is such that the inscribed angle of the membrane is 3/2 π (at the attachment points of the membrane to the cover, $\theta = \pm 3/4\ \pi$). The distance from the cover to the membrane bottom is thus 1.707*R*. The cover and membrane are moved down such that the submerged depth is 0.5*R*. This depth is then fixed for the exact solution example. We first calculate an initial estimate for the tension using $T = q_0 R = 10.14\,\text{kN}$. The configuration for the submerged portion of the membrane is then calculated using Equations (2.17) and (2.21). The resulting geometry at the waterline then allows solution for the top portion. In other words, the coordinates and the slope of the end of the submerged portion is used as a starting point for the top portion.

For the second iteration, another value close to the first iteration value is chosen for tension equal to $T = 9.632\,\text{kN}$. This value is then used to determine the solution of the submerged geometry. Table 2.1 shows a summary of results obtained for these first two iterations for our example.

Table 2.1. First and second iterations for the analytic solution.

	Iteration 1	Iteration 2
K1 (m^{-1})	0.5005	0.5267
K2 (m^{-2})	0.9990	1.051
C1 (m^{-2})	2.249	2.379
θ	0.8958	0.9207
xw (m)	1.211	1.175
sw (m)	1.353	1.321
xTotal (m)	1.377	1.278
xTop (m)	0.7071	0.7071
T (kN)	10.14	9.632

Based on Equation (2.27), we next find $m = 0.1949$ and the tension in the membrane for the third iteration can be calculated from Equation (2.28), $T_{new} = 6.751\text{kN}$. This process continues in the same manner and after eight iterations the value for tension is found to be 7.481 kN. Tension values after each iteration are shown in Table 2.2 and Figure 2.7.

Table 2.2. Values of tension in membrane during the Newton-Raphson iterations.

Iteration	Tension in the membrane(kN)
1	10.14
2	9.632
3	6.751
4	7.688
5	7.432
6	7.479
7	7.482
8	7.481

Based on this final deformed geometry, the vertical distance from the highest point of the membrane to its lowest point is 1.516 m. We denote the out of water height of the membrane as Y_{Top}. Recall that the submerged depth of the membrane in 0.5000 m and

therefore our solution yields for our example a final configuration with

$Y_{Top} = 1.516\,\text{m} - 0.5000\,\text{m} = 1.016\,\text{m}$.

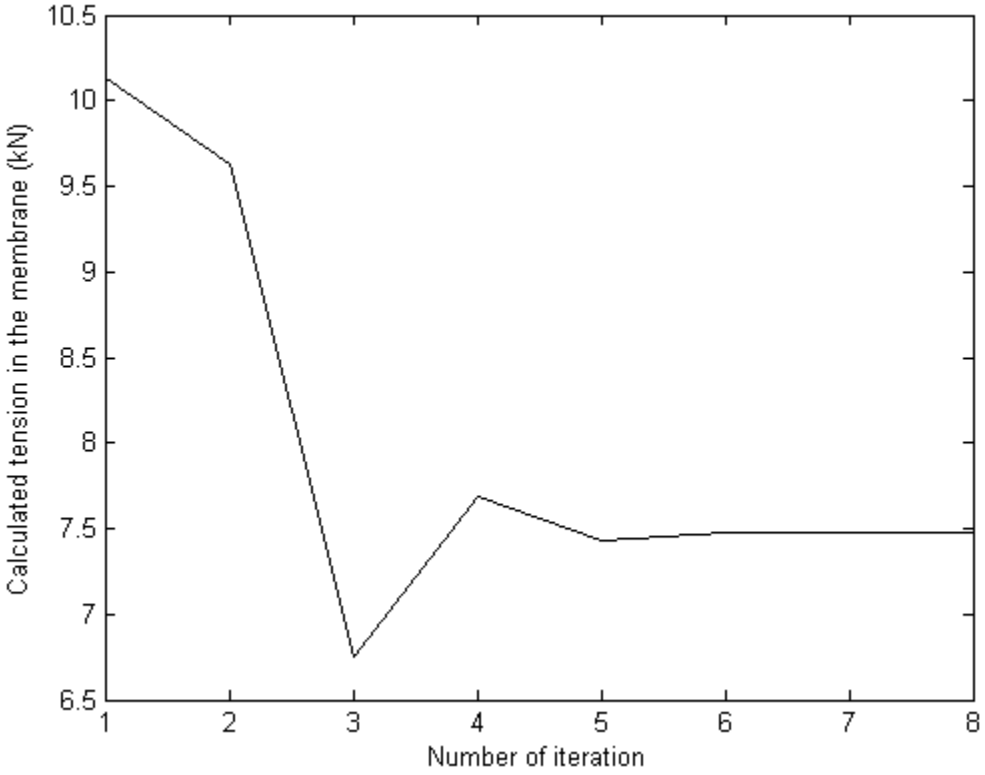

Figure 2.7. Convergence of tension versus the number of elements

Figure 2.8. shows the membrane of this example in a deformed configuration where it is partially submerged and the submerged depth is 0.7609 m. The lowest point of the undeformed geometry is set to the origin. The diagram of the membrane in this example along with some other examples are shown and discussed in Chapters 4 and 5. It is also of great interest to consider the case the membrane loses its symmetry as it is immersed in the fluid. At this configuration the largest width of the profile of the membrane and the waterline overlap.

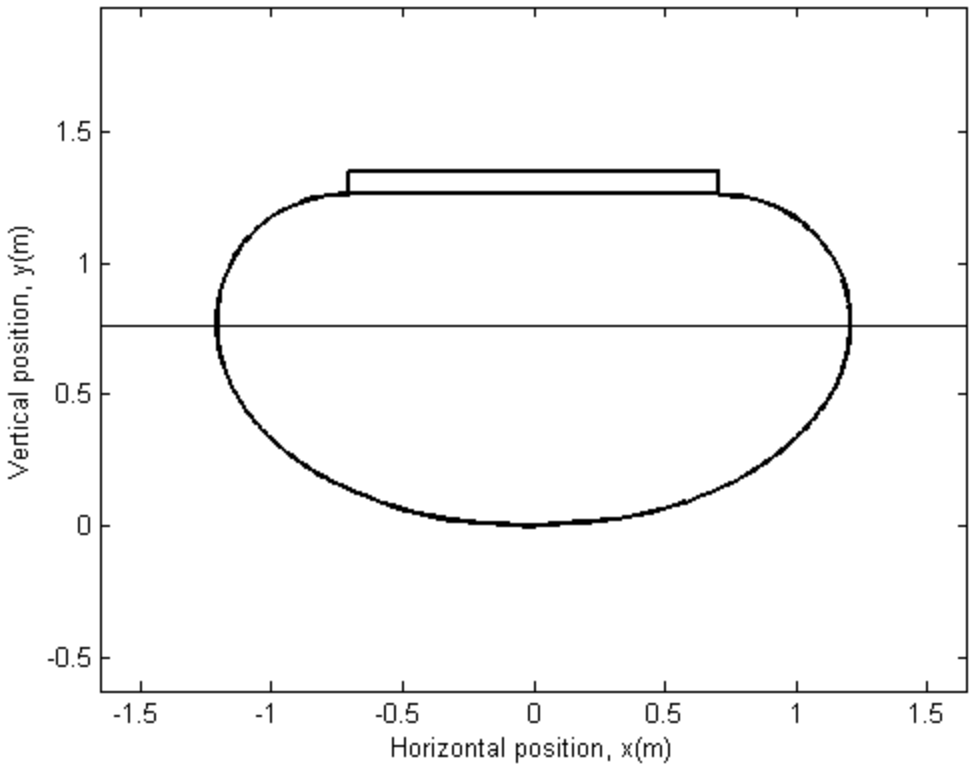

Figure 2.8. Deformed profile of a membrane with 0.7609 m submerged depth

The solution to the problem of 0.7609 m submerged depth for this membrane is unique if symmetry is imposed. In the case that symmetry is not enforced there are other solutions to the problem, such as the profile demonstrated in Figure 2.9. This solution has the same submerged profile and length. In this case, out of the fluid part is located only at one side of the cover. The boundary condition that needs to be satisfied (the coordinate of the point that the membrane is attached to the cover) by Newton-Raphson iterative method is different in this case.

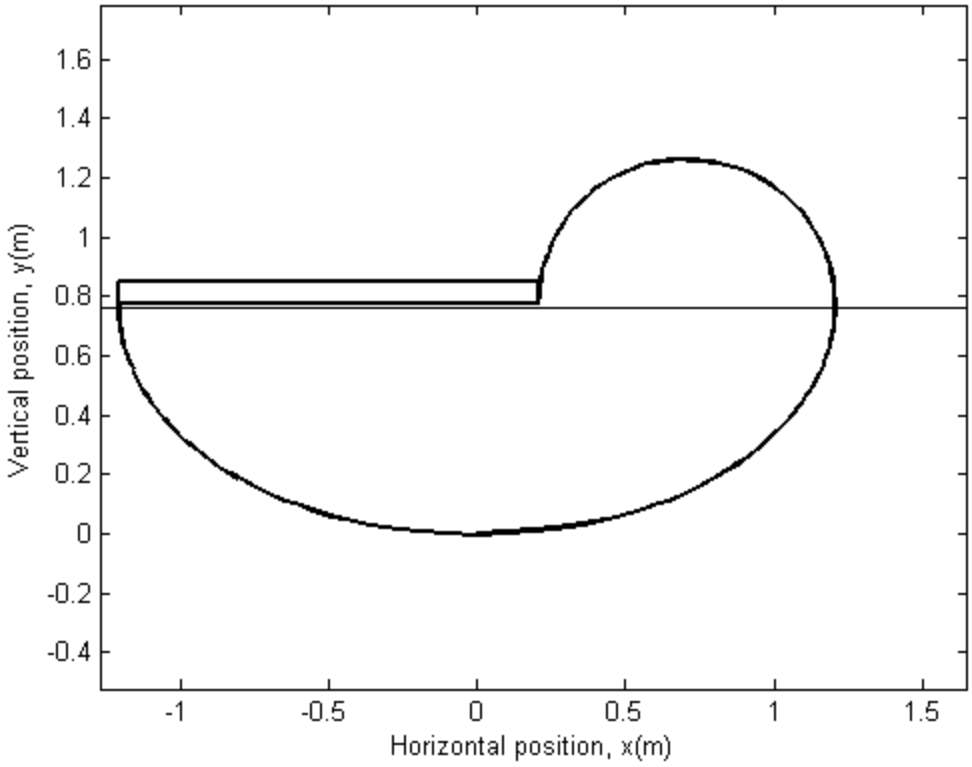

Figure 2.9. The non-symmetrical deformed profile of a membrane with 0.7609 m submerged depth

2.8. Conclusion

The methodology presented in this Chapter applies specifically to partially submerged membranes. The methods discussed in Chapters 4 and 5 can be applied to more general geometries, also the results of different methods will be compared.

2.9. References

[1] Wu, C.H., (1971), "On the contact problems of inflated cylindrical membranes with a life raft as an example", Journal of Applied Mechanics, 38(3), 615-622.

[2] Szyszkowski, W. and Glockner, P. C. (1987), "On the Statics of Large Scale Cylindrical Floating Membrane Containers", International Journal of Nonlinear Mechanics, 22(4), 275-282.

[3] Plaut, R.H. and Suherman, S. (1998), "Two-Dimensional Analysis of Geosynthetic Tubes", Acta Mechanica, 129, 207-218.

[4] Zhao, R. (1995), "A Complete Linear Theory for a Two-Dimensional Floating and Liquid-Filled Membrane Structure in Waves", Journal of Fluid Structures, 9, 937-956.

[5] Ghavanloo, E., and Daneshmand, F. (2009), "The Equilibrium Shapes of Air-Filled Heavy Membrane Tubes Resting on Inclined Planes", Mechanics Research Communications, 36(3), 405-412.

[6] Hawthorne, W.R. (1961), "The early development of the Dracone flexible barge," Proceedings of the Institution of Mechanical Engineers, 175, 52-83.

Chapter 3

Numerical Modeling of a Surface Effect Ship Bow Seal

In this Chapter, the beam bending theory is employed to determine the hydrodynamic pressure in the bow seal system of Surface Effect Ships (SESs). The flexural rigidity of the seal membrane is determined by beam bending tests and other geometric information is collected from visual snapshots taken during an experiment involving a test apparatus in a towing tank. In addition to hydrodynamic pressure, the seal membrane is under constant cushion pressure, shear forces, and its own weight.

3.1. Introduction

Previous experimental analyses have considered the overall resistance of SESs [1, 2]. The SES finger-type seal performance has also been investigated in detail from the vibration and material durability stand point [3]. However, there is a lack of experimental data required for conducting and validating numerical analysis methods. As such, existing numerical methods need to be improved to be able to effectively determine the structural

behavior of air cushion vessels under the complex environment at sea. An advanced knowledge of seal membrane characteristics is essential for such an improvement.

In this Chapter, the seal system of SESs is modeled using beam bending theory to find the hydrodynamic pressure required to achieve a specific geometry determined during an experiment. The experiment [4] was conducted in a towing tank facility with a test apparatus of 3.660 m long by 1.219 m high by 1.524 m wide, equipped with a flat bow seal membrane. The seal was selected according to the two-dimensional theoretical seal model devised by Doctors and McKesson [5].

The result of this analysis was also compared with the results of a Computational Fluid Dynamics (CFD) analysis based on the same experimental information [4]. Figure 3.1 shows a snapshot of the seal membrane and the test apparatus during the experiment with the following conditions:

- Forward speed of 2.438 m/s
- Cushion pressure of 107.7 mm H_2O
- Initial submerged depth of 0.2286 m
- Total calculated hydrodynamic thrust force of approximately 551.6 N

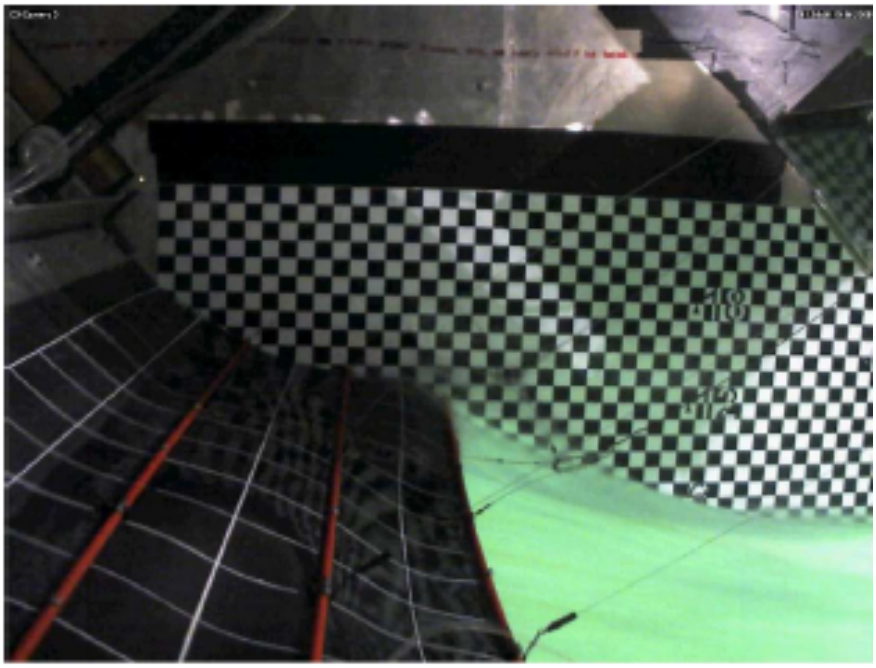

Figure 3.1. Transverse view of the bow seal (courtesy of [4])

The membrane was marked with a 7.620 cm × 7.620 cm grid in contrasting color of white to allow digital optical analysis. In addition, the wall of the test apparatus was also marked with a 2.540 cm × 2.540 cm black and white checkerboard grid. The upper portion of the bow seal was made of stiffened aluminum plate connected to the front wall of test apparatus at a 45 degree angle. The lower part of the bow seal was a flexible membrane made of vulcanized neoprene rubber with the thickness of 3.175 mm. The membrane was equipped with two nylon mesh inserts to minimize stretching.

3.2. Model Assumptions

In order to conduct seal deflection analysis, a strip of the seal along its length is selected from Figure 3.1. This seal strip is treated as a flexible elastic beam under hydrodynamic pressure on one side and constant cushion pressure on the other side. The equilibrium is established for quasi-static steady state conditions and the pressures are assumed to act normal to the surface of the seal. In addition, large displacements are presumed.

3.3. Mathematical Establishments

For a seal membrane described in Section 3.1 the net transverse pressure is calculated as the difference between the cushion and hydrodynamic pressure,

$$q = p_{cushion} - p_{hydro} \tag{3.1}$$

Contributing components to the applied normal pressure to the membrane is shown in Figure 3.2. In addition to the normal pressure, a number of other forces act on the membrane, including, membrane's weight, w, and shear load, V which acts in the direction normal to the displaced surface. Also, due to large displacements, an axial tension force is generated in the membrane. The density of the seal membrane weight is approximated to be $w = 34.47\ \text{N/m}^2$.

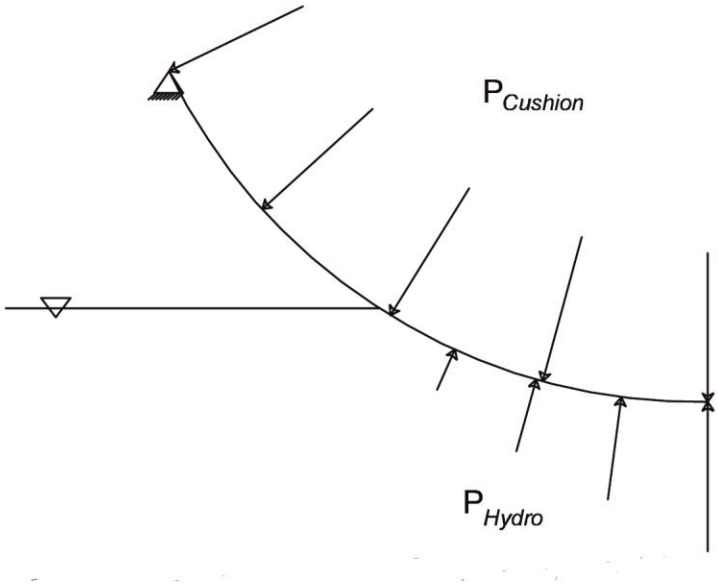

Figure 3.2. Contributing components to the total normal pressure applied to the membrane

If the slope of the seal membrane with respect to the horizontal direction at any point along its length is shown with θ, establishing equilibrium equations in the transverse and tangential directions for an element of arc length , ds, will lead to Equations (3.2) and (3.3) respectively,

$$\frac{dV}{ds} = q + w\cos\theta - T\frac{d\theta}{ds} \tag{3.2}$$

$$\frac{dT}{ds} = w\sin\theta - V\frac{d\theta}{ds} \tag{3.3}$$

Due to the flexural rigidity, the moment at any point of the seal is related to the change of inclination angle through the length of the membrane,

$$M = EI\frac{d\theta}{ds} \tag{3.4}$$

On the other hand, establishing equilibrium equations for moments yields,

$$\frac{dM}{ds} = -V \tag{3.5}$$

By substituting Equations (3.4) and (3.5) into Equation (3.3) and integrating, shear and tension forces are expressed in Equations (3.6) and (3.7), respectively in terms of weight density, flexural rigidity, seal slope and its first and second derivatives with respect to arc length,

$$V = -EI\frac{d^2\theta}{ds^2} \tag{3.6}$$

$$\begin{aligned} T &= \int w\sin\theta\, ds - \int V\left(\frac{d\theta}{ds}\right)ds + C \\ &= \int\left[w\sin\theta + EI\left(\frac{d^2\theta}{ds^2}\right)\left(\frac{d\theta}{ds}\right)\right]ds + C \end{aligned} \tag{3.7}$$

Again, substituting Equations (3.6) and (3.7) into Equation (3.2) will result in an expression for net transverse pressure, q, in terms of the seal inclination angle , θ, the weight density, w, the flexural rigidity, and the seal axial tension in the form of Equation (3.8),

$$q = -EI\frac{d^3\theta}{ds^3} - w\cos\theta + T\left(\frac{d\theta}{ds}\right) \tag{3.8}$$

Accordingly, the hydrodynamic pressure acting on the seal is easily calculated knowing the internal pressure of cushion, using Equation (3.8) and rearranging Equation (3.1),

$$p_{hydro} = p_{cushion} - q \tag{3.9}$$

3.4. Model Results

Figure 3.1 is used to derive the geometry of the seal during the test described in Section 3.1 by selecting 99 data points and obtaining their coordinates in the plane of the Figure by determining their horizontal and vertical distance from the upper left corner of the seal membrane, where it is connected to the vessel bow frame. For smoothing purposes, a 7th order polynomial fit, based on least squares, was established. The inclination angle is calculated as a function of the arc length, $\theta = \theta(s)$, based on the relative position of the data points. This defines a geometry shown in Figure 3.3. The flexural rigidity of the seal was determined to be approximately 0.04519 N-m^2 per unit width, based on beam bending tests [4]. It should be noted that there is variability in this value due to the existence of the fibers added to the membrane to add extensional stiffness in the plane of the seal. By differentiating slope with respect to arc length and using Equation (3.4), the moment is determined as a function of arc length. This is illustrated in Figure 3.4.

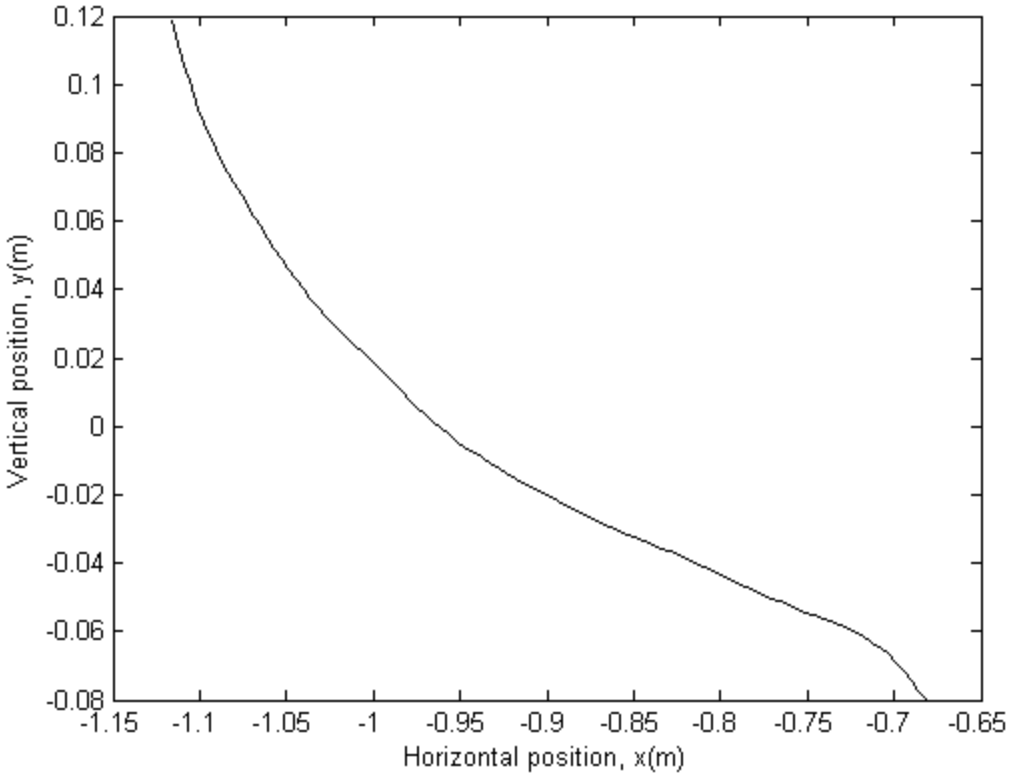

Figure 3.3. Seal geometrical configuration example of a two-dimensional structural analysis

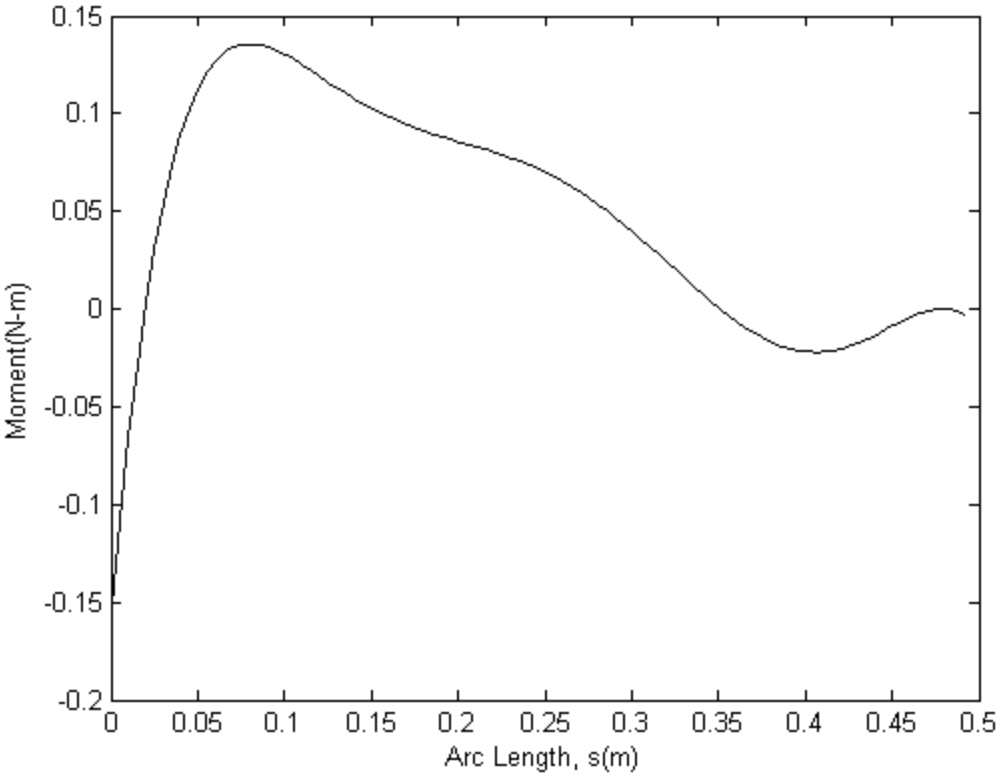

Figure 3.4. Seal moment intensity determined from the example structural analysis

Knowing the geometry of the seal, the net transverse pressure is calculated considering only bending resistance and shear forces. The hydrodynamic pressure is calculated based on Equation (3.9) knowing constant cushion pressure. The results are shown by a dashed line in Figure 3.5. However, based on Equation (3.8), other factors, specifically weight of the seal and the axial tension generated due to nonlinear geometric effects also contribute to bending resistance. The effects of these factors are considered in the calculation of hydrodynamic pressure which is illustrated by a solid line in Figure 3.5.

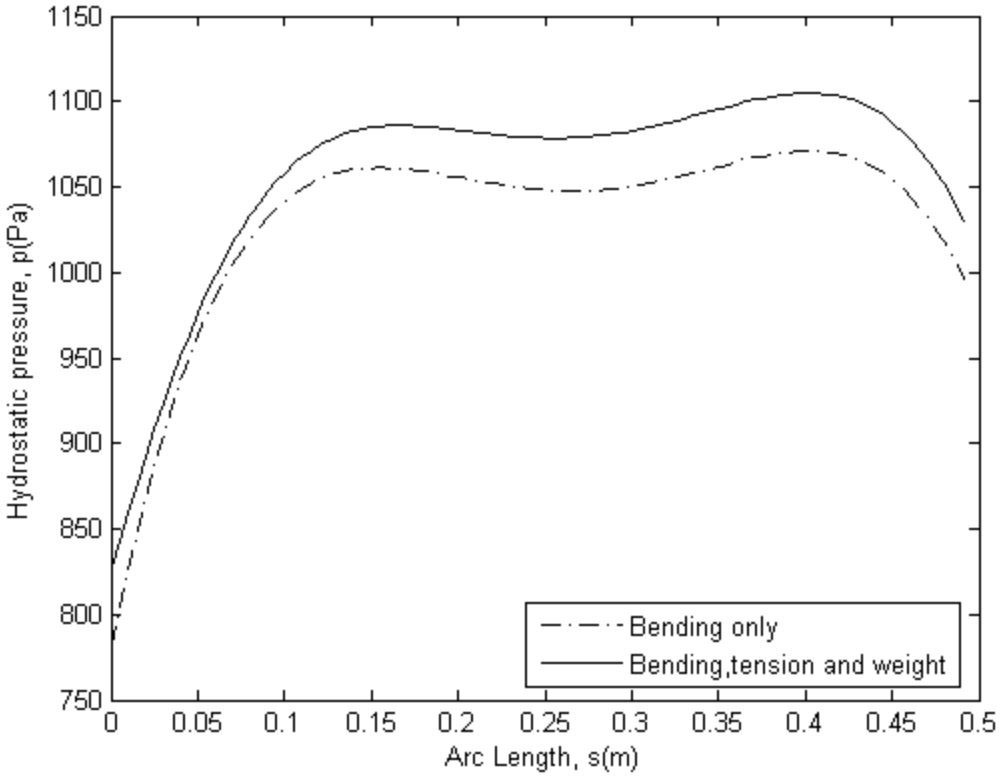

Figure 3.5. Hydrodynamic pressures determined from the example structural analysis

It should be noted that these analyses highly depend on the seal's inclination angle as its third derivative with respect to arc length is involved in the calculation of the hydrodynamic pressure. As shown in Figure 3.5, the hydrodynamic pressure decreases in the vicinity of the connection point to the vessel frame. This is due to the fact that unlike most parts of the seal membrane, at this area, for a very short distance, the seal profile has a slight negative curvature which results in lower hydrodynamic pressure values.

The opposite edge of the seal is completely free; this results in minimum tension in the seal. The cases where ends of seal membrane are fixed have been previously analyzed [5, 6]. Fixed ends allow the tensile forces in the membrane to increase and subsequently to

resist normal pressures. In this research, due to the free end of the seal, the effect of the tensile forces is not very high and the resulting hydrodynamic pressure is mostly a function of bending resistance. This is confirmed by the difference between two cases shown in Figure 3.5. Therefore, the structural behavior of the seal depends highly on boundary conditions as well as material characteristics.

3.5. Conclusion

The beam bending theory was used to model a two-dimensional seal membrane of SESs under quasi-static conditions. The required information for conducting the analysis was determined by experiments. The beam bending theory analysis showed that the results were very sensitive to local element inclination angle, θ.

3.6. References

[1] Bresch, P.K. (1976), "Motions of bow seal fingers in a surface effect ship flexible seal," David W. Taylor, Naval Ship Research and Development Center Report No. 76-0026.

[2] Wilson, R.A. et al. (1979), "Powering predictions for surface effect ships based on model results", Journal of Hydronautics, 13(4), 113-119.

[3] Malakhoff, A. and Davis, S. (1981), “Dynamics of SES bow seal fingers”, Proceedings of the American Institute of Aeronautics and Astronautics Sixth Marine Systems Conference, Seattle, Washington.

[4] Zalek, S.F. et al. (2011), “Modeling of air cushion vehicle’s flexible seals under steady state conditions”, Ocean Systems Engineering, 1(1), 17-29.

[5] Doctors, L.J. and McKesson, C.B. (2006), “The resistance components of a surface-effect ship”, Proceedings of the 26th Symposium on Naval Hydrodynamics, Rome, Italy.

[6] Ulstein, T. and O.D. Faltinsen (1998), “Cobblestone effect on SES”, NATO Research and Technology Organisation”, Proceedings of the AVT Symposium on Fluid Dynamics Problems of Vehicles Operating near or in the Air-Sea Interface, Amsterdam, The Netherlands.

Chapter 4

Finite Element Approach of Inextensible Membranes

In this Chapter, an innovative Finite Element (FE) methodology to analyze two-dimensional inextensible curved membranes with negligible flexural rigidity is presented. To accommodate for curved geometries, arc elements with constant radii through their lengths are used. Each element has two nodes and two degrees of freedom (DOFs) expressed in terms of displacement per node. The "stiffness influence coefficient" method is used to calculate the stiffness matrix. Also, in addition to normal pressure, the effects of shear and membrane weight are investigated.

4.1. Introduction

In our FE development, the elements are presumed inextensible with negligible flexural rigidity. Each element is assumed to have a constant radius of curvature which varies with pressure loading. The applied forces are resisted by the membrane tension in the element in its deformed configuration. In the analysis, equilibrium is satisfied using the

deformed geometry. The analysis is thus nonlinear in nature. The solution approach is to linearize the equilibrium equations using a "current state" for which the linearized force-displacement relations are established. Increments in loading are thus related to increments in displacements. The resulting new geometry can then be used to update the stiffness matrix of the elements and to determine the forces for computing the displacement increments for the next iteration.

Although some analytical solutions (e.g. the method described in Chapter 2) have been previously published, deriving an analytical solution for more complicated problems may be infeasible. The FE method, on the other hand, enables the solution to be easily programmable in a variety of computer applications. This results in solutions with high precision in a remarkably short processing time.

4.2. Prior Work in Finite Element Analysis of Membranes

If extensibility, flexural rigidity and compressive strength are added to an ideal membrane, the result is categorized as a shell element. As a result of their small thickness, they are usually used in applications where light structures are needed, e.g. watercrafts, airplanes and also as roof systems for large buildings.

A FE formulation for a general shaped shell was developed by Ahmed et al. [1]. Based on this formulation, two and three-dimensional situations were analyzed by Hughes and

Liu ([2] and [3]). These shell elements were also analyzed under dynamic loading [4]. Hughes and Carnoy developed this concept for the cases where large strains may develop [5]. These methods are based on the principle of minimum total potential energy using an elastic potential function.

In a comprehensive work, Bushnell [6] used finite difference energy method to develop a FE formulation for shells. Considering a one-dimensional curved beam, he used the energy method and presented the components of the total potential energy as strain energy, kinetic energy, constraint energy and work done by external loads. The systems were defined to have five DOFs: displacement in two directions: along the curved beam and perpendicular to that, rotation, strain and change in curvature. Each of these DOFs and terms of total energy were defined as a function of displacement vector. This vector was made of tangential displacement at the two ends of the element in addition to the normal displacement of the element and its adjacent ones. Equilibrium equation was then developed by making the potential energy stationary. It should be noticed that although somewhat similar, shells and membranes cannot be analyzed by the same methods considering the extra strength and rigidity and lack of flexibility in shells.

Oden and Sato analyzed the large deformation in elastic membranes by modeling them with flat triangular elements [7]. A nonlinear stiffness matrix was derived and numerical examples were provided to illustrate the procedure. The deformation process was assumed reversible and isothermal and therefore an elastic potential function existed which described the strain energy. According to Rivlin [8] strain energy is appropriately

quantified as a function of the strain invariants. The stiffness was then found by differentiating the strain energy with respect to displacement. A similar FE formulation for membrane shells was developed by Gruttmann and Taylor using the tangential stiffness matrix [9]. The stiffness matrix was derived in a similar manner to Oden and Sato's, but the strain energy was defined as a function of principal strain.

The theory for large deformations has also received considerable attention. In an effort to model blood vessels, Holzapfel et al. developed a FE formulation for large strain in membranes following the same theory [10]. Demiroz developed a FE method to predict large deformations in a flexible cantilever beam under buckling to model fabrics [11]. The Galerkin method [12] was used to develop a FE solution where rotation and curvature were defined as two DOFs. Newton-Raphson iteration method was used to solve for rotation and curvature and the FE formulation was established. The results were compared with previously published work. A few methods have already been developed for membranes with drilling DOFs. Ibrahimbegovic et al. [13], and Iura and Atluri [14] both derived a quadrilateral membrane FE for such membranes.

None of the previously established methods account for inextensible membranes. Thus, this Chapter aims to develop a new numerical method that can be easily applied to curved inextensible membranes with no bending stiffness. Another advantage is that in this method the boundary conditions are often defined in terms of displacements, hence readily adapted to the FE approach.

4.3. Local Stiffness of an Element Due to Normal Pressure

In order to find the stiffness matrix, the stiffness influence coefficient method is used. The stiffness component, k_{ij}, is the force at degree of freedom *i* due to a unit displacement at degree of freedom *j* with all other displacements equal to zero.

Figure 4.1 illustrates an element in the local coordinate system, with chord length, l, and its local DOFs. The arc length of the element is denoted by L, and the radius is R. These are shown in Figure 4.2. Each element has four DOFs, the (x_e, y_e) coordinate of each nodal end point.

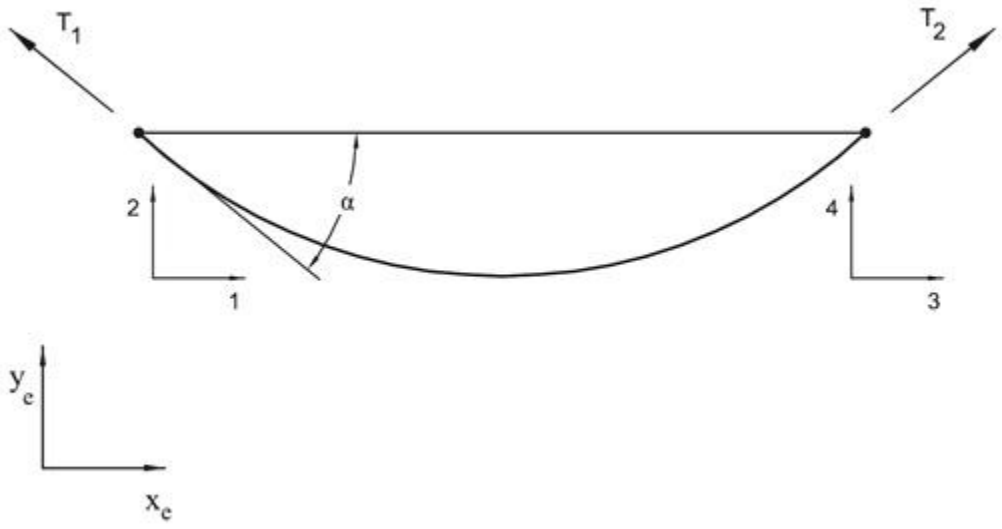

Figure 4.1. An element in the local coordinate system

From geometry by considering the angle α, the defining parameters of this element, arc length L, radius of curvature R, angle α and cord length l are related by

$$\alpha = \frac{L}{2R} \tag{4.1}$$

Also, from geometry,

$$\frac{l}{2R} = \sin(\frac{L}{2R}) \tag{4.2}$$

Forces associated with all four DOFs are,

$$\begin{cases} T_{e1} = -T_1 \cos\alpha \\ T_{e2} = T_1 \sin\alpha \\ T_{e3} = T_2 \cos\alpha \\ T_{e4} = T_2 \sin\alpha \end{cases} \tag{4.3}$$

where the subscript "e" denotes the local element DOF.

Assuming that the membrane element is of unit width and subjected to a constant pressure p , the resulting force, per unit length along the membrane arc length can be written as,

$$q = p(1) \tag{4.4}$$

The loading q per unit length along the membrane arc length resulted from applied constant pressure p on a membrane element of unit width has a dimension of force per

unit length. In this section, with weight and shear loading ignored, from equilibrium we have,

$$T = qR \tag{4.5}$$

where $T = T_1 = T_2$ is the constant force in the membrane.

As an example of the application of the stiffness influence coefficient method, consider the case where displacement in the third DOF is unity while other displacements are zero (Figure 4.2).

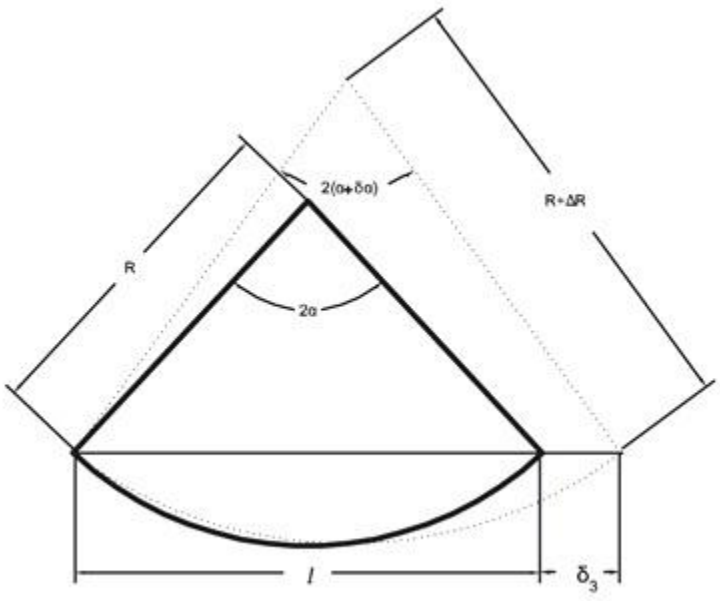

Figure 4.2. Unit displacement at the element third degree of freedom

Then due to the elongation of the chord length l, the radius R and the angle α also change when,

$$l \Rightarrow l + \delta_3 \tag{4.6}$$

As an example, the change in tension in first local DOF due to a change in nodal displacement, δ_3, can be expressed as,

$$\frac{dT}{d\delta_3} = \frac{dT}{d\alpha}\frac{d\alpha}{dR}\frac{dR}{dl}\frac{dl}{d\delta_3} \tag{4.7}$$

For this example,

$$K_{13}^{e} = \frac{dT_1}{d\delta_3} = \frac{dT_1}{d\alpha}\frac{d\alpha}{dR}\frac{dR}{dl}\frac{dl}{d\delta_3} \tag{4.8}$$

where,

$$\frac{dT_1}{d\alpha} = \frac{qL}{2\alpha^2}(\alpha \sin\alpha + \cos\alpha) \tag{4.9}$$

$$\frac{d\alpha}{dR} = -2\frac{\alpha^2}{L} \tag{4.10}$$

$$\frac{dR}{dl} = \frac{1}{2(\sin\alpha - \alpha\cos\alpha)} \tag{4.11}$$

$$\frac{dl}{d\delta_3} = 1 \tag{4.12}$$

and thus,

$$K_{13}^{e} = -\frac{1}{2} q\left(\frac{\alpha \sin\alpha + \cos\alpha}{\sin\alpha - \alpha\cos\alpha}\right) \tag{4.13}$$

By repeating the analysis in this manner, the other elements of the stiffness matrix are determined. Therefore, the stiffness matrix of the element due to pressure is found to be

$$K_{q_0}^{e} = \frac{1}{2} q \begin{bmatrix} K_1 & 1 & -K_1 & -1 \\ -1 & K_2 & 1 & -K_2 \\ -K_1 & 1 & K_1 & -1 \\ -1 & -K_2 & 1 & K_2 \end{bmatrix} \tag{4.14}$$

where,

$$\begin{cases} K_1 \equiv \dfrac{\alpha \sin\alpha + \cos\alpha}{\sin\alpha - \alpha\cos\alpha} \\ K_2 \equiv \cot\alpha \end{cases} \tag{4.15}$$

4.4. Local Stiffness of an Element Due to Shear Load

Consider an element in the local coordinate system (Figure 4.3). Suppose that a pressure loading, q_0, is applied simultaneously with a uniformly distributed shear load, q_s, applied in the tangential direction. Due to this load, the tension through the length of the membrane is not constant and the two tension forces at the ends are different.

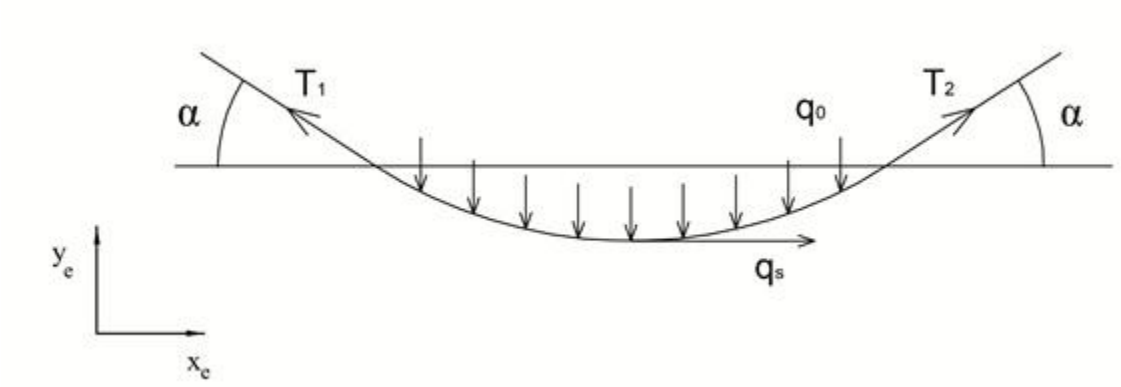

Figure 4.3. Pressure and shear loading applied on an element

From the equilibrium equations, these two forces are found to be

$$\begin{cases} T_1 = q_0 R + q_s R \ \tan\alpha \\ T_2 = q_0 R - q_s R \ \tan\alpha \end{cases} \tag{4.16}$$

Note there must be sufficient pressure to maintain equilibrium; for example equilibrium without pressure is generally not possible for a curved shape under shear loading alone.

4.5. Local Stiffness of an Element Due to Element Weight

Consider the element in the global coordinate system shown in Figure 4.4, where the angle between the chord line and horizontal line is γ. The uniformly distributed weight load ω is applied on the element in the -y_G direction. The tension forces on the two ends are also different in this case.

From the equilibrium equations, these two forces are found to be

$$\begin{cases} T_1 = \frac{1}{2}\omega L(\frac{\cos\gamma}{\sin\alpha} - \frac{\sin\gamma}{\cos\alpha}) \\ T_2 = \frac{1}{2}\omega L(\frac{\cos\gamma}{\sin\alpha} + \frac{\sin\gamma}{\cos\alpha}) \end{cases} \tag{4.17}$$

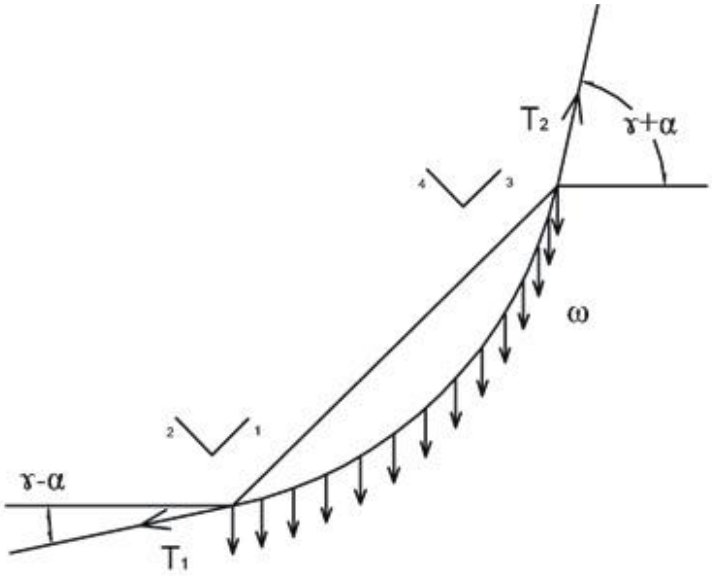

Figure 4.4. An element with uniformly distributed weight

Again applying the stiffness influence coefficient method, we find the stiffness due to weight:

$$K_w = \frac{1}{2} w \begin{bmatrix} -k_a \frac{\cos\gamma}{\sin^2\alpha} & -k_b(\cos\gamma + \cot\alpha\sin\gamma) & k_a \frac{\cos\gamma}{\sin^2\alpha} & k_b(\cos\gamma + \cot\alpha\sin\gamma) \\ k_a \frac{\sin\gamma}{\cos^2\alpha} & k_b(\sin\gamma + \tan\alpha\cos\gamma) & -k_a \frac{\sin\gamma}{\cos^2\alpha} & -k_b(\sin\gamma + \tan\alpha\cos\gamma) \\ k_a \frac{\cos\gamma}{\sin^2\alpha} & -k_b(\cos\gamma - \cot\alpha\sin\gamma) & -k_a \frac{\cos\gamma}{\sin^2\alpha} & k_b(\cos\gamma - \cot\alpha\sin\gamma) \\ -k_a \frac{\sin\gamma}{\cos^2\alpha} & k_b(\sin\gamma - \tan\alpha\cos\gamma) & k_a \frac{\sin\gamma}{\cos^2\alpha} & -k_b(\sin\gamma - \tan\alpha\cos\gamma) \end{bmatrix} \tag{4.18}$$

where:

$$\begin{cases} k_a = \dfrac{\alpha^2}{(\alpha\cos\alpha - \sin\alpha)} \\ k_b = \dfrac{L}{l} \end{cases} \tag{4.19}$$

4.6. Global Stiffness of an Element

Figure 4.5 shows the membrane element in an arbitrary orientation (an arbitrary value for angle γ). As an example of calculating an element of the global stiffness matrix, suppose the first node of the element moves 1 unit in the $+1_G$ direction when all other nodal displacements are zero. This displacement has two components in the x_e and y_e directions. We denote these displacements x_1 and y_1 as shown in Figure 4.6.

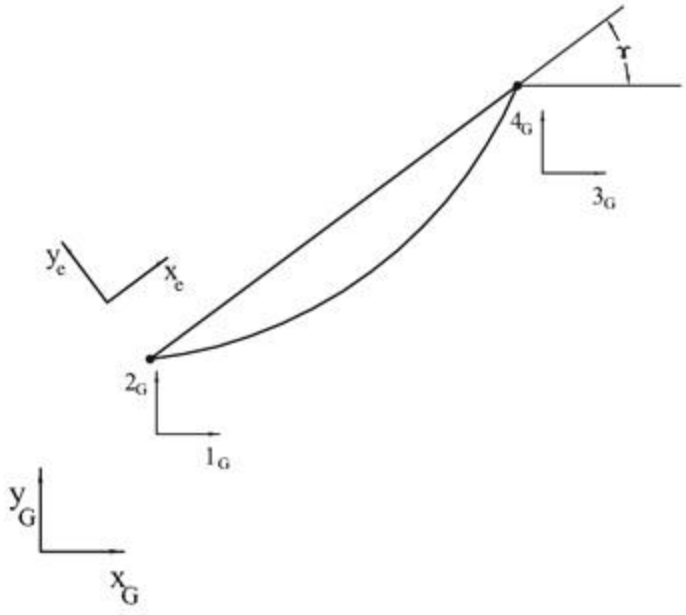

Figure 4.5. An element in the global coordinate system

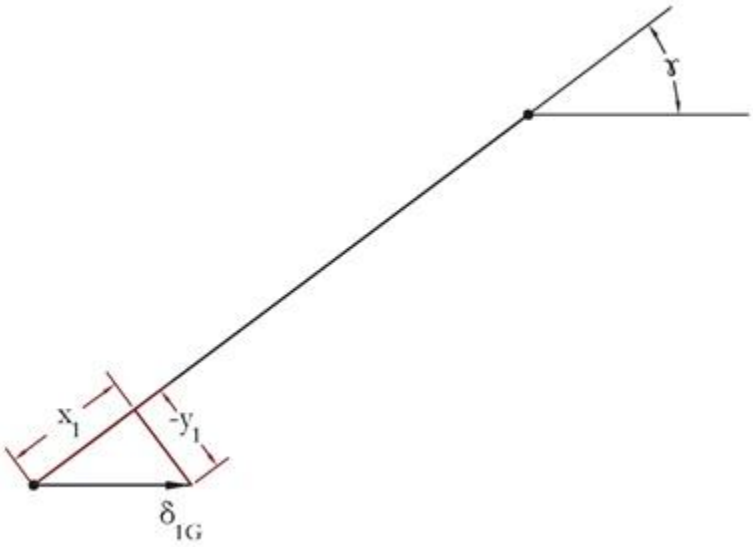

Figure 4.6. Decomposition of unit nodal displacement in the local degrees of freedom

From geometry, the value of the displacement components in the x_e and y_e direction respectively are,

$$\begin{cases} x_1 = \delta_{1G} \cos\gamma \\ y_1 = -\delta_{1G} \sin\gamma \end{cases} \tag{4.20}$$

The resulting force in the $+1_G$ direction ($K_{G_{11}}$) also has two components: F_{1x} and F_{1y} in the x_e and y_e directions respectively. Again from geometry we find,

$$K_{G_{11}} = F_{1x} \cos\gamma - F_{1y} \sin\gamma \tag{4.21}$$

where,

$$\begin{cases} F_{1x} = K_{11}^e x_1 + K_{12}^e y_1 \\ F_{1y} = K_{21}^e x_1 + K_{22}^e y \end{cases} \tag{4.22}$$

$K_{G_{11}}$ is found by substituting Equations (4.20) and (4.22) into Equation (4.21). The components of the global stiffness matrix are found in this manner and are expressed in the following set of formulae:

$$
\begin{cases}
K_{G_{11}} = K_{11}^e \cos^2\gamma - (K_{12}^e + K_{21}^e)\cos\gamma\sin\gamma + K_{22}^e \sin^2\gamma \\
K_{G_{21}} = K_{21}^e \cos^2\gamma + (K_{11}^e - K_{22}^e)\cos\gamma\sin\gamma - K_{12}^e \sin^2\gamma \\
K_{G_{31}} = K_{31}^e \cos^2\gamma - (K_{32}^e + K_{41}^e)\cos\gamma\sin\gamma + K_{42}^e \sin^2\gamma \\
K_{G_{41}} = K_{41}^e \cos^2\gamma + (K_{31}^e - K_{42}^e)\cos\gamma\sin\gamma - K_{32}^e \sin^2\gamma \\
K_{G_{12}} = K_{12}^e \cos^2\gamma + (K_{11}^e - K_{22}^e)\cos\gamma\sin\gamma - K_{21}^e \sin^2\gamma \\
K_{G_{22}} = K_{22}^e \cos^2\gamma + (K_{12}^e + K_{21}^e)\cos\gamma\sin\gamma + K_{11}^e \sin^2\gamma \\
K_{G_{32}} = K_{32}^e \cos^2\gamma + (K_{31}^e - K_{42}^e)\cos\gamma\sin\gamma - K_{41}^e \sin^2\gamma \\
K_{G_{42}} = K_{42}^e \cos^2\gamma + (K_{32}^e + K_{41}^e)\cos\gamma\sin\gamma + K_{31}^e \sin^2\gamma \\
K_{G_{13}} = K_{13}^e \cos^2\gamma - (K_{14}^e + K_{23}^e)\cos\gamma\sin\gamma + K_{24}^e \sin^2\gamma \\
K_{G_{23}} = K_{23}^e \cos^2\gamma + (K_{13}^e - K_{24}^e)\cos\gamma\sin\gamma - K_{14}^e \sin^2\gamma \\
K_{G_{33}} = K_{33}^e \cos^2\gamma - (K_{34}^e + K_{43}^e)\cos\gamma\sin\gamma + K_{44}^e \sin^2\gamma \\
K_{G_{43}} = K_{43}^e \cos^2\gamma + (K_{33}^e - K_{44}^e)\cos\gamma\sin\gamma - K_{34}^e \sin^2\gamma \\
K_{G_{14}} = K_{14}^e \cos^2\gamma + (K_{13}^e - K_{24}^e)\cos\gamma\sin\gamma - K_{23}^e \sin^2\gamma \\
K_{G_{24}} = K_{24}^e \cos^2\gamma + (K_{14}^e + K_{23}^e)\cos\gamma\sin\gamma + K_{13}^e \sin^2\gamma \\
K_{G_{34}} = K_{34}^e \cos^2\gamma + (K_{33}^e - K_{44}^e)\cos\gamma\sin\gamma - K_{43}^e \sin^2\gamma \\
K_{G_{44}} = K_{44}^e \cos^2\gamma + (K_{34}^e + K_{43}^e)\cos\gamma\sin\gamma + K_{33}^e \sin^2\gamma
\end{cases}
\tag{4.23}
$$

4.7. Total Stiffness Matrix of an Element

The total stiffness matrix can be calculated by adding all the stiffness matrices due to different factors which were considered.

$$
K = K_{q_0} + K_{q_s} + K_{\omega} \tag{4.24}
$$

This should be done either before or after transformation to the global coordinate system when all the elements of the total stiffness matrix are in one coordinate system. The stiffness matrices of all elements then will be assembled to make the total stiffness

matrix. Again we note the stiffness matrix is geometry dependent and is therefore updated based upon the membrane "current state".

4.8. Assembled Global Stiffness Matrix

The stiffness matrix of the entire membrane structure is determined by first modeling the structure as an assemblage of elements (Figure 4.7). The position of each nodal point and each element should be determined with respect to others in the overall model. The local element DOFs must be mapped to the global DOFs, and the total stiffness components are found by adding the element stiffness components having common global DOFs.

For example, in Figure 4.7, for each nodal point, both of the elements connected to it contribute to the stiffness associated with that nodal point. The components of the total global stiffness matrix which have contributions from element i are shown in the following:

$$\begin{bmatrix} \ddots & & & & \\ & K_{33}^{i-1}+K_{11}^{i} & K_{34}^{i-1}+K_{12}^{i} & K_{13}^{i} & K_{14}^{i} \\ & K_{43}^{i-1}+K_{21}^{i} & K_{44}^{i-1}+K_{22}^{i} & K_{23}^{i} & K_{24}^{i} \\ & K_{31}^{i} & K_{32}^{i} & K_{33}^{i}+K_{11}^{i+1} & K_{34}^{i}+K_{12}^{i+1} \\ & K_{41}^{i} & K_{42}^{i} & K_{43}^{i}+K_{21}^{i+1} & K_{44}^{i}+K_{22}^{i+1} \\ & & & & \ddots \end{bmatrix} \tag{4.25}$$

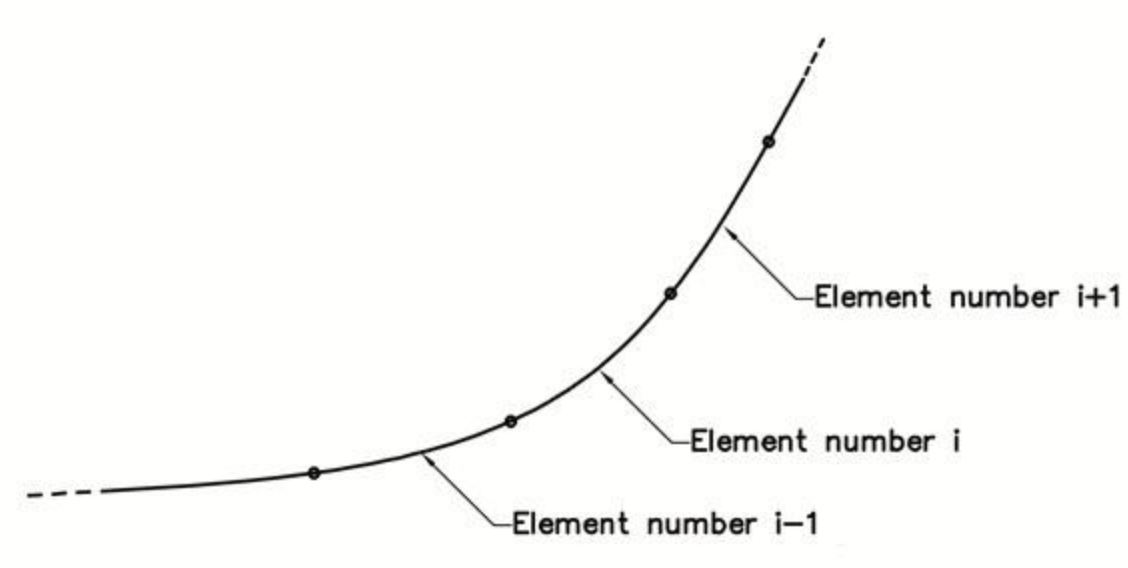

Figure 4.7. The position of element number "i" in a model consisting of several elements

4.9. Force Vector

In general, before an equilibrium configuration is determined, there may be an equivalent load applied on each node due to an imbalance of forces at the node. Consider the node between "element i" and "element j" (Figure 4.8). This node has a DOF "m" in the x_G direction and a DOF "n" in the y_G direction. At the node, force T_i is applied by element "i" and force T_j is applied by element "j" as shown in Figure 4.9. The resulting force vector is computed by the following steps:

a) Decompose each element's force applied on the node in the x_G and y_G directions

b) Compute the net force vectors in the x_G and y_G direction. This yields,

$$\begin{cases} F_m = T_i \cos(\gamma_i - \alpha_i) - T_j \cos(\gamma_j + \alpha_j) \\ F_n = T_i \sin(\gamma_i - \alpha_i) - T_j \sin(\gamma_j + \alpha_j) \end{cases} \tag{4.26}$$

c) To counteract the force imbalance, consider the force components in their related position to calculate the forcing vector.

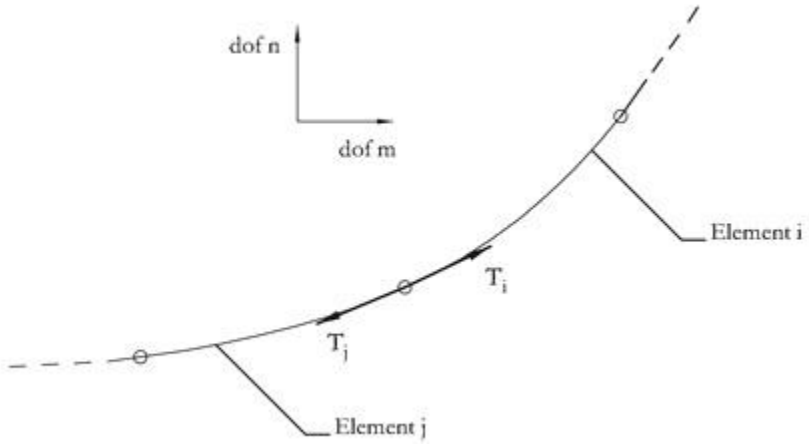

Figure 4.8. Forces applied on a node by its adjacent elements

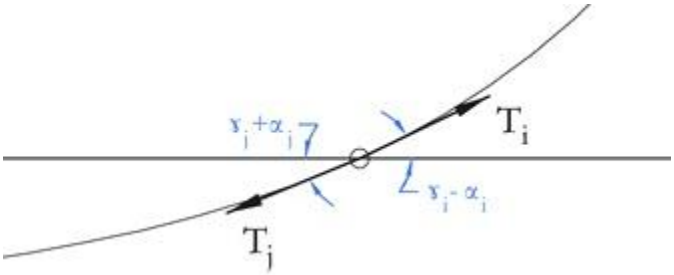

Figure 4.9. Orientation of the applied membrane forces on a node

Figure 4.10 shows the resultant components of the applied load corresponding to the two nodal DOFs. F_m and F_n are respectively the mth and nth elements of the forcing vector.

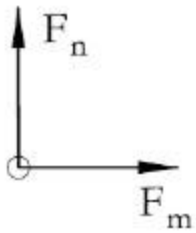

Figure 4.10. Nodal force resultants corresponding to global degrees of freedom m and n

4.10. The Global System of Equations

For a particular structural analysis, the membrane is modeled as an assemblage of finite elements as discussed in the previous section. An initial geometrical configuration is first established and the global DOFs determined. A mapping of the local element DOFs to global DOFs is also required. This allows one to establish the global stiffness matrix from the total local stiffness matrix for each element. Also using the initial geometry, the total forcing vector is calculated and the system displacements can be solved using

$$\{F\}^G = [K]^G \{d\}^G \tag{4.27}$$

where $\{d\}^G$ is the vector of displacements.

4.11. Example Analyses and Results

4.11.1. A Partially Submerged Membrane

Recall the example discussed in Section 2.7. The radius of the undeformed membrane is R=1.000 m and the internal gauge pressure is 10.14 kPa. First, four elements are used to mesh the membrane, each 0.5890 m. Then the mesh is refined and six 0.3925 m elements are used. Due to symmetry about the y-axis, only the right-hand half of the system is modeled. The origin of the coordinate system is set to the lowest point of the undeformed membrane when it is partially submerged with a given Y_{Top}. The boundary conditions are thus x = 0 m at s = 0 m, and a fixed value of position at the top end of the membrane given by ($x = X_{Top} = 0.7071$ m, y = 1.707 m) for our example.

For each element, a mean pressure is calculated based on the mean depth of that element and using Equation (2.2). Supposing that each element is an arc with constant radius, the radius of the element is calculated from geometry using Equation (2.5). Tension in each element is calculated based on the mean calculated pressure. The values of the stiffness matrix elements in the local coordinate system can then be determined. This matrix is transformed to the global coordinate system. This process is repeated for every element in the model and ultimately, the stiffness matrices for all elements can be assembled using the method described in Section 4.8.

The elements of the forcing vector are also found following the method discussed in subsection 4.9. The system of equations is solved for changes in the values of the DOFs.

After the DOFs are adjusted based on the solution to the system of equations, this process is repeated until convergence, which can be analyzed based on either displacement or the tension in the membrane. In the examples presented in this section the goal is to derive the displacement to zero.

As noted previously, we let Y_{Top} denote the distance of the rigid cover from the waterline. This value is fixed for a FE solution. As it was calculated in the example described in Section 2.7, the value of Y_{Top} from the analytical solution is 1.016 m. In the FE calculations, if Y_{Top} is relatively small, which means the submerged depth is relatively high and the change in geometry before and after the process is considerable, the process must be broken down to smaller steps. To solve a problem with a small Y_{Top}, it might be necessary to first solve for the case where the out of water height is larger and use this deformed geometry as the starting point to solve for the case of a smaller Y_{Top}. Therefore, in case on a small Y_{Top}, the submerged depth is increased in displacement increments. At each increment, new geometry and tension is found through iterations.

We found this to be the case when we compare our FE analysis to the analytical solution analysis. We first attempted to solve for the condition with $Y_{Top} = 1.016\,\mathrm{m}$. Convergence failed for this attempt, so a smaller depth of submergence of 0.25*R* was analyzed. This reduced depth results in a larger $Y_{Top} = 1.390\,\mathrm{m}$, which was found using the analytical solution following the procedure of Section 2.7. Figure 4.11 demonstrates the resulted value of tension in the membrane versus the number of elements where $Y_{Top} = 1.390\,\mathrm{m}$.

When compared with the analytical method the error in tension from less than 2% in a two element model was rapidly reduced to almost 0.1% in an eight element model. Using this initial geometry, the process of finding the resulting equilibrium configuration and membrane tension converged in five iterations (the convergence threshold was set at 1N). As the next step, $Y_{Top} = 1.016\,\mathrm{m}$ was considered. This process converged in seven iterations. Tension values during these seven iterations are summarized in Table 4.1.

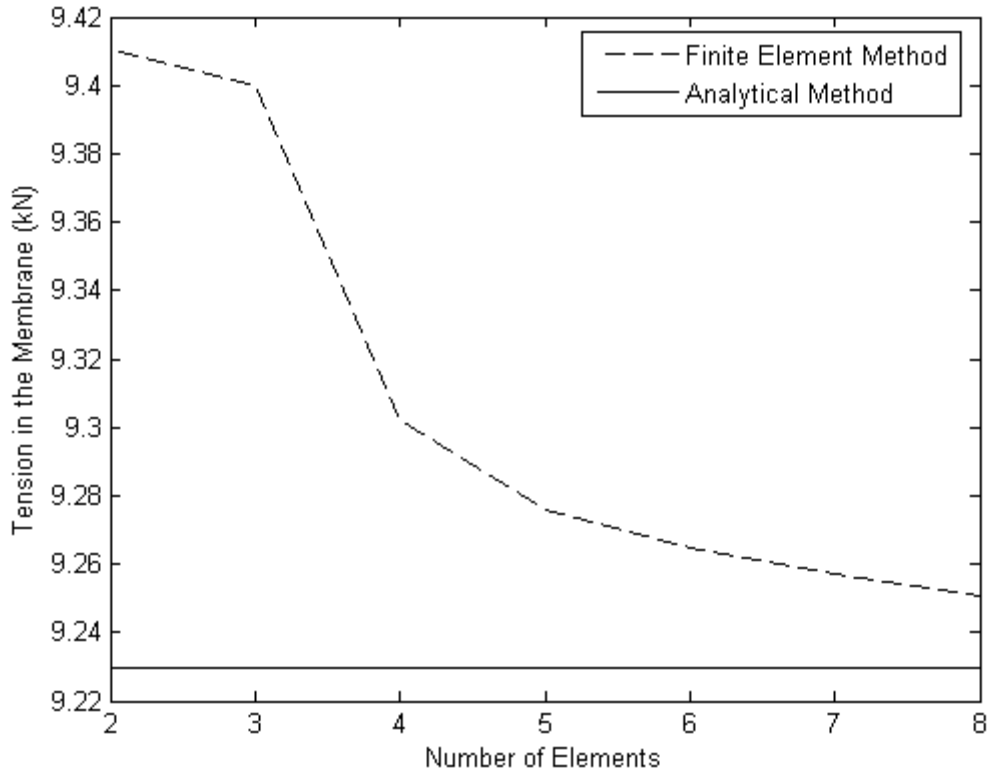

Figure 4.11. Convergence of tension versus the number of elements

Table 4.1. Values of tension in the four-element model during the finite element method iterations

	Tension(kN)			
Iteration	Element 1	Element 2	Element 3	Element 4
1	5.345	6.896	8.822	9.078
2	11.96	8.470	7.352	9.345
3	8.836	7.247	6.960	7.599
4	7.386	6.945	6.923	7.000
5	6.963	6.924	6.924	6.925
6	6.924	6.924	6.924	6.924

The solution for the model with six elements once again started with $Y_{Top} = 1.390\,\mathrm{m}$ and converged in seven iterations. As the second step, Y_{Top} was set to 1.173 m. This process converged in eight iterations. For the final step, $Y_{Top} = 1.016\,\mathrm{m}$ was considered. The values of tension converged in five iterations. Table 4.2 shows these values.

Table 4.2. Values of tension in the six-element method during the finite element method iterations

	Tension(kN)					
Iteration	Element1	Element2	Element3	Element4	Element5	Element6
1	7.915	7.602	7.372	7.485	7.485	7.485
2	7.607	7.634	7.609	7.563	7.568	7.582
3	7.562	7.562	7.558	7.561	7.561	7.561
4	7.561	7.561	7.562	7.561	7.561	7.561
5	7.561	7.561	7.561	7.561	7.561	7.561

The magnitudes of the displacement vector at each iteration are plotted in Figure 4.12. The jumps at iterations 9 and 18 correspond to a new iteration on geometry.

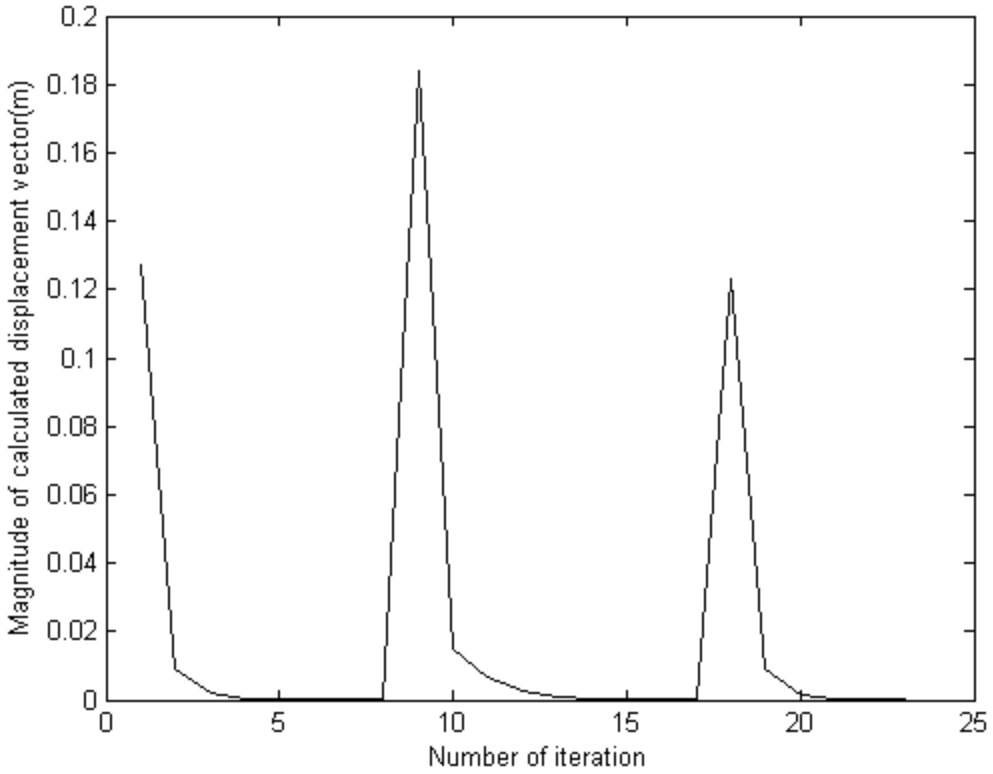

Figure 4.12. Convergence of Finite element method for a membrane with 0.5R submerged depth

Figure 4.13 shows the FE solutions in comparison with the analytical solution. As it can be seen in this Figure, there is a very good agreement between these two methods. The error of the FE solution for the four elements model (dashed line) in the displacement on the lowest point of the membrane is about 16%. This is the point where the maximum difference between the two methods occurs. For the six-element model (circles), this error is about 7%. The difference tension between the six-element model and the analytical solution is 1.1%.

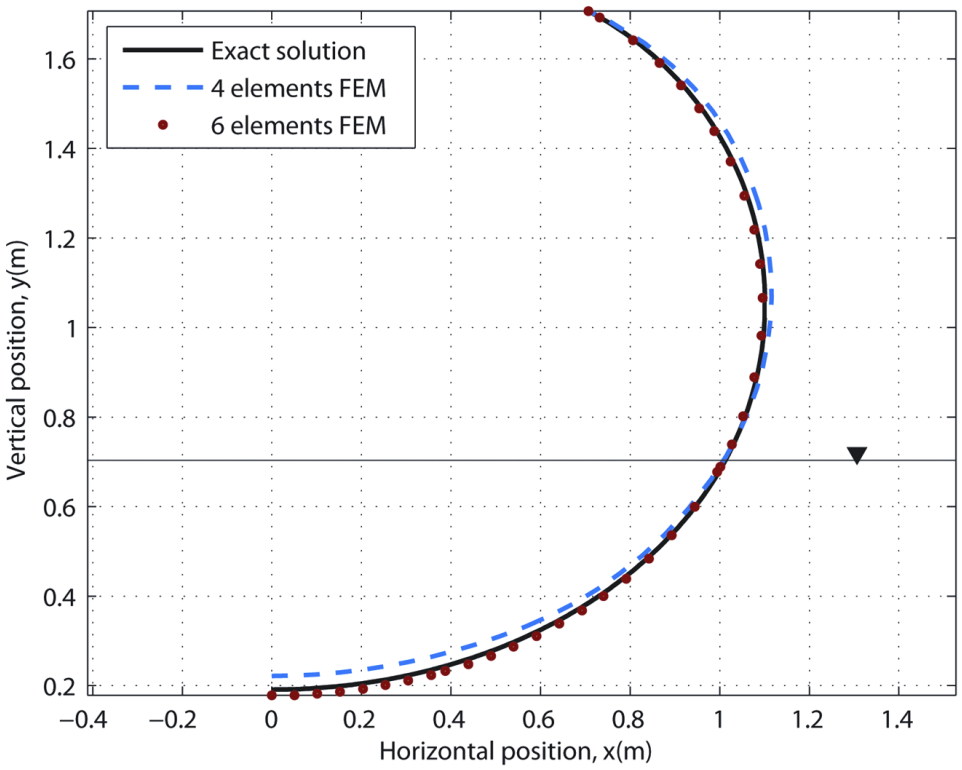

Figure 4.13. Analytical and finite element solution for deformed membrane under pressure

Figure 4.14 shows the undeformed profile of the membrane in comparison with the deformed solution by analytical and FE method.

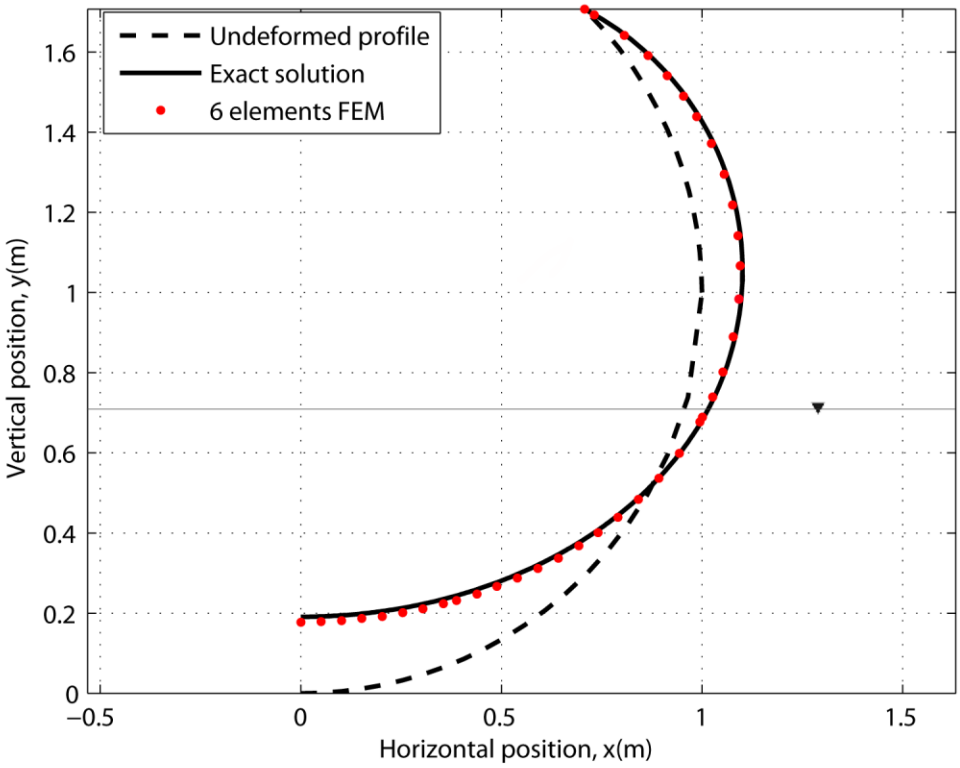

Figure 4.14. Profile of the deformed and undeformed membrane

Figure 4.15 illustrates the output of the presented FE solution with four elements in comparison with the result of another FE method [11] with three elements in which DOFs are in terms of rotation and curvature. The rotation based FE has two elements in the submerged part of the membrane while in our method four equal length elements are used. Each of these methods may result in a more accurate solution when compared with the other one, depending on where along the length of the membrane the point of interest is located. But, it should be noted that the rotation based FE solution does not satisfy the boundary condition at the top point as its calculated top point is higher than the point where the actual membrane and lid are connected. On the other hand, the displacement based FE method presented here totally satisfies the displacement boundary conditions at

this point and this is the major advantage of this method over the methods published in the past.

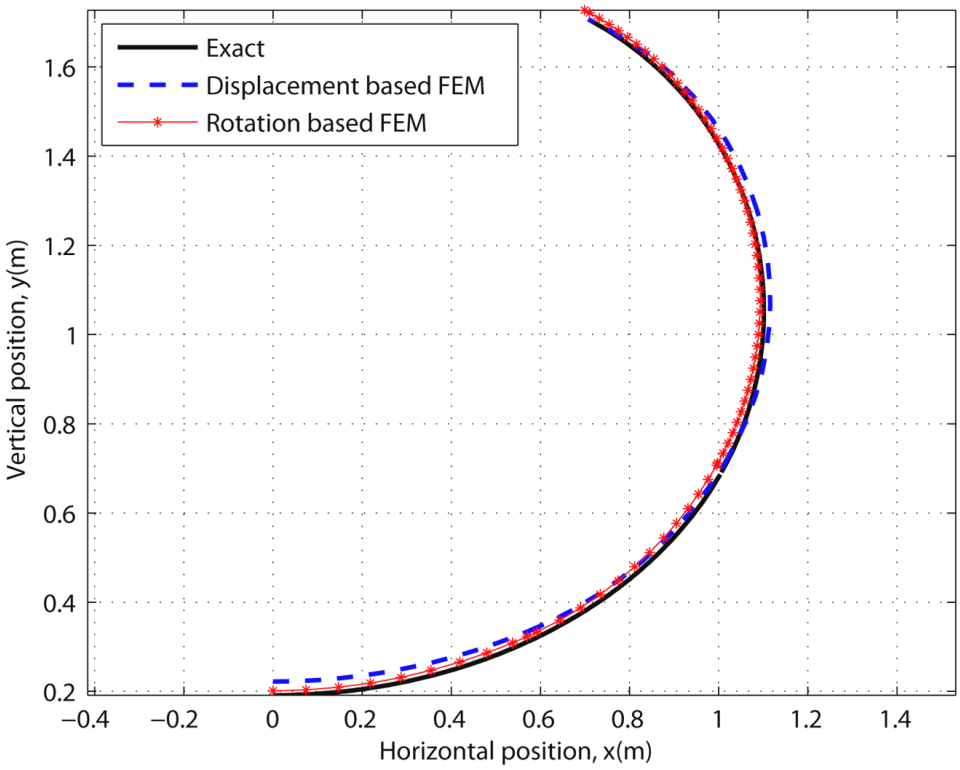

Figure 4.15. The presented finite element method in comparison with another one

4.11.2. A Weighted Membrane Under Internal Pressure

In this section a distributed weight load of 34.47 N/m is added to a membrane with the same geometry as the membrane analyzed in Subsection 4.11.1. The width of the membrane is 1 m. In the first example, the internal pressure is 344.7 N/m. The membrane is first analyzed with a four element model, then the mesh is refined and ten elements are used. The lengths of the elements from the lowest element to the highest in the four element model are $\frac{1}{10}L, \frac{2}{10}L, \frac{3}{10}L$ and $\frac{4}{10}L$ respectively. The lengths of the

elements in the ten element model are $\frac{1}{55}L, \frac{2}{55}L, ..., \frac{10}{55}L$ respectively, where L is half of the length of the cross section of the membrane. The smallest element is the one which is the closest to the lowest point.

The stiffness matrix for each element is calculated based on Equation (4.18), and will be added to the stiffness due to pressure (based on Equation (4.14)). Then every matrix will be transformed to the global coordinate system and assembled. The system of the equations for the model can be solved for changes in the values of the DOFs after the forcing vector is calculated. After the DOFs are adjusted based on the solution to the system of equations, this process is repeated until convergence.

Figure 4.16 shows the FE solutions in comparison with the previously developed analytical solution presented in [15]. The origin of the coordinate system is set to the lowest point of the undeformed membrane. As it can be seen in this Figure; there is a very good agreement between these two methods. Also the improvement of the result due to refinement is noticeable.

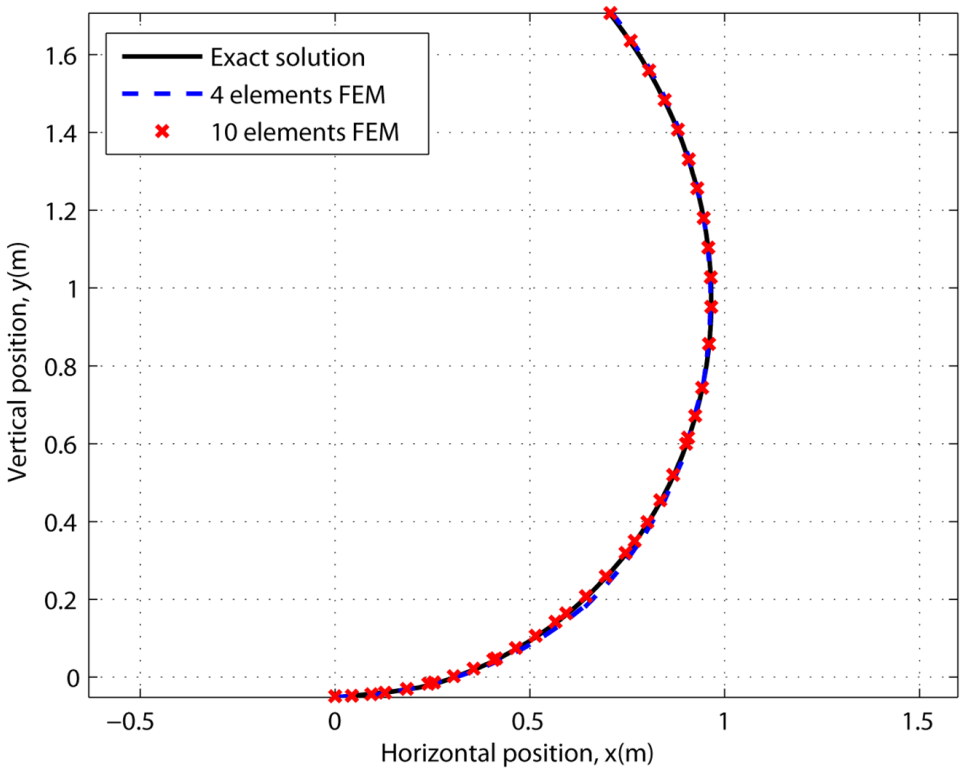

Figure 4.16. Analytical and Finite element solution for deformed weighted membrane with internal pressure of 344.7 N/m

The internal pressure is then reduced to 34.47 N/m which is equal to the membrane weight. The result of the FE analysis in comparison with analytical analysis is shown in Figure 4.17. Since the change in geometry before and after deformation is considerable, this process was broken to smaller steps, meaning the internal pressure was reduced gradually. The result of the case with 344.7 N/m internal pressure was used as the first step and it was reduced in four steps to 34.47 N/m.

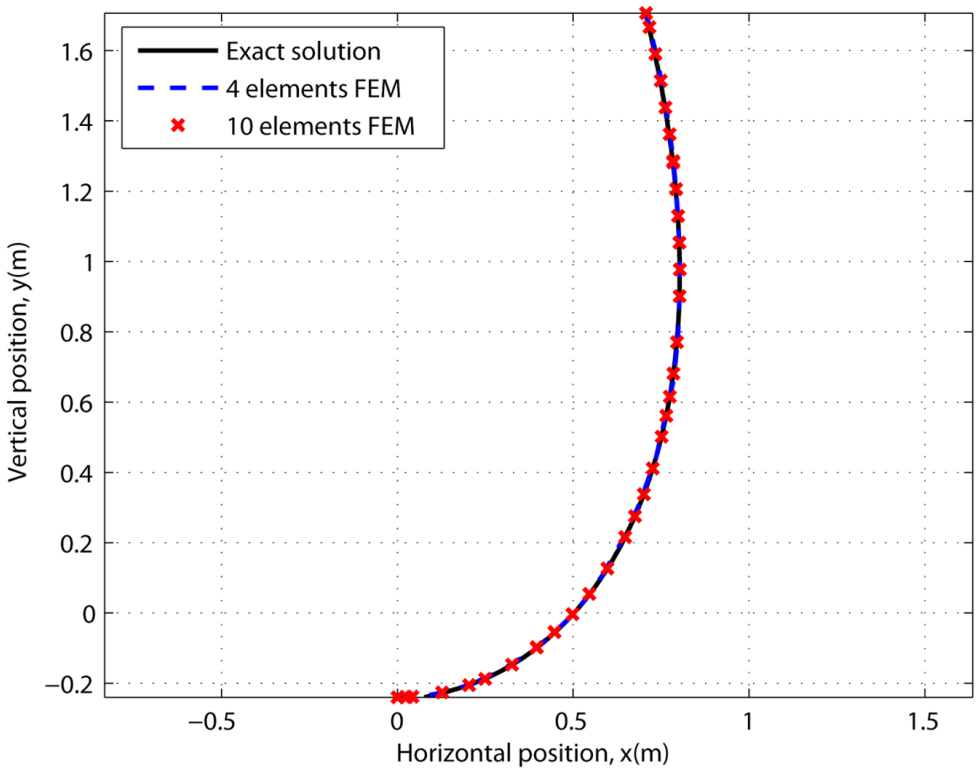

Figure 4.17. Analytical and Finite element solution for deformed weighted membrane with internal pressure equal to its weight

As the internal pressure decreases, the shapes of the elements get closer to a straight line and the assumption of constant radius is not accurate anymore. Therefore, there is a lowest limit for the internal pressure in any FE model with the constant radius assumption. Higher number of the elements results to shorter elements and therefore more straight elements. This means that for analysis with higher number of elements the lowest limit of internal pressure has a higher value. Figure 4.18 shows the four-element FE solution compared with analytical solution. Internal pressure is 21.37 N/m which is less than membrane weight.

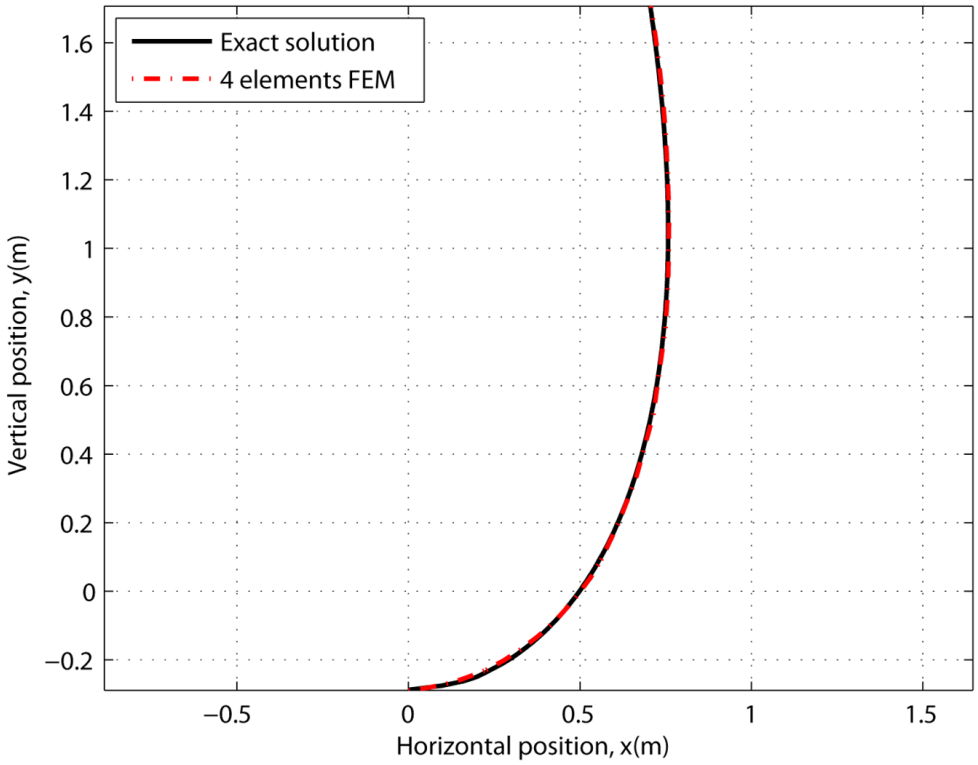

Figure 4.18. Analytical and Finite element solution for deformed weighted membrane with internal pressure of 21.37 N/m

Figure 4.19 shows the ten-element FE solution compared with analytical solution. Internal pressure is 31.03 N/m. This is the lowest limit for this analysis which is higher than the lowest limit for four element analysis. As it can be seen in deformed shape, the membrane is closer to a straight line in upper part of the membrane and it has more curvature in lower part of the membrane. This requires longer elements in lower curvature positions. Therefore, choosing elements with different lengths speeds up the convergence process. That is the reason of the specific element length selection in this problem.

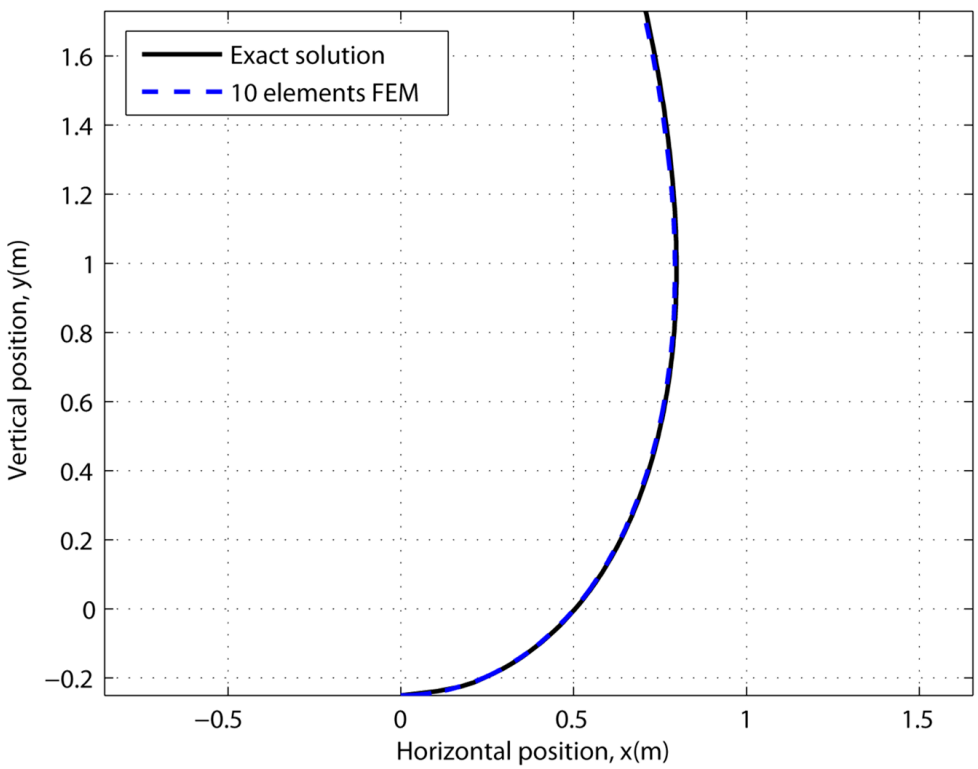

Figure 4.19. Analytical and Finite element solution for deformed weighted membrane with internal pressure of 31.03 N/m

4.11.3. A Membrane Under Internal Pressure and Shear loading

Consider now a membrane 2.310 m long with radius 0.9655 m. This membrane is symmetric with respect to the y axis, such that the origin of the coordinate system is set to the lowest point of the membrane. The shear loading is applied as horizontal distributed load in $-x$ direction. The boundary conditions are fixed value of position at the two top ends of the membrane given by (x = 0.8985 m, y = 0.6121 m) and (x = -0.8985 m, y = 0.6121 m).

Internal pressure is 6.895 kN/m and shear distributed load is 3.447 kN/m. First, two equal length elements are used to mesh the membrane. Then, the mesh is refined and four elements are used. Again the analysis is done based on the method and equations described in Sections 4.3 and 4.4. Figure 4.20 illustrates the deformed shape of the membrane under shear loading and internal pressure.

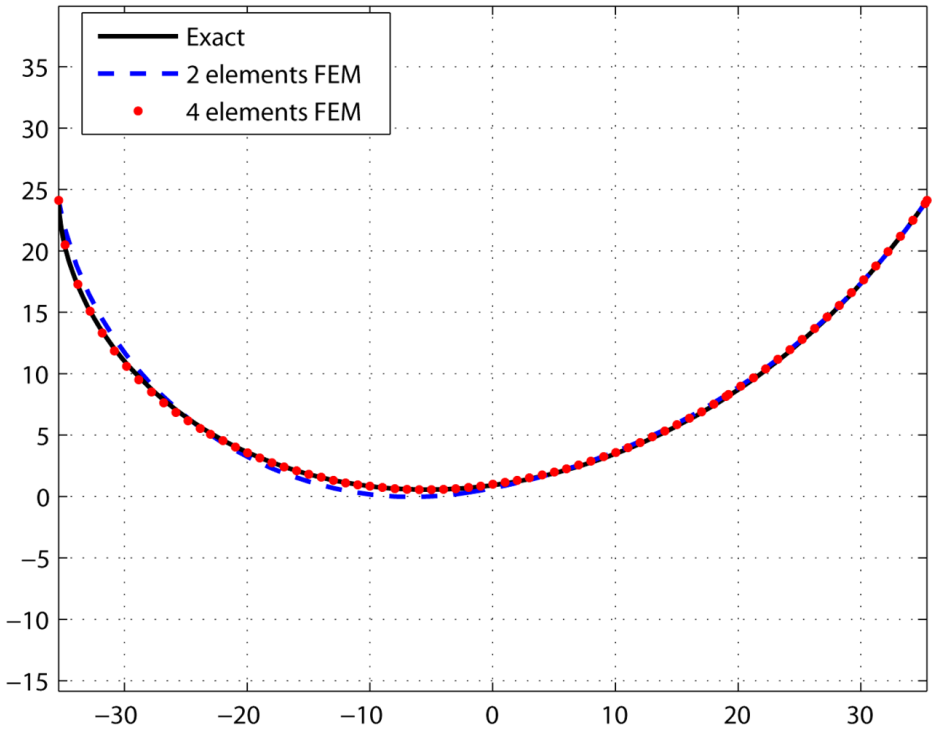

Figure 4.20. Analytical and Finite element solution for deformed membrane under shear loading and internal pressure

4.11.4. A Weighted Membrane Under Internal Pressure and Shear loading

Reconsider again the membrane described in Subsection 4.11.2. A weight equal to 34.47 N/m is also applied to the membrane. The internal pressure is distributed gradually. The membrane is modeled using two, four and six elements. In the six element model the internal pressure is reduced from 14.20 kN/m to 4.247 kN/m which is the lowest amount of internal pressure to which the presented FE solution can be applied. The reduction of internal pressure in this model was achieved in three steps. In the four element model the internal pressure is reduced from 9.439 kN/m to 4.123 kN/m which is the lowest amount of internal pressure to which the presented FE solution can be applied. The reduction of internal pressure in this model was achieved in three steps.

In the two element model, the internal pressure is reduced from 6.895 kN/m to 110.3 N/m in eight steps. Figure 4.21 shows the deformed profiles of the membrane modeled with two, four and six elements. In this Figure, the lowest limit of internal pressure for the six element model is used to derive the deformed profiles. Figure 4.22 compares the deformed profile of the membrane modeled with two elements in the lowest limit of internal pressure corresponding to the four element model (i.e. 4.123 kN/m) with the deformed profile of the same membrane in the lowest limit of internal pressure corresponding to the two element model (i.e. 110.3 N/m). Due to the lack of analytical methods considering shear and normal pressures for weighted membranes, these results are not compared with results of other methods.

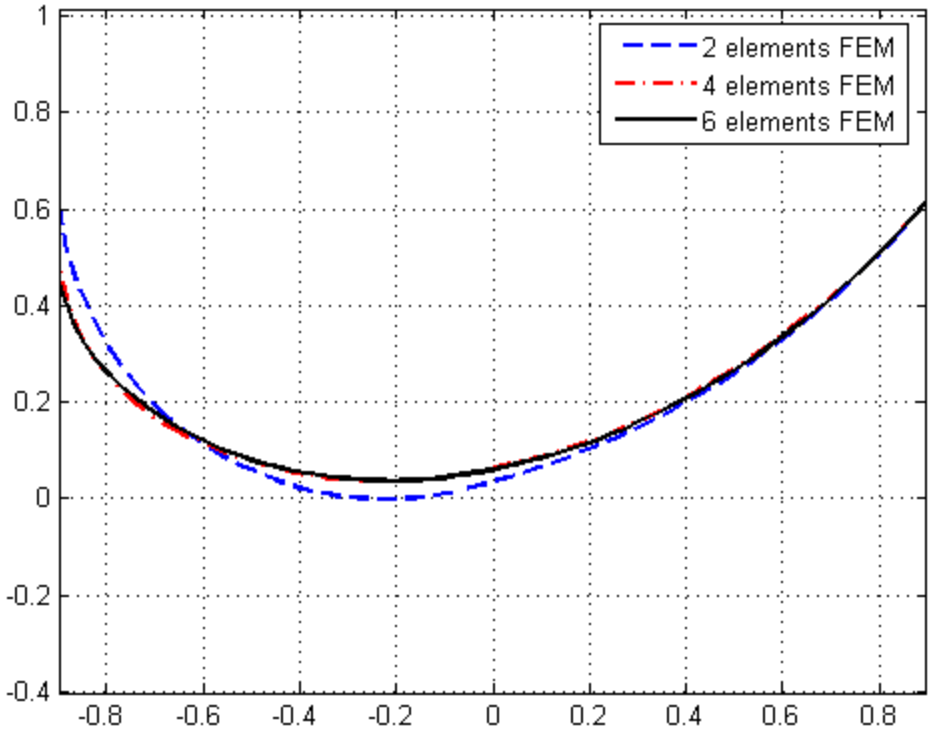

Figure 4.21. Deformed membrane with lowest limit of internal pressure modeled with six elements

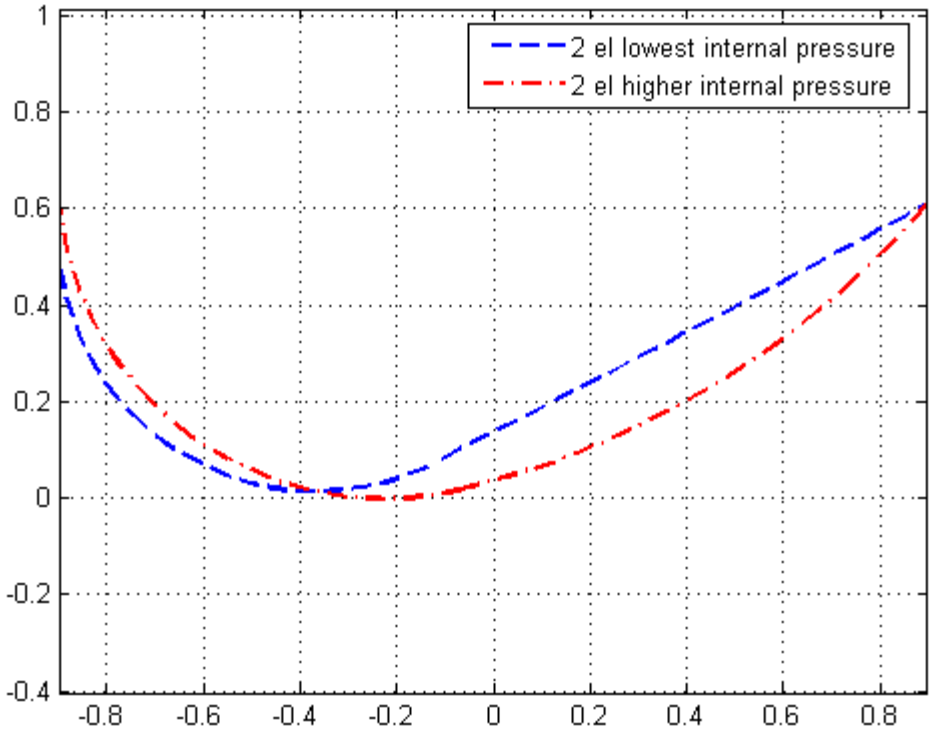

Figure 4.22. Deformed shape of the membrane in two different internal pressures

4.12. Conclusions

The developed FE formulation can be effectively used to model any loading conditions for the two-dimensional membranes where deformation in terms of displacements is desired. The developed results will contribute tremendously in modeling the response of the flexible seals of surface effect ships and inflatable pontoons, which is the main motivation, although it can also be applied to any membrane deformation problem in other fields than marine engineering. The FE applications are more general than the examples provided here; the approach can be used to model membranes subjected to general loading and various boundary conditions.

The FE solution is defined in terms of nodal displacements in the *x* and *y* directions. The stiffness influence coefficient method is used to find the stiffness matrix of the elements. The result from the developed FE solutions when compared with the result obtained from the analytical solution for the partially submerged membranes is found to be very accurate. In the example discussed in Section 4, the coverage rate is comparable to that of the analytical solution. This rate is a function of increments in the submerged depth or deformation in general. The process is very fast when the submerged depth increment is small. As the depth increment increases the convergence rate decreases. Therefore for large depth increments, the FE solution may need intermediate steps. This is similar to the behavior of load stepping increments when applied loading is prescribed in nonlinear FE simulations. The number of intermediate steps increases where the number of elements are higher, since elements are closer to a straight line and their chord length cannot be stretched more than their arc length.

In case of applied shear force, the existence of the internal pressure is essential to maintain equilibrium equations as shown in Figure 4.3 and Equations 4.16. The analysis does not converge when internal pressure is lower than a specific amount. This amount depends on the number of elements and it is lower when the number of elements is small.

One important assumption in deriving the presented FE method is that each element has a constant radius. When this radius increases and the elements get closer to a straight line, either because of the large radius of the membrane or high number of elements, the convergence rate decreases. Therefore, although increasing the number of elements

improves the results, which in some cases might be negligible depending on the problem, it reduces the convergence rate.

One of the significant advantages of the presented method is its accuracy when compared with the previously developed method for the cases where satisfaction of displacement boundary conditions is essential. This is very important due to the fact that displacement is usually prescribed in many engineering problems and the previous methods fail in imposing this condition.

4.13. References

[1] Ahmad, S., Irons, B.M. and Zienkiewicz, O.C. (1970), "Analysis of thick and thin shell structures by curved finite elements," International Journal of Numerical Methods in Engineering, 2, pp. 419-451.

[2] Hughes, T.J.R. and Liu, W.K. (1981), "Nonlinear finite element analysis of shells: Part II. Two-dimensional shells," Computer Methods in Applied Mechanics and Engineering, 27, pp. 167-181.

[3] Hughes, T.J.R. and Liu, W.K. (1981), "Nonlinear finite element analysis of shells: Part I. Three-dimensional shells," Computer Methods in Applied Mechanics and Engineering, 26, pp. 331-362.

[4] Hughes, T.J.R., Liu, W.K. and Levit, I. (1981), "Nonlinear dynamic finite element analysis of shells," W. Wunderlich, E. Stein and K.J. Bathe eds., Nonlinear Finite Element Analysis in Structural Mechanics, pp. 151-161., Springer-Verlag, Berlin.

[5] Hughes, T.J.R. and Carnoy, E. (1983), "Nonlinear Finite Element Shell Formulation Accounting For Large Membrane Strains," Computer Methods in Applied Mechanics and Engineering, 39, pp. 69-82.

[6] Bushnell, D. (1984), "Computerized analysis of shells-Governing equations," Computers and Structures, 18(3), pp. 471-536.

[7] Oden, J.T. and Sato, T. (1967), "Finite strains and displacements of elastic membranes by the finite element method," International Journal of Solids and Structures, 3, pp. 471-488.

[8] Rivlin, R. S. (1960), "Some Topics in Finite Elasticity," Proceedings of the First Symposium on Naval Structural Mechanics, pp. 169-198., Pergamon Press, London.

[9] Gruttmann, F. and Taylor, R.L. (1992), "Theory and finite element formulation of rubberlike membrane shells using principal stretches," International Journal of Numerical Methods in Engineering, 35, pp. 1111-1126.

[10] Holzapfel, G.A., Eberlein, R., Wriggers, P. and Weizsacker, H.W. (1996), "Large strain analysis of soft biological membranes: Formulation and finite element analysis," Computer Methods in Applied Mechanics and Engineering, 132, pp. 45-61.

[11] Demiroz, A (2005), "Prediction of large deformation behavior of fabric using galerkin finite element method," Textile Research Journal, 75(9), pp. 662-669.

[12] Gallagher, R.H. (1975), Finite Element Analysis Fundamental, Prentice-Hall Inc, New Jersey, 126-132, Chap. 5.5

[13] Ibrahimbegovic , A., Taylor, R.L. and Wilson, E.L. (1990), "A robust quadrilateral membrane finite element with drilling degrees of freedom," International Journal of Numerical Methods in Engineering, 30, pp. 445-457.

[14] Iura, M. and Atluri, S.N. (1992), "Formulation of a membrane finite element with drilling degrees of freedom," Computational Mechanics, 9, pp. 417-428.

[15] Yu, B. and Karr D.G., "Analytical Solutions of 2D Membrane Shapes within Different Inflation and Deflation Regimes", The Quarterly Journal of Mechanics and Applied Mathematics,(In preparation).

Chapter 5

Isogeometric Approach for Membrane Structural Analysis

In this Chapter, a numerical method is developed based on the Isogeometric analysis to investigate the deformation of two-dimensional membranes under different loading and boundary conditions. To adequately represent complex geometries and shapes, each element is selected as a quadratic Bezier curve. Therefore, each element will have three control points and two degrees of freedom (DOFs) per control point expressed in terms of displacement. In addition to inextensible membranes, linear elastic membranes with uniaxial extension and membranes with bending stiffness and small strains are also considered. Due to the fact that the problem at hand is a non-conservative system, the principle of virtual work is used to calculate the total virtual work including the strain energy in case of extensible membranes, as well as the constraint energy.

5.1. Introduction

Isogeometric Analysis [1] is a computational mechanics method that integrates Computer Aided Design (CAD) and Finite Element (FE) analysis. The need for Isogeometric Analysis is rooted in the fact that an FE model is only an approximation of the geometry, and that data must often be translated from one system (i.e. CAD modeling) to the other (i.e. mesh generation). In many cases, the results of the analysis highly depend on the exact geometry and the main goal of the Isogeometric Analysis is to achieve geometric accuracy and systematic treatment by integrating CAD and FE analysis. Another advantage of Isogeometric Analysis is that it reduces the overall computational cost. In traditional practice, most of the analysis time is spent on creating CAD models that are suitable for FE analysis and remeshing. Another reason to develop Isogeometric methods is the desire to reduce the analysis time by integrating CAD and FE method and eliminating the need to communicate between them. This concept is shown in Figure 5.1.

In this research, analysis is based on “Bezier Curves”, which is one of the earliest parametric curve approximation methods used in CAD [2]. A Bezier curve is a polynomial curve. The terms of the polynomial are weighted points of a polyline that fits the curve. The Bernstein polynomial is used by Bezier to describe weight values of the ploy line. This polynomial is a function of the number of points as well as a dimensionless parameter which is usually the location of the multiplier point with respect to the first and last points of the curve.

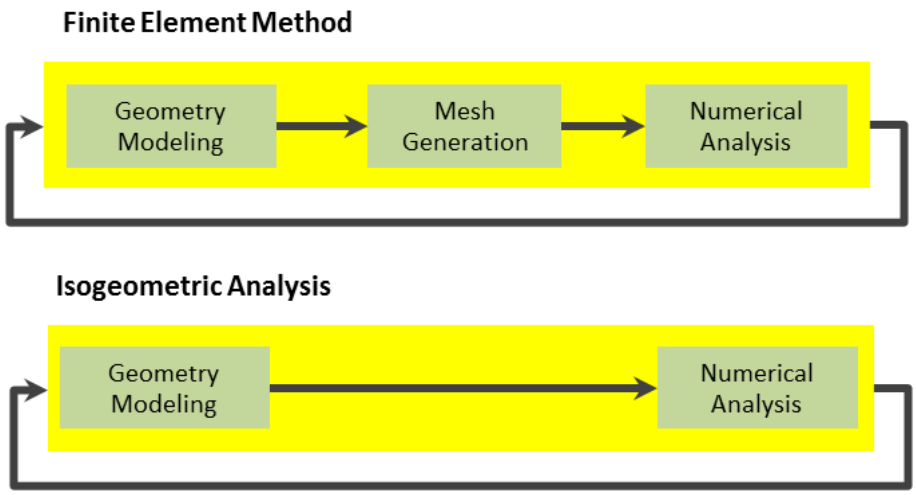

Figure 5.1. The schematic comparison of FE method and Isogeometric Analysis

Verron and Marckmann [3] developed a model based on B-spline curves. This method was established to study the free inflation of axisymmetric hyper-elastic membranes based on Mooney-Rivlin solid model. The non-linear system of equations was iteratively solved. Based on their method the instability and complex equilibrium path in the problem of the inflation of two connected rubber balloons was studied [4].

Due to its ability in modeling complex geometries, Isogeometric Analysis can benefit Fluid Structure Interaction (FSI) problems especially when there are large deformations in the structure. Accordingly, there are a few FSI problems analyzed by Isogeometric Analysis such as blood flow in veins, ventricular assist devices, and the arterial wall which was treated as a hyper-elastic solid [5, 6].

5.2. Bezier Description for an Element with Six Degrees of Freedom

The coordinates of any point on a Bezier curve can be expressed in terms of the coordinates of its controlling points as well as its position with respect to the two end points. Knowing the geometric description of a Bezier curve, the curve length can be conveniently calculated as a function of its control points' coordinates.

5.2.1. Geometric Description

To reduce computational complexity and easily control the geometry, a Bezier curve of second degree is selected. It should be noted that a quadratic curve does not have an inflection point and therefore, when the problem involves an inflection point, this point must be located where elements are connected. Still, at inflection point, unless the curvature is zero, there will be discontinuity between elements.

A quadratic Bezier curve is the path defined by the following function,

$$\vec{C}(u) = (1-u)^2 \vec{P}_0 + 2u(1-u)\vec{P}_1 + u^2 \vec{P}_2 \qquad (5.1)$$

, where $P_0(X_0, Y_0), P_1(X_1, Y_1)$ and $P_2(X_2, Y_2)$ are control points and $u \in [0,1]$. The path described by Equation (5.1) is shown in Figure 5.2. Therefore the (x, y) coordinates of any point on the path can be defined by,

$$\begin{cases} X(u) = (1-u)^2 X_0 + 2u(1-u)X_1 + u^2 X_2 \\ Y(u) = (1-u)^2 Y_0 + 2u(1-u)Y_1 + u^2 Y_2 \end{cases} \tag{5.2}$$

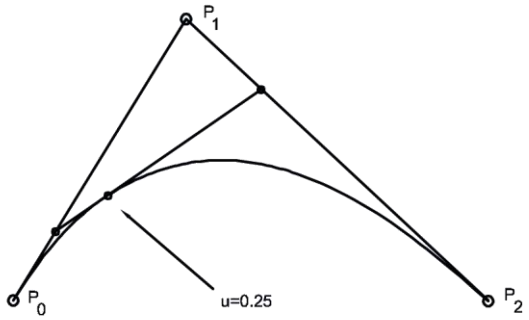

Figure 5.2. A quadratic Bezier curve and the point corresponding to u=0.25

5.2.2. Length of an Element

The rate of change of the curve length with respect to u can be calculated from,

$$(\frac{ds}{du})^2 = (\frac{dX}{du})^2 + (\frac{dY}{du})^2 \tag{5.3}$$

Based on Equation (5.2),

$$\begin{cases} \frac{dX}{du} = 2(X_1 - X_0) + 2u(X_0 - 2X_1 + X_2) \\ \frac{dY}{du} = 2(Y_1 - Y_0) + 2u(Y_0 - 2Y_1 + Y_2) \end{cases} \tag{5.4}$$

Now let,

$$\begin{cases} a_x \equiv X_1 - X_0 \\ a_y \equiv Y_1 - Y_0 \end{cases} \tag{5.5}$$

and,

$$\begin{cases} b_x \equiv X_0 - 2X_1 + X_2 \\ b_y \equiv Y_0 - 2Y_1 + Y \end{cases} \tag{5.6}$$

Therefore,

$$\begin{cases} \dfrac{dX}{du} = 2(a_x + b_x u) \\ \dfrac{dY}{du} = 2(a_y + b_y u) \end{cases} \tag{5.7}$$

and,

$$\begin{cases} ds^2 = 4[(a_x + ub_x)^2 + (a_y + ub_y)^2]du^2 \\ ds^2 = 4[{a_x}^2 + {a_y}^2 + 2u(a_x b_x + a_y b_y) + u^2({b_x}^2 + {b_y}^2)]du^2 \end{cases} \tag{5.8}$$

Again, let,

$$\begin{cases} a \equiv a_x{}^2 + a_y{}^2 \\ b \equiv 2(a_x b_x + a_y b_y) \\ c \equiv b_x{}^2 + b_y{}^2 \\ d \equiv a + b + c \\ f \equiv \dfrac{4ac - b^2}{4} \end{cases} \tag{5.9}$$

From Equations (5.7) and (5.8),

$$ds^2 = 4(a + bu + uc^2)du^2 \tag{5.10}$$

$$ds = 2\sqrt{a + bu + c^2 u}\,du \tag{5.11}$$

Therefore, the length of an element can be calculated by integrating *ds*. After simplifying and considering that at u=0, length (L) is zero,

$$L = \int_0^L ds = 2\int_0^1 \sqrt{a + bu + c^2 u}\,du = \frac{(2c + b)\sqrt{d} - b\sqrt{a}}{2c} + \frac{f}{c^{\frac{3}{2}}} \ln\left(\frac{2\sqrt{cd} + 2c + b}{2\sqrt{ac} + b}\right) \tag{5.12}$$

5.3. Stiffness Matrix Calculations

5.3.1. The Principle of Virtual Work

It should be considered that pressure is a follower force. In other words, it is not a conservative force and thus, the Principle of Minimum Total Potential Energy cannot be applied to it. On the other hand, the Principle of Virtual Work can be applied to conservative and non-conservative forces and therefore, this principle is used to derive the stiffness matrix [7].

According to this Principle, the sum of the virtual external work done by real external forces acting through virtual displacements and the virtual internal work done by the real internal forces acting through the virtual displacements is equal to zero. When external work is denoted as W_e and internal work is denoted as W_i, this principle can be expressed as,

$$\delta W_e + \delta W_i = 0 \tag{5.13}$$

The internal virtual work is stored in the body in the form of virtual strain energy, denoted by U, in other words,

$$\delta W_i = -\delta U \tag{5.14}$$

Combining Equations (5.13) and (5.14) will result in the new form for the principle of virtual work,

$$\delta W_e - \delta U = 0 \tag{5.15}$$

5.3.2. General Solution Procedure

In general, total work includes work done by external forces, internal work which is equal to strain energy, and work done by constraints which have the form of energy, denoted by T .The latter will be explained in more details in Section 5.4.

$$W = W_e + U + T \tag{5.16}$$

In this research, the external work done by normal and shear pressures as well as the distributed weight of the membrane is considered,

$$W_e = W_q + W_s + W_w \tag{5.17}$$

To find the deformed shape of the membrane, the force vector and stiffness matrix corresponding to all DOFs should be calculated. These will be used to calculate the displacement. To find the deformed geometry, the Newton-Raphson iterative method is employed to solve the following equation to obtain increments in displacement where

N is the number of DOFs, f_i is a generic element of the force vector and ξ_j is a generic DOF,

$$\sum_{1}^{N} \frac{\partial f_i}{\partial \xi_j} \Delta \xi_j = -f_i \tag{5.18}$$

In order to apply this method, the force vector and stiffness matrix are calculated for initial geometry and applied forces. Comparing Equation (5.18) with the general formula,

$$K \Delta \vec{\xi} = -\vec{f} \tag{5.19}$$

the stiffness matrix can be calculated using,

$$K_{ij} = \frac{\partial f_i}{\partial \xi_j} \tag{5.20}$$

To calculate the force vector, the virtual work is defined in terms of increments in DOFs, as follows,

$$\delta W = \Delta \xi_j \frac{\partial W}{\partial \xi_j} \tag{5.21}$$

Comparing Equation (5.21) with the definition of work we have,

$$\delta W = \Delta\bar{\xi}\ \bar{f} \tag{5.22}$$

After calculating the virtual work based on the known applied loads, strain energies and constraint, the elements of the force vector corresponding to each DOF can be easily determined to be,

$$f_i = \frac{\partial W}{\partial \xi_i} \tag{5.23}$$

After the increments in DOFs are found using Equation (5.18), the values of DOFs are updated and Equation (5.18) is used again to find the new increments and this process continues until convergence.

5.4. Inextensible Membrane

No strain is generated in inextensible membranes. Therefore the virtual strain energy and virtual internal work are zero. In addition, if a membrane is inextensible, the length of each element at every step of the iteration process should remain constant. This can be introduced as a constraint and included in the process, using the "Lagrange Multipliers". The term that is added to the overall Virtual Work to ensure the constant length is $T = \lambda(L - L_0)$ in which λ is the Lagrange Multiplier, L is the length of the element, and L_0 is the initial length of the element. This term has been called "constraint energy" [8]. Then the Principle of Virtual Work can then be expressed as,

$$\delta W_e + \delta T = 0 \tag{5.24}$$

This constraint adds another degree of freedom (DOF) to the problem. Therefore, for an element with six DOFs and length constraint, Equation (5.24) can be rewritten as,

$$\sum_{1}^{7} \delta\xi_i \left(\frac{\partial W_e}{\partial \xi_i} + \frac{\partial T}{\partial \xi_i}\right) = 0 \tag{5.25}$$

or,

$$\begin{cases} \dfrac{\partial W_e}{\partial \xi_i} + \dfrac{\partial T}{\partial \xi_i} = 0 \\ i = 1,2,...,7 \end{cases} \tag{5.26}$$

where ξ_i is a generic or generalized DOF.

$$\begin{cases} \xi_1 = X_0 \\ \xi_2 = Y_0 \\ \xi_3 = X_1 \\ \xi_4 = Y_1 \\ \xi_5 = X_2 \\ \xi_6 = Y_2 \\ \xi_7 = \lambda \end{cases} \tag{5.27}$$

5.5. Contribution of Normal Pressure to External Work

Figure 5.3 shows a membrane under internal pressure q. As shown in this Figure, the components of the total applied internal pressure to a portion of the membrane with length *ds*, are $q\,dy$ and $q\,dx$, along x and y directions, respectively.

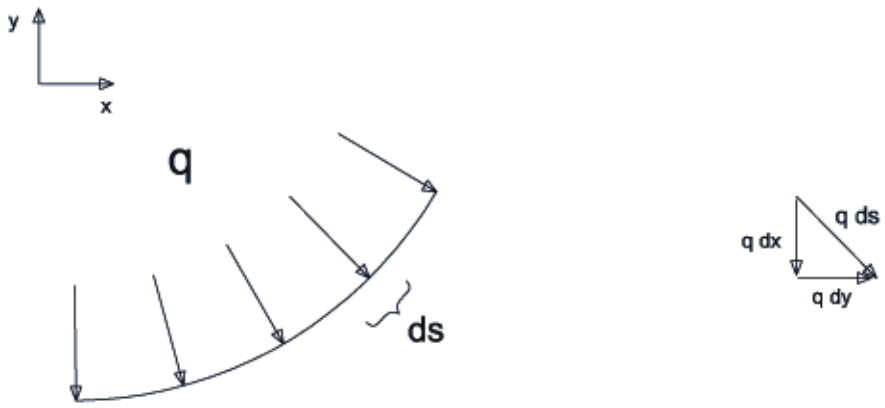

Figure 5.3. The components of the applied internal pressure to a membrane

Therefore, the virtual work done by *q* is the sum of force components multiplied by the virtual displacement in the same direction as the applied force,

$$d(\delta W_q) = q\,dy\,\delta x - q\,dx\,\delta y \qquad (5.28)$$

where δx and δy can be calculated as follows using Equation (5.2),

$$\begin{cases} \delta x = (1-u)^2(\delta x_0) + 2u(1-u)(\delta x_1) + u^2(\delta x_2) \\ \delta y = (1-u)^2(\delta y_0) + 2u(1-u)(\delta y_1) + u^2(\delta y_2) \end{cases} \tag{5.29}$$

By integrating Equation (5.28) along the length of the membrane, the virtual work of the internal pressure can be calculated,

$$\delta W_q = \int d(\delta W_q) \tag{5.30}$$

After a few steps of integration and simplification, the external force of normal pressure is found to be:

$$\begin{aligned} \delta W_q = q[&\delta x_0(-\frac{1}{2}y_0 + \frac{1}{3}y_1 + \frac{1}{6}y_2) \\ &+ \delta x_1(-\frac{1}{3}y_0 + 0y_1 + \frac{1}{3}y_2) \\ &+ \delta x_2(-\frac{1}{6}y_0 - \frac{1}{3}y_1 + \frac{1}{2}y_2) \\ &+ \delta y_0(\frac{1}{2}x_0 - \frac{1}{3}x_1 - \frac{1}{6}x_2) \\ &+ \delta y_1(\frac{1}{3}x_0 + 0x_1 - \frac{1}{3}x_2) \\ &+ \delta y_2(\frac{1}{6}x_0 + \frac{1}{3}x_1 - \frac{1}{2}x_2)] \end{aligned} \tag{5.31}$$

5.6. Contribution of Axial Extension to Internal Work

For a membrane that is extensible, the contribution of the strain energy should be considered in calculating the force vector and stiffness matrix. In this case, the total work W includes the internal work which is equal to the strain energy generated by the extension of the membrane, δU . Therefore from Equation (5.16),

$$\delta W = \delta W_e + \delta U + \delta T \tag{5.32}$$

The strain energy generated by axial extension is calculated using,

$$U_A = \frac{1}{2}\iiint \sigma \varepsilon dV \tag{5.33}$$

For a linear elastic material, uniaxial stress is,

$$\sigma = E\varepsilon \tag{5.34}$$

Substituting equation (5.34) into equation (5.33),

$$U = \frac{1}{2}\iiint E\varepsilon^2 dV \tag{5.35}$$

with constant modulus of elasticity and cross section,

$$U_A = \frac{1}{2} EA \int_0^{L_0} \varepsilon^2 dz \tag{5.36}$$

If the elongation with respect to initial length of the element is small, the Cauchy strain can be defined as follows,

$$\varepsilon_{Axial} \cong \frac{\Delta L}{L} \tag{5.37}$$

By substituting this into Equation (5.36) and integrating,

$$U_A = \frac{1}{2} EA \frac{(\Delta L)^2}{L_0} \tag{5.38}$$

To calculate the force vector and stiffness matrix, derivative of strain energy with respect to DOFs is calculated as follows,

$$\frac{\partial U_A}{\partial \xi_i} = EA \frac{\Delta L}{L_0} \left(\frac{\partial L}{\partial \xi_i} \right) \tag{5.39}$$

5.7. Contribution of Uniformly Distributed Weight to External Work

Figure 5.4 shows a membrane with weight intensity w, which has the unit of force per unit arc length.

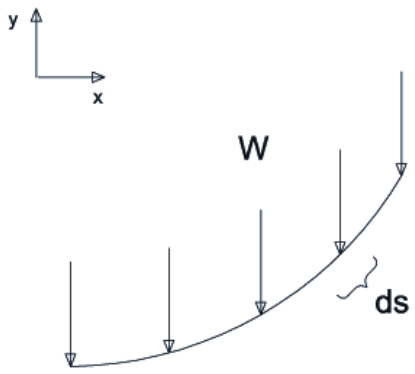

Figure 5.4. A membrane under uniformly distributed weight

Considering that weight has no components along x direction, the virtual work done by uniformly distributed weight on a portion of the membrane with length *ds* is,

$$d(\delta W_w) = -w\, ds\, \delta y \tag{5.40}$$

Substituting from Equations (5.11) and (5.29) and integrating, the work done by uniformly distributed load is found to be,

$$\delta W_w = -w[\delta y_0 \frac{1}{64c^3}(\frac{2}{3}(\sqrt{d}\,(2bc(6c-13a)+8c^2(2c-13a)+15b^3+38b^2c) - \sqrt{a}\,(4bc(12c-13a)-128c^2a+15b^3+48b^2c)) + \frac{1}{\sqrt{c}}\ln(\frac{2\sqrt{cd}+b+2c}{2\sqrt{ca}+b})(8b^2c(3a-2c)+64abc^2 - 16ac^2(a-4c)-5b^4-16b^3c) + \delta y_1 \frac{1}{32c^3}(\frac{2}{3}(\sqrt{d}\,(-4bc(2c+13a)-8c^2(2c+5a)+15b^3+14b^2c) - \sqrt{a}\,(-52abc-64c^2a+15b^3+24b^2c)) + \frac{1}{\sqrt{c}}\ln(\frac{2\sqrt{cd}+b+2c}{2\sqrt{ca}+b})(-16a^2c^2+32abc^2 + 24ab^2c-5b^4-8b^3c) + \delta y_2 \frac{1}{192c^3}(2(\sqrt{d}\,(4bc(2c-13a)+24c^2(a+2c)+15b^3-10b^2c) - \sqrt{a}\,(-52abc+15b^3)) + \frac{3}{\sqrt{c}}\ln(\frac{2\sqrt{cd}+b+2c}{2\sqrt{ca}+b})(-16a^2c^2+24ab^2c-5b^4)] \quad (5.41)$$

5.8. Contribution from Shear Loading

Figure 5.5 shows a membrane under shear load. As shown in this Figure, the shear load applied to an infinitesimal portion of the membrane with length ds has a component with the magnitude equal to $q_s dx$ along x direction and a component equal to $q_s dy$ along y direction.

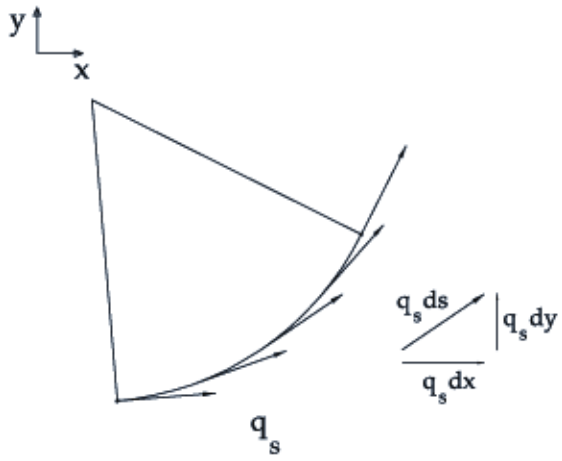

Figure 5.5. A membrane under shear load

The work done by the shear load on the infinitesimal portion of the membrane (*ds*) is equal to,

$$d(\delta W_{q_s}) = q_s dx\, \delta x + q_s dy\, \delta y \tag{5.42}$$

Again, substituting from Equations (5.11) and (5.29) and integrating,

$$\begin{aligned}\delta W_{q_s} = q_s[&\delta x_0(-\frac{1}{2}x_0 + \frac{1}{3}x_1 + \frac{1}{6}x_2)\\ &+ \delta x_1(-\frac{1}{3}x_0 + 0x_1 + \frac{1}{3}x_2)\\ &+ \delta x_2(-\frac{1}{6}x_0 - \frac{1}{3}x_1 + \frac{1}{2}x_2)\\ &+ \delta y_0(-\frac{1}{2}y_0 + \frac{1}{3}y_1 + \frac{1}{6}y_2)\\ &+ \delta y_1(-\frac{1}{3}y_0 + 0y_1 + \frac{1}{3}y_2)\\ &+ \delta y_2(-\frac{1}{6}y_0 - \frac{1}{3}y_1 + \frac{1}{2}y_2)]\end{aligned} \tag{5.43}$$

5.9. Contribution of Bending Strain Energy to Internal Work

Figure 5.6 shows an infinitesimal portion of a membrane. The radius of the membrane profile is denoted by ρ.

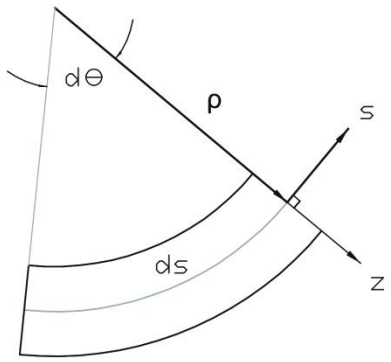

Figure 5.6. An infinitesimal portion of a membrane under shear load

If the midplane is inextensible, the length is related to the radius by,

$$ds = \rho \, d\theta \tag{5.44}$$

For any other plane,

$$ds^* = (\rho + z) \, d\theta \tag{5.45}$$

For small strains, Green strain is defined as,

$$\varepsilon = \frac{ds^* - ds}{ds} \tag{5.46}$$

Substituting Equations (5.44) and (5.45) into Equation (5.46),

$$\varepsilon = \frac{z}{\rho} \tag{5.47}$$

To calculate the strain energy, Equation (5.47) is substituted in Equation (5.35). Denoting the length of the membrane perpendicular to the profile shown in Figure 5.5 by b, and thickness of the membrane with t,

$$U_b = \frac{Eb}{2}\int[\int_{-\frac{t}{2}}^{\frac{t}{2}} \varepsilon^2 dz]ds = \frac{Eb}{2}\int[\int_{-\frac{t}{2}}^{\frac{t}{2}} (\frac{z}{\rho})^2 dz]ds \tag{5.48}$$

By integration,

$$U_b = \frac{1}{2}\frac{Ebt^3}{12}\int \frac{1}{\rho^2} ds \tag{5.49}$$

The moment of inertia for a membrane with the geometry depicted in Figure 5.5 is,

$$I = \frac{bt^3}{12} \tag{5.50}$$

Substituting Equation (5.50) into Equation (5.49),

$$U_b = \frac{1}{2} EI \int \frac{1}{\rho^2} ds \tag{5.51}$$

Considering the fact that curvature is the inverse of radius,

$$\kappa = \frac{1}{\rho} \tag{5.52}$$

Equation (5.51) can be rewritten as,

$$U_b = \frac{1}{2} EI \int \kappa^2 \, ds \tag{5.53}$$

After substituting equation (5.44) and integrating,

$$U_b = \frac{EI}{24} [\frac{e}{d^{\frac{3}{2}}} - \frac{b}{a^{\frac{3}{2}}} + \frac{2c}{f} (\frac{e}{d^{\frac{1}{2}}} - \frac{b}{a^{\frac{1}{2}}})] \tag{5.54}$$

5.9.1. Curvature in Terms of Degrees of Freedom

For a two-dimensional curve with Cartesian coordinates (x,y), the curvature is,

$$\kappa = \frac{|\dot{x}\ddot{y} - \dot{y}\ddot{x}|}{(\dot{x}^2 + \dot{y}^2)^{\frac{3}{2}}} \tag{5.55}$$

, where $\dot{x} = \frac{dX}{du}$ and $\dot{y} = \frac{dY}{du}$. Differentiating $\dot{x}$ and $\dot{y}$ with respect to u using Equation (5.7),

$$\begin{cases} \ddot{x} = 2b_x \\ \ddot{y} = 2b_y \end{cases} \tag{5.56}$$

By substituting Equations (5.7) and (5.56) into Equation (5.55),

$$\kappa = \frac{1}{2} \frac{\left| a_x b_y - a_y b_x \right|}{(a + bu + cu^2)^{\frac{3}{2}}} \tag{5.57}$$

From Equation (5.9) by substituting *a*, *b*, and *c* into *f*,

$$f = \frac{4ac - b^2}{4} = (a_x b_y - b_x a_y)^2 \tag{5.58}$$

Substituting Equation (5.58) into Equation (5.57) simplifies the equation of curvature,

$$\kappa = \frac{1}{2} \frac{\sqrt{f}}{(a + bu + cu^2)^{\frac{3}{2}}} \tag{5.59}$$

5.10. Example Analyses and Results

5.10.1. A Two-Element Model with Variable Pressure

Consider the profile of a circular membrane. The length of the membrane is 3.141 m and it is positioned symmetrically with respect to the vertical radius (*y* axis). The undeformed shape is such that the inscribed angle of the membrane is $\pi/2$. The radius of undeformed membrane is *R*=1 m and the internal gauge pressure is 6.895 kN/m. Two elements are used to mesh the membrane, each 0.393 m long. Due to symmetry about the *y*-axis, only the right-hand half of the system is modeled. The origin of the coordinate system is set to be the lowest point of the undeformed membrane. For this example, the boundary conditions are $x = 0$ m at $s = 0$ m, and the fixed position at the top end of the membrane as given by ($x = 1$ m, $y = 1$ m). The internal pressure of the second (rightmost) element is kept constant (6.895 kN/m) and the internal pressure of the first (leftmost) element was reduced in several steps from 6.895 kN/m to -6.895 kN/m. The result of the deformed geometry is shown in Figure 5.6. In each step, the virtual work of the internal pressure is calculated using Equation (5.31). The geometry of this model is shown in Figure 5.7.

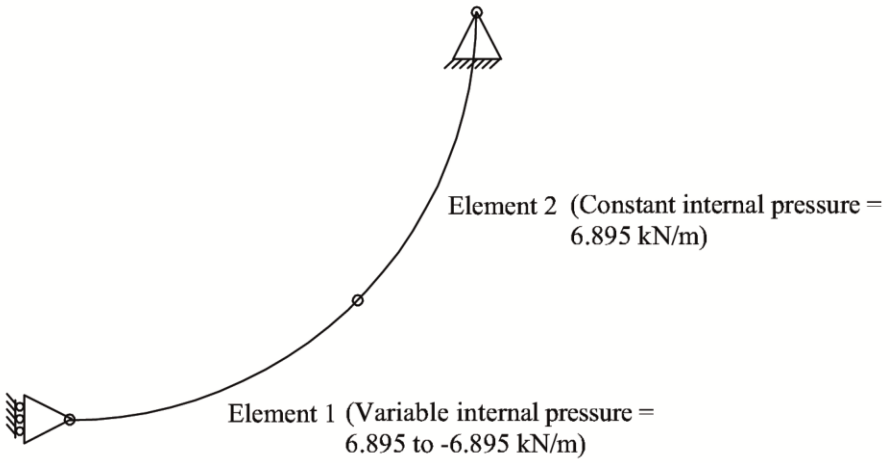

Figure 5.7. The geometry of the model investigated in Subsection 5.10.1 in undeformed geometry

There are a few constraints that are taken into consideration. The length of each element is fixed by applying the Lagrange Multiplier method. Another constraint is the C1 continuity of the two elements where they meet, which can be considered again by applying the Lagrange Multiplier method. In addition, the slope at x=0 m should be equal to zero due to symmetry.

Since the control point at which the two elements are connected is a common control point, the contributing terms from both elements is considered at that point. The stiffness matrix and forcing vector for DOFs including the Lagrange multipliers are calculated using Equations (5.20) and (5.23), respectively. The result of the deformed geometry is shown in Figure 5.8.

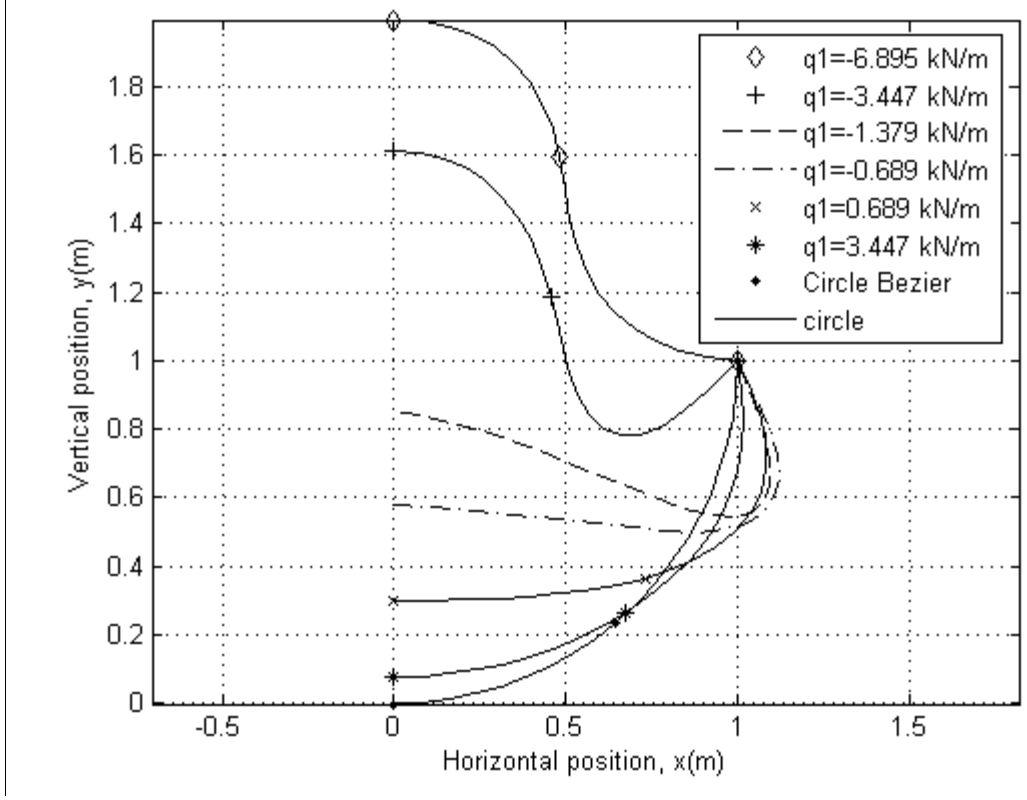

Figure 5.8. A membrane under variable pressure

It is worth mentioning that when no pressure is applied on the left element, the membrane becomes a completely straight horizontal line. At this point the analysis experiences a discontinuity due to the fact that the position of the middle control point in not unique for this case. This matter will be discussed in more detail in Chapter 6.

5.10.2. A Partially Submerged Membrane

Consider a circular membrane with a radius of undeformed geometry equal to R=1 m. The length of the membrane is 4.712 m and similar to the example presented in Subsection 4.11.1, it is positioned symmetrically with respect to the y-axis. The

undeformed shape is such that the inscribed angle of the membrane is $3\pi/2$. Also, the internal gauge pressure is 10.135 kN/m. Due to symmetry about the *y*-axis, only the right-hand half of the system is modeled. First three elements were used to conduct the analysis, each 0.7854 m long. Then the number of elements were increaded to five 0.4712 m long elements. The origin of the coordinate system is set to the lowest point of the undeformed membrane. Similar to previous case, the boundary conditions are $x = 0$ m at $s = 0$ m, and a fixed position at the top end of the membrane given by ($x = 0.707$ m, $y = 1.707$ m). Suppose that this membrane is submerged in water with underwater depth equal to $0.5R = 0.5\,\text{m}$. Similar to the problem discussed is Subsection 5.10.1, constant length, C1 continuity and symmetry at $x = 0$ m are enforced.

The results of the analysis with three- and five- element models are shown in Figure 5.9 and compared to the analytical solution. This Figure shows a very good agreement between these two methods. The difference in the vertical position of the lowest point of the membrane based on the Bezier curve analysis with three elements (dashed curve) in comparison with analytical solution is 5.6 cm which is 5.6% of the initial radius of the membrane. It should be noted that this is the point where the maximum deviation from the analytical model occurs. For the four-element model, this difference is about 2% of the initial radius and for the five-element model (dotted curve), it is about 1.1% of the initial radius. Recalling from Chapter 4, these differences in the results of FE analysis were 3.1% and 1.3% for a four-element and six-element model respectively. This shows that the Bezier curve method results in noticeable improvements in the displacement analysis.

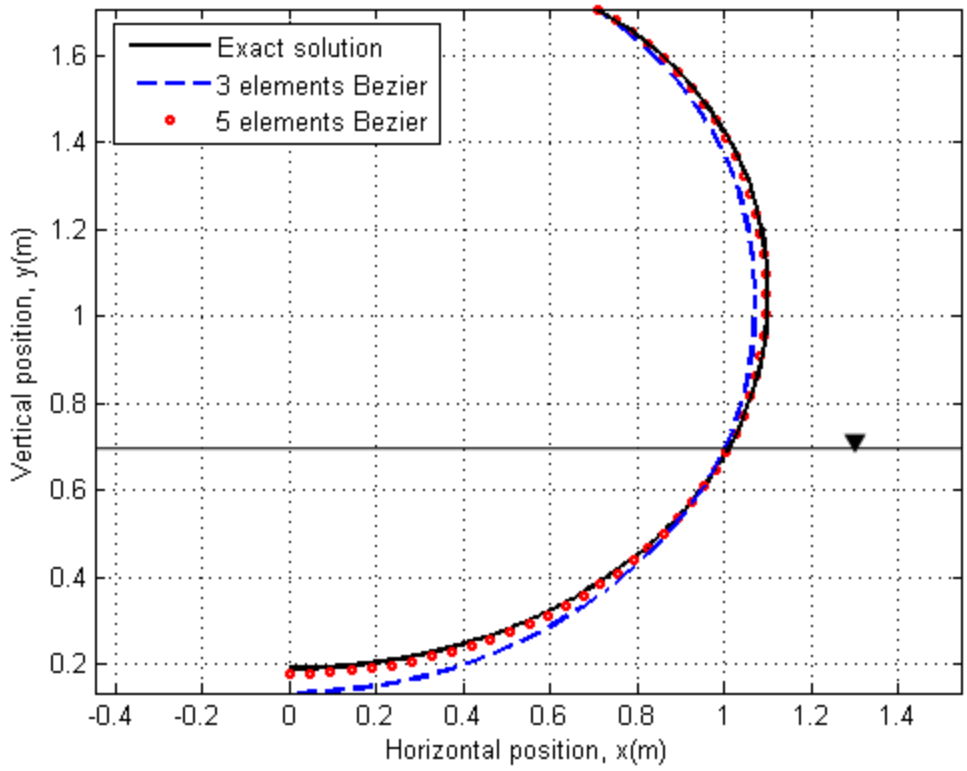

Figure 5.9. Deformed membrane under hydrostatic pressure modeled by 3 and 5 elements

5.10.3. A Weighted Membrane under Internal Pressure

In this Subsection, the same problem studied in Subsection 3.11.2 is considered. In summary, a distributed weight load of 34.474N/m is added to the same membrane described in Subsection 5.11.2. The width of the element is considered to be 1 m. Initially, the internal pressure is set at 344.736 N/m. The membrane is analyzed with one-, three-, and five- element models. In case of more than one element, elements of same length are used.

In calculating the stiffness matrix and force vector, the contribution by the weight of the elements based on Equation (5.41) is added to that of the normal pressure based on Equation (5.31), along with the contributions due to constraints on the length of the elements, and slope continuity at points where elements are connected. After finding the stiffness matrix and force vector, Newton-Raphson iterative method is employed to find the deformed geometry.

Figure 5.10 shows the finite element solutions in comparison with the analytical solution presented in [9]. The origin of the coordinate system is set at the lowest point of the undeformed membrane. As shown in this Figure, the improvement of the result due to refinement is noticeable. For instance, the difference in the vertical position of the lowest point of the membrane based on Bezier curve analysis with one element in comparison with analytical solution for one element model is 49.5 cm or 49.5% of the initial radius of the membrane, while the same value for three- and five-element model is 3.2 cm and 3.1 cm, respectively. Although the results presented in Subsection 3.11.2 were closer to the results of analytical methods, it should be noted that the results of FE method were enhanced by selecting elements with different lengths based on their anticipated curvature.

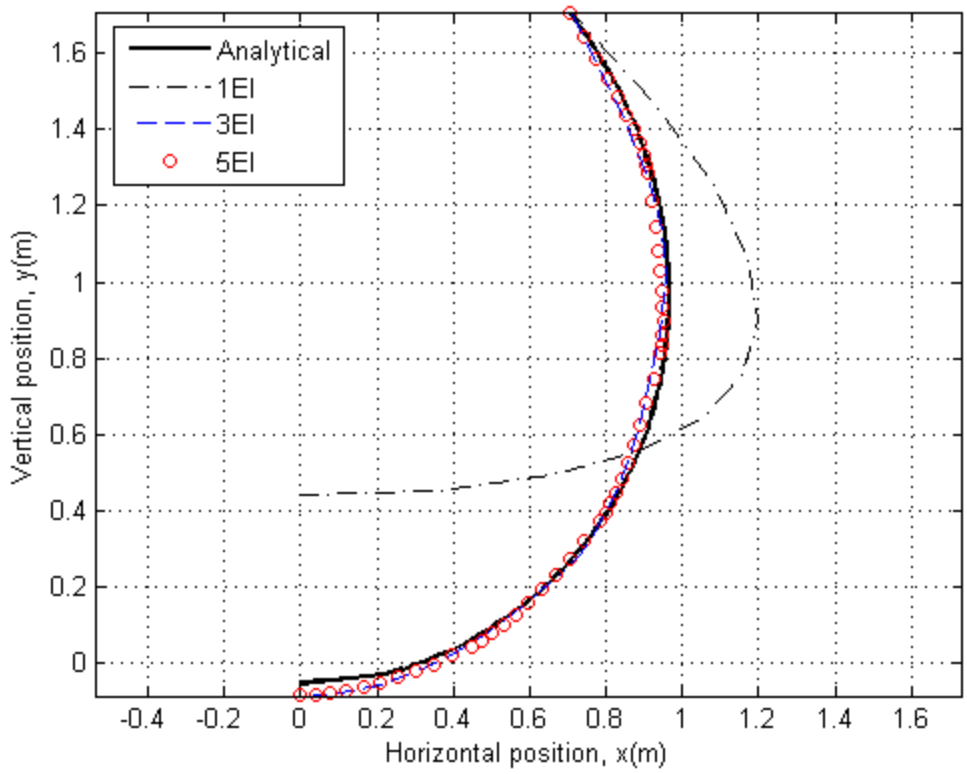

Figure 5.10. Bezier curve based analysis for deformed weighted membrane with internal pressure of 344.736N/min comparison with analytical results

Figure 5.11 shows the result of the case where the internal pressure is reduced to as low as the membrane weight, which is 34.474 N/m. The difference in the vertical position of the lowest point of the membrane based on Bezier curve analysis with four elements in comparison with analytical solution is 4.2 cm or 4.2% of the initial radius of the membrane. It is also observed that the curvature continuity is not maintained. This problem appears as the curvature of the part of membrane modeled by an element approaches zero. As an example, the curvature discontinuity grows as the internal pressure decreases.

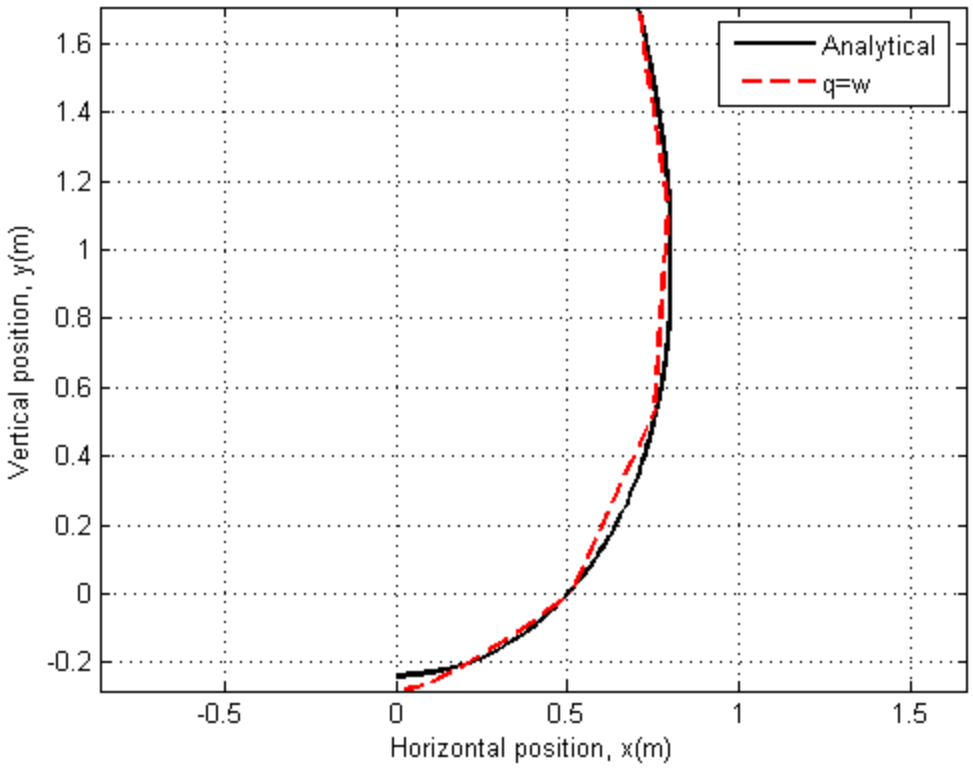

Figure 5.11. Bezier curve based analysis for deformed weighted membrane with internal pressure equal to membrane weight in comparison with analytical results

The next example considers the catenary case. When compared to the example presented in Subsection 4.11.2, it is seen that unlike the FE method example, in which there was a low internal pressure limit, Bezier curve analysis allows for the internal pressure to be dropped to zero. In FE solution, the problem occurred when the arc elements modeled straight lines; although this introduces continuity problems in Bezier curve analysis, it still converges to a solution. This is in fact one of the major benefits of the Bezier curve analysis in comparison with the FE method introduced in Chapter 4.

The results of the catenary analysis are shown in Figure 5.12. The difference in the vertical position of the lowest point based on Bezier curve analysis and analytical

solution is 4.8 cm, although this is not the point with maximum deviation from the analytical solution.

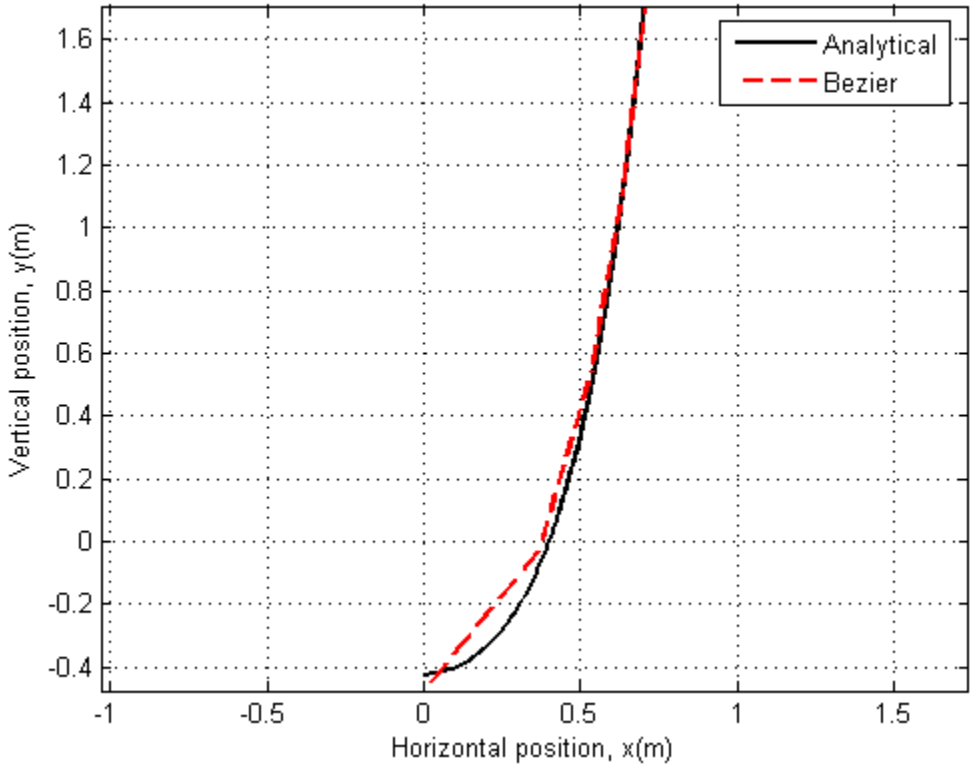

Figure 5.12. Bezier curve based analysis of catenary solution for deformed weighted membrane in comparison with analytical results

5.10.4. A Membrane under Internal Pressure and Shear Loading

In this Subsection, the problem considered in Subsection 4.11.3 is analyzed using Bezier curve analysis. The membrane is 2.310 m long and before the application of any shear pressure, the radius is 0.966 m. This membrane is symmetric with respect to the *y*-axis, such that the origin of the coordinate system is located at the lowest point of the membrane. The boundary conditions are fixed values of position at the two top ends of the membrane given by (x = 0.899 m, y = 0.612 m) and (x = -0.899 m, y = 0.612 m).

In this problem, internal pressure is 6.895 kN/m and shear distributed load is 3.447 kN/m. The analysis is done using one, three and five elements. The contribution of the normal pressure (Equation (5.31)) as well as shear pressure (Equation (5.43)), constant length constraint and C1 continuity were considered in calculating the total virtual work for the membrane. Figure 5.13 illustrates the deformed shape of the membrane under shear loading and internal pressure.

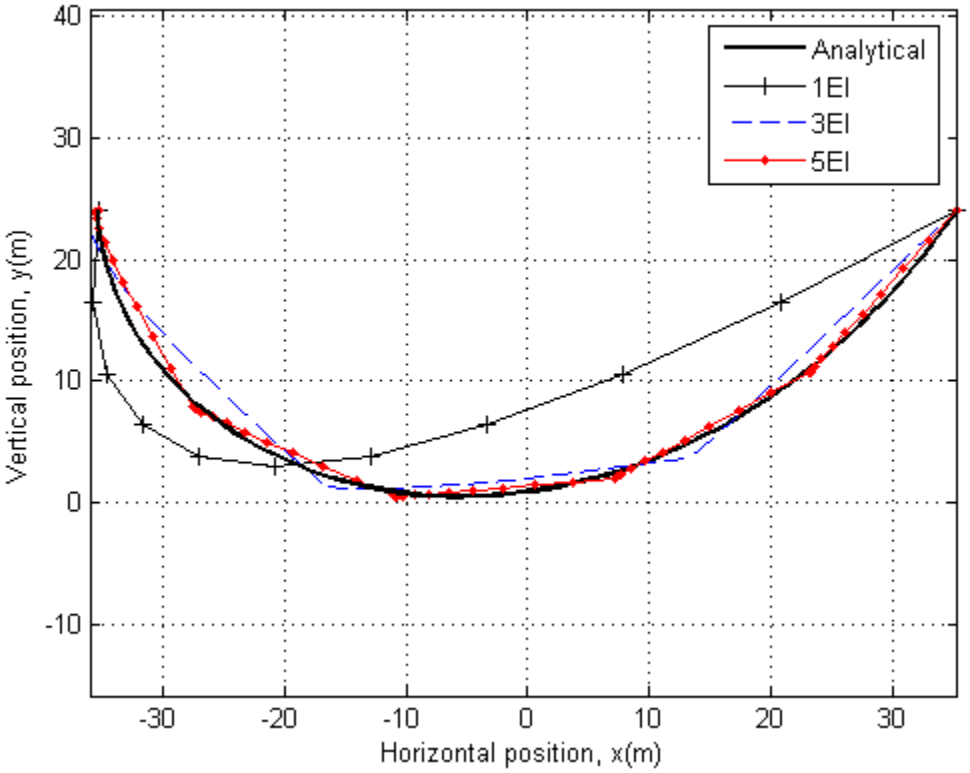

Figure 5.13. Bezier curve based analysis of a membrane under internal pressure and shear loading in comparison with analytical results

5.10.5. Elastic Membranes

5.10.5.1. A Membrane under Increasing Internal Pressure

Consider ¼ of the circle as the initial shape of a membrane that can be axially expanded and has bending stiffness. It is symmetric with respect to the *y*-axis, such that the origin of the coordinate system is at the lowest point of the membrane. The boundary conditions are fixed values of position at the two top ends of the membrane given by (x = 0.7071 m, y = 0.2929 m) and (x = -0.7071 m, y = 0.2929 m). The membrane has flexural rigidity of 0.001148 N-m^2 and its modulus of elasticity multiplied by its cross-sectional area is 1.366 kN. The membrane is modeled with four elements of equal length.

In calculating the total virtual work on the membrane, the work of normal pressure was added to the contribution of the applied constraint of having C1 continuity as well as axial extension and flexural rigidity based on Equations (5.38) and (5.54), respectively. It should be noted that the constraint of constant length elements is not valid in this example. The internal pressure of 34.474 kN/m was applied to the membrane, and was later reduced to 6.895 kN/m and 0.689 kN/m in two steps. The result of the analysis which led to the expansion of the membrane is illustrated in Figure 5.14. As the internal pressure reduces the membrane becomes shorter. The accuracy of the results decreases when the internal pressure approaches zero, the point where the curvature changes. This inaccuracy in the results is shown in Figure 5.14 where the internal pressure is 0.689 kN/m.

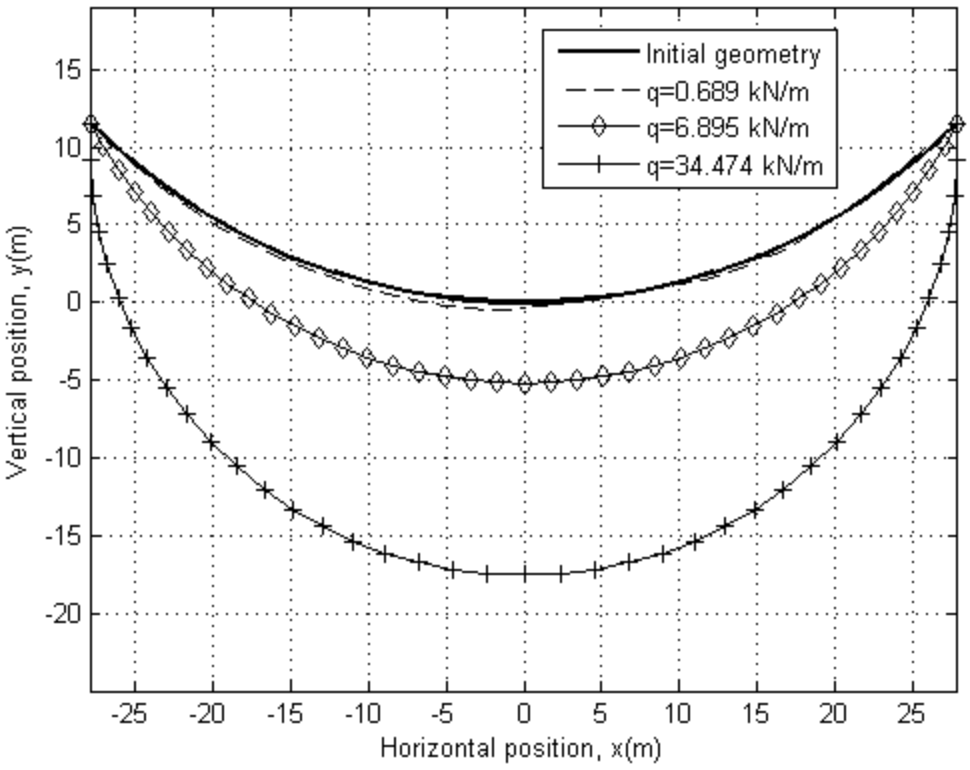

Figure 5.14. Bezier curve based analysis of an elastic membrane under increasing internal pressure

5.10.5.2. A Weighted Membrane under Internal Pressure

A modified version of the example discussed in Subsection 5.11.3 is revisited in this Subsection. Here, the membrane has axial extension and bending stiffness. The flexural rigidity of membrane is 0.001148 N-m^2 and its modulus of elasticity multiplied by its cross-sectional area is 1.366 kN. It is modeled with four elements of equal length. The internal pressure is initially equal to 6.895 kN/m and then reduced to 25.511 N/m. The contributing components in the calculation of virtual work are internal normal pressure (Equation (5.31)), membrane mass (Equation (5.41)), axial extension (Equation (5.38)),

flexural rigidity (Equation (5.54)), and C1 continuity constraint. The change in the geometry of the membrane during internal pressure reduction is shown in Figure 5.15.

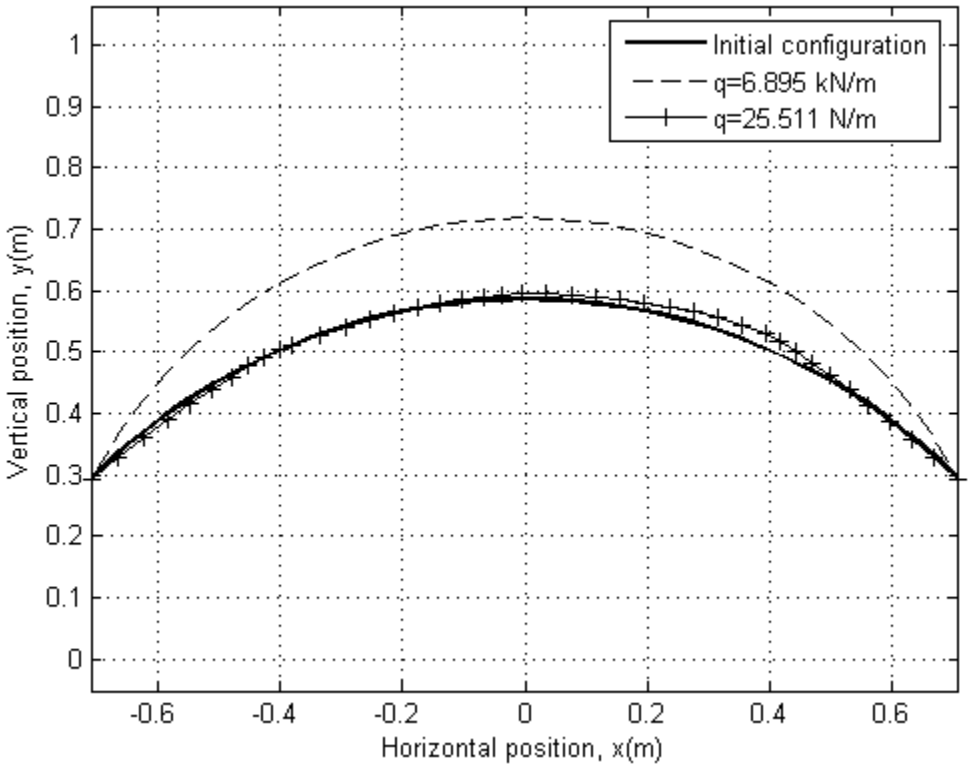

Figure 5.15. Deformation of an elastic weighted membrane due to decreasing internal pressure

Figure 5.16 shows the geometry of an inextensible membrane and an elastic membrane under internal pressure of 6.895 kN/m and distributed weight of 34.474 N/m. As shown in this Figure, although deformation of the inextensible membrane from initial geometry is almost negligible, the elastic membrane significantly deforms upward.

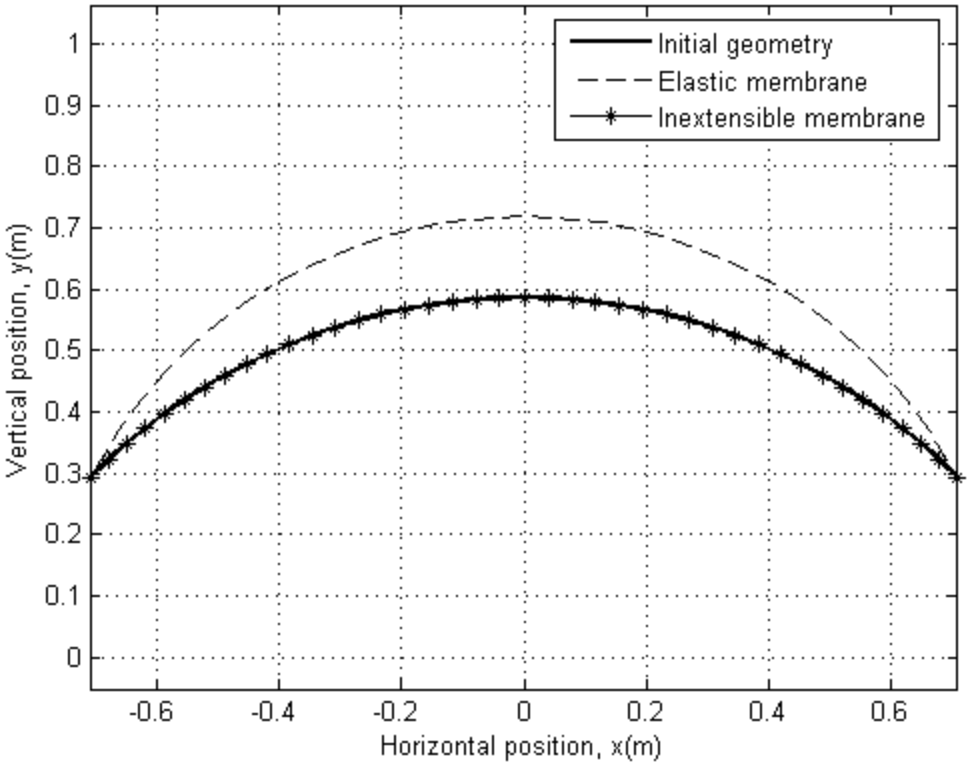

Figure 5.16. Geometry of an inextensible weighted membrane and an elastic weighted membrane in identical conditions

5.10.5.3. A Membrane under Internal Pressure and Shear Loading

The problem discussed in Subsection 5.10.4 is modified by adding axial extension and bending stiffness. The flexural rigidity of membrane is 0.001148 N-m^2 and its modulus of elasticity multiplied by its cross-sectional area is 1.366 kN. The membrane is modeled using four elements of equal length. Internal pressure is kept at 6.895 kN/m, and shear pressure is increased from -0.689 kN/m to -3.447 kN/m and to -6.895 kN/m. The deformation of the membrane due to an increase in shear pressure is illustrated in Figure 5.17.

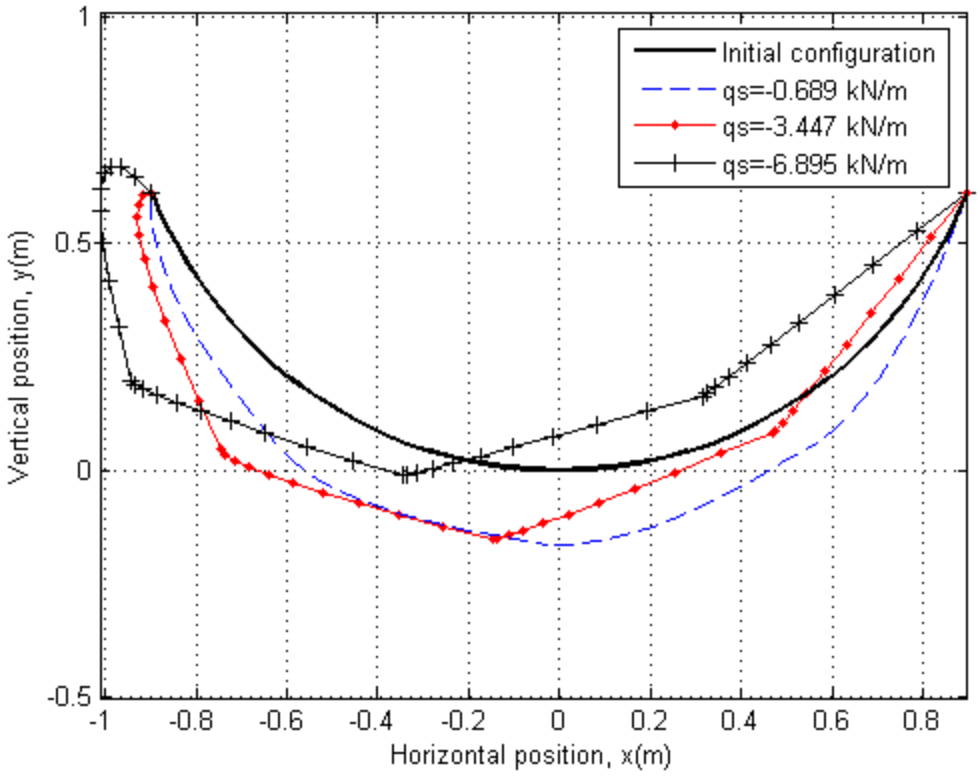

Figure 5.17. Deformation of an elastic membrane under increasing shear pressure

5.10.5.4. Multiple Solutions for a Set of Forces and Boundary Conditions

The method described in Chapter 5 in some cases results in multiple solutions. As an example, the deformation of a circular membrane under external pressure is considered. The membrane in its original configuration is ¼ of a circle with radius of 1 m. The flexural rigidity of membrane is 0.001148 N-m^2 and its modulus of elasticity multiplied by its cross-sectional area is 1.366 kN. The membrane is modeled using two elements of equal length where C1 continuity is enforced. The position is fixed at the two top ends of the membrane and external pressure of 2.068 kN/m is applied upward. Figure 5.18 shows the multiple solutions resulted from Bezier curve based analysis. It should be

noted that not all of these solutions are acceptable. For instance, the solution in bold black line crosses itself which is physically impossible for a three dimensional membrane. The dashed blue line and the solid red line with dot markers represent two unstable solutions before the membrane reaches the stable solution represented by the dash-dot line in black.

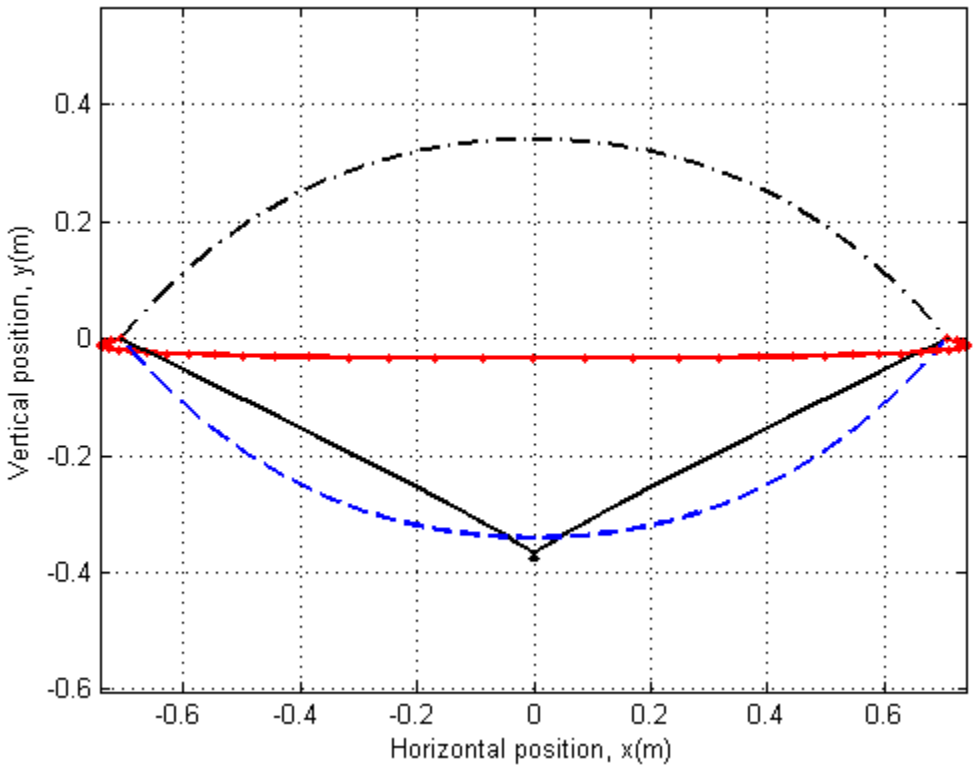

Figure 5.18. Multiple solutions for a unique initial and boundary conditions

5.11. Conclusions

The methodology presented in this Chapter to structurally analyze membranes based on quadratic Bezier curve, can be used to model any class of simple or complex geometry

and its applications are beyond the examples discussed herein. In order to demonstrate the applicability of the developed method to cases that involve elastic membranes, membranes with axial extension and bending stiffness were also included in the analysis.

The developed methodology considered the deformation of two-dimensional membranes, using elements with three control point and two DOFs in term of displacements along *x* and *y* directions for each control point. The stiffness matrix and force vector were calculated based on the principle of total virtual work. The terms contributing to the total virtual work were the results of external loads (i.e. normal and shear pressure), membrane mass, and constraint conditions such as constant length, and C1 continuity. In case of an elastic membrane, the effects of axial extension and bending stiffness were added to the total virtual work; in this case, the constraint of constant length did not hold. The results of the analysis were compared to the analytical solutions, and a very good agreement was observed between these methods. In addition, in some cases the method based on Bezier curve showed improvement over the FE method presented in Chapter 4 in terms of the displacement analysis, the range of the problems they could solve, and even the convergence rate. However, it should be noted that compared to the method presented in Chapter 3, due to the increased number of DOFs and complexity of formulations, higher convergence ratio was expected. Similar to the FE method in Chapter 3, displacement stepping increments were required for large displacements

There are several issues that potentially benefit from further studies and improvement of the developed methodology. An example is the discontinuity of the solution in situations

where the curvature of an element changes from positive to negative or vice versa. In addition, the quality of the results can be enhanced by increasing the degree of continuity. Another concern originates from the fact that due to nonlinear characteristics of the problem, the analysis may lead to multiple solutions, depending on the initial values of the contributing parameters. As such, a method to further analyze these solutions to select the most appropriate one will enormously improves the analysis. A more detailed discussion on these subjects will be presented in Chapter 6.

The most important advantage of the methodology presented in this Chapter is its ability to represent complex geometries. This is especially important in cases where displacements are large in comparison with the dimensions of the model such as FSI problems. Due to the same reason, the developed methodology results in more accurate analysis compared to the FE analysis. In particular, in several cases, when compared to the FE analysis presented in Chapter 4, it resulted in better results in terms of displacements. In addition, problems that could not be solved with the FE method due to low internal pressure, can be solved using Bezier curve based analysis.

5.12. References

[1] Hughes, T.J.R. et al. (2005), “Isogeometric analysis: CAD, finite elements, NURBS, exact geometry and mesh refinement”, Computer Methods in Applied Mechanics and Engineering, 194, pp. 4135-4195.

[2] Farin, G.E. (2002), Curves and Surfaces for CAGD: A Practical Guide, Academic Press, 57-62, Chap. 5.1-5.2.

[3] Vrron, E. and Marckmann, G. (2001) "An Axisymmetric B-spline Model for the Non-Linear Inflation of Rubberlike Membranes", Computer Methods in Applied Mechanics and Engineering, 190, pp. 6271-6289.

[4] Verron, E. and Marckmann, G. (2003) "Numerical Analysis of Rubber Balloons", Thin-Walled Structures, 41(8), pp. 731-746.

[5] Bazilevs, Y. et al. (2009) "Patient-specific isogeometric fluid–structure interaction analysis of thoracic aortic blood flow due to implantation of the Jarvik 2000 left ventricular assist device", Computer Methods in Applied Mechanics and Engineering, 198(45-46), pp. 3534-3550.

[6] Bazilevs, Y. et al. (2010) "A fully-coupled fluid-structure interaction simulation of cerebral aneurysms", Computational Mechanics, 46(1), pp. 3-16.

[7] Bauchau, O.A. (2011), Flexible Multibody Dynamics, Springer Science+Business Media, 284-292, Chap. 7.5.

[8] Bushnell, D. (1984), “Computerized analysis of shells-Governing equations,” Computers and Structures, 18(3), pp. 471-536.

[9] Yu, B. and Karr D.G., “Analytical Solutions of 2D Membrane Shapes within Different Inflation and Deflation Regimes”, (In preparation).

Chapter 6

Conclusion

Understanding the structural behavior of membranes is the first and one of the essential steps in their design process. This behavior is a function of the membrane material, geometry, boundary conditions, and applied loads. Depending on the application, any combination of these characteristics may be selected to construct a membrane that best satisfies all design criteria. A few membrane types have been studied previously using existing analytical and numerical methods [1-4]. However, there are types of membranes the structural behavior of which is not considered by previously developed methods. As an example, elastic and hyper-elastic membranes have been frequently studied by numerical, experimental and analytical methods; yet, the structural behavior of inextensible membranes which have marine applications specifically in inflatable pontoon or the skirt system of Air Cushion Vehicle (ACVs), have not been thoroughly analyzed in the past. Thus, the presented research in this dissertation was to a large extent, motivated by this identified gap in knowledge.

This dissertation documented the research that led to the development of analytical and numerical methods to analyze two-dimensional curved membranes under different loading and boundary conditions, and constraints.

Prior developed methods in this area, do not fully apply to inextensible membranes. Since they mostly considered some degrees of elasticity, to impose inextensibility, a high modulus of elasticity should be selected which results in high bending stiffness. This contrasts with the almost negligible bending stiffness of membranes. On the other hand, considering that membranes are constructed from fabrics coated with rubberlike material, there might be some similarities in the behavior of fabrics and membranes. As an example, some analyzed fabrics by modeling them as cantilever beams with flexural rigidity to study their buckling and bending performance where degrees of freedom (DOFs) were in terms of slope and curvature of the beam.

This dissertation successfully developed methods to find how inextensible and elastic two-dimensional curved membranes react to different loading conditions. The developed numerical analyses in this research pick DOFs in terms of displacement. This facilitates the analysis especially since very often; known boundary conditions as well as the output of the analysis are also expressed in terms of displacements. This research also takes advantage of new numerical methods (Isogeometric Analysis) that promise more accuracy in geometric modeling. All numerical methods were validated by comparing their results to the analytical method.

In **Chapter 2**, an analytical solution to the problem of initially circular two-dimensional membranes partially submerged in fluid was established. It was assumed that the membranes were weightless and that they were only under constant normal internal and hydrostatic external pressure. The solution was in the form of a system of equations that related the deformed geometry to membrane tension and was solved for both deformed geometry and tension through an iterative method. The results of this Chapter were used as a point of reference to validate the methodologies developed in the following Chapters.

In **Chapter 3**, beam bending theory was used to study the two-dimensional seal of a Surface Effect Ship (SES). The pressure field required to achieve the seal geometry for the given test conditions was derived from a beam-bending theory approach. The results of this analysis were compared to an experimental study previously conducted by [5].
In **Chapter 4**, a Finite Element (FE) solution based on the stiffness influence coefficient method was established to model two-dimensional curved membranes. In this respect, constant-length arc-shaped elements with two nodes and two DOFs per node were selected. In addition to the normal pressure, the deformation of membrane under shear loading and self-weight was also considered. Deformation and DOFs were expressed in terms of displacements. This method was then validated using the results obtained in Chapter 2. It was shown that there was a very good agreement between the two methods in terms of calculated deformation. It was also observed that there was a limitation in the applications of this method where elements were expected to represent curves with very low curvatures, such as a weighted membrane with low internal pressure or a membrane under high shear pressure. Moreover, in case of large deformations, displacements were

required to be incremented in several steps rather than one. One of the significant advantages of this methodology is its ability in satisfying the “displacement” boundary conditions. This aspect is where some of the previous methods to model fabrics failed [6].

Chapter 5 introduced an alternative solution to the problem of two-dimensional membrane deformation under different loading and boundary conditions. The work in this Chapter was inspired by the “Isogeometric Analysis”, a computational method that deploys the same Computer Aided Design (CAD) basis functions used in geometric modeling for structural analysis. In this research, a quadratic Bezier curve was used to represent an element. This indicates that each element has three control points and two DOFs per control point. The principle of virtual work (that is valid for conservative and non-conservative systems) was used to formulate the problem. The total virtual work consisted of work of external applied pressure as well as membrane’s weight. Constraints such as constant length and C1 continuity were also enforced by means of Lagrange multiplier method. Also, to consider membranes that can be axially extended and membranes with bending stiffness, their contributing energies were added to the total virtual work. Computations to calculate the stiffness matrix and force vector were easier when compared to FE method since there was no need for assembly and transformation from local to global coordinate system. The results were validated by comparing them with the results presented in Chapter 2. An overall improvement in terms of displacement analysis was observed when compared with the FE method. When elements were to represent low curvature curves, a discontinuity in curvature was observed. Yet, unlike the FE method discussed in Chapter 4, the analysis converged to a solution. Similar to the FE

method, displacement stepping increments were required for large displacements. In the case where curvature changed sign during the analysis, discontinuity in the analysis was detected. Despite these issues, based on the analysis results, the Bezier curve approach turned out to be very promising. In addition, methods to improve many of the abovementioned issues are deliberated in Section 6.1. The essential advantage of this methodology is its capability in precise geometric modeling which in turn will result in more accurate structural analysis.

In summary, although the motivation of this research was the need for methods capable of analyzing the skirt system of ACVs, the developed methods can be used to model a wide range of membranes in many engineering or non-engineering applications.

6.1. Recommendations for Future Work

The FE method discussed in Chapter 4 provided a solution with a high convergence rate capable of modeling relatively simple geometries. The Bezier curve based analysis described in Chapter 5, is potentially able to model more complex geometries and provide better results. As discussed earlier, there are still a few issues that can significantly benefit from further studies. Selecting a more appropriate basis function, can contribute to the issue of curvature discontinuity that appeared in parts of the results obtained from the Bezier curve based analysis. In cubic Bezier curves, the curvature changes continuously and can have an inflection point. In cases when local control is an issue such as when a material should react locally to a pointed or local load rather than an

overall deformation of the model, a B-spline is a proper choice. This also helps conduct a more accurate geometric modeling which leads to a more accurate analysis, and therefore fewer numbers of elements. The representation of a circular arc with $3\pi/4$ angle by quadratic Bezier curve is shown in Figure 6.1. The representation of the same arc by cubic Bezier curve is shown in Figure 6.2 and they are compared in Figure 6.3. For a quadratic Bezier curve, by matching the two end points and the slope of the curve at these point with those of the arc, the Bezier polygon is determined. Figure 6.1 shows that the resulted curve is has a different length than the arc. The polygon of the cubic Bezier curve can be determined in the same manner which results in a family of solutions. By enforcing symmetry, this family of solutions is narrowed down to the polygon and the curve in Figure 6.2 which is the geometrically exact representation of the arc. Therefore, increasing the degree of basis function will benefit the analysis especially for complex geometries. Figure 6.3 shows these two Bezier curves in comparison with the arc.

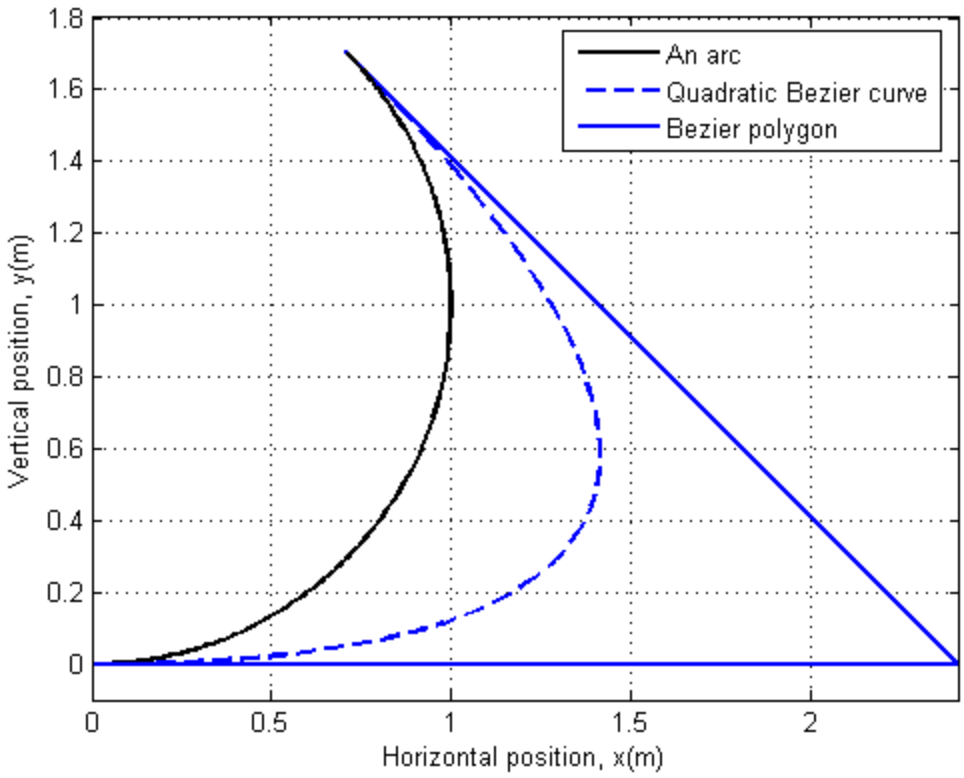

Figure 6.1. Representation of an arc with quadratic Bezier curves

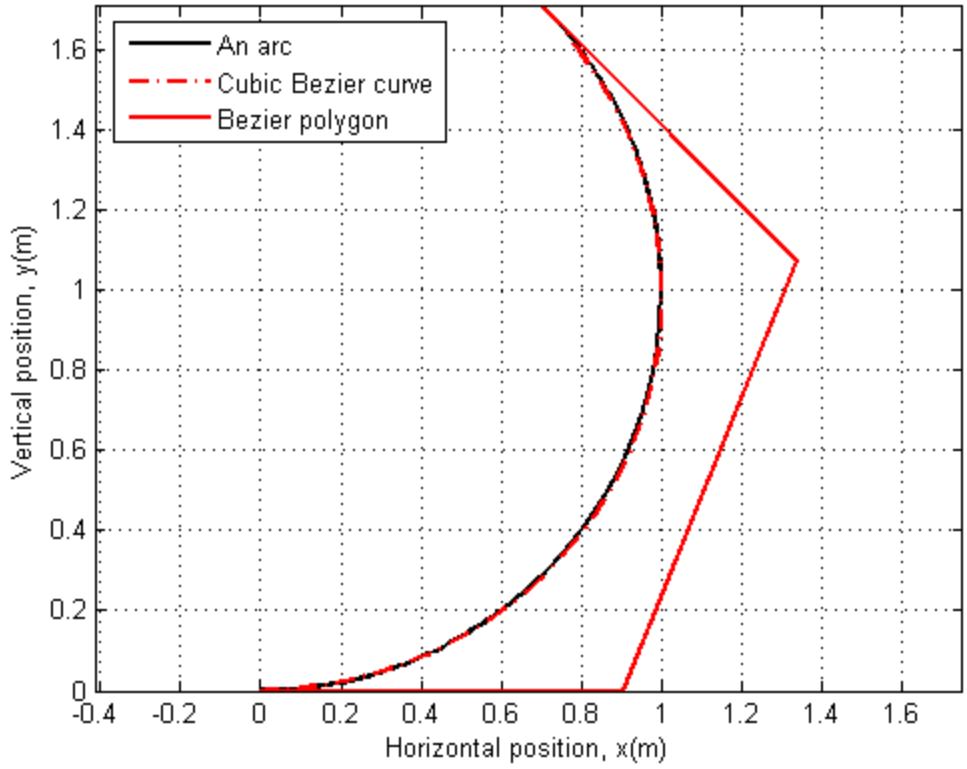

Figure 6.2. Representation of an arc with cubic Bezier curves

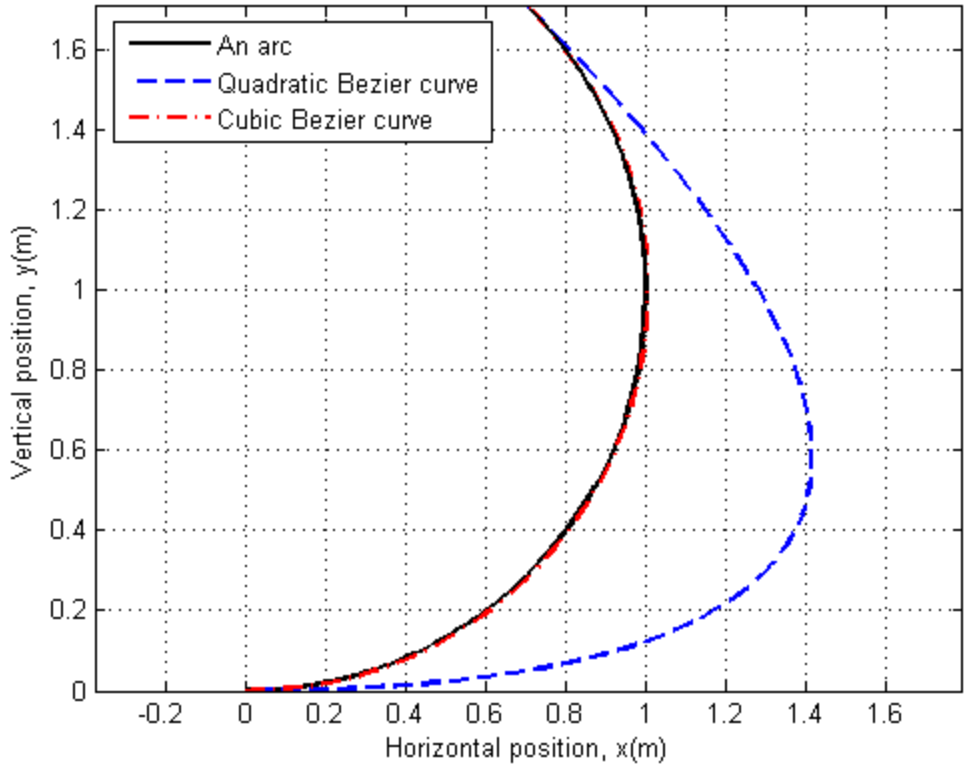

Figure 6.3. Representation of an arc with quadratic and cubic Bezier curves

When curvature in a part of geometry changes sign, a discontinuity in the solution may be experienced. An example of this situation was explained in Subsection 4.11.1.Considering that problem, the discontinuity happened due to the fact that the three control points defining a straight line lie on the line itself. The first and last points were located on the right and left end of the line, respectively; but in order to define a straight line, the middle point could be anywhere on the line. Therefore, under no internal pressure, there was no unique solution to the problem in terms of the location of the central control point. As the pressure was reduced and approached a small value close to zero, the middle control point got closer to the right control point. The movement of the middle point was completely symmetric with respect to the case of "*no internal*

pressure". In other words, for small negative internal pressures close to zero, the middle control point was very close to the left control point. It can thus be concluded that as the pressure changes from a small positive value to a small negative value, the middle control point moves from the far right to the far left on the membrane curve that is very close to a straight line, and therefore, there is a discontinuity about the position of the middle control point as internal pressure approaches zero. This sudden change in the position of the middle point is illustrated in Figure 6.4 in which solid circles indicate end control points and hollow circles show the middle control point. This issue can be solved by introducing and including a parameter (e.g. such as slope of the curve at end points) that changes continuously as the curvature changes sign.

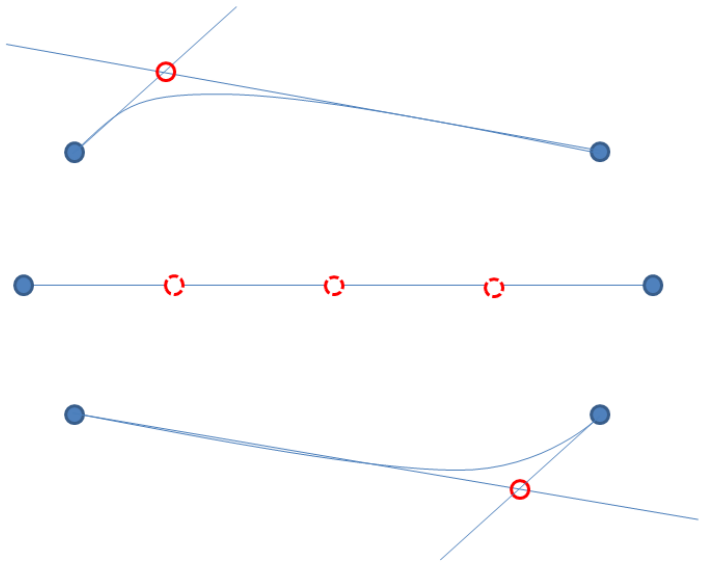

Figure 6.4. The position of the middle point is not defined for zero curvature

Another aspect of the developed Bezier curve analysis method is that depending on the initial values of Lagrange multipliers and geometry, multiple solutions may exist for a

certain combination of loading and boundary conditions. An example of these circumstances is shown in Figure 6.5. This Figure illustrates the results of analysis conducted using two elements (the right element is dashed and the left one is solid line). In all solutions, slope continuity at points where the two elements are connected is maintained. An algorithm to select the correct solution or to optimize the initial value of Lagrange multipliers based on loads and geometry conditions will tremendously contribute to the robustness of the solution.

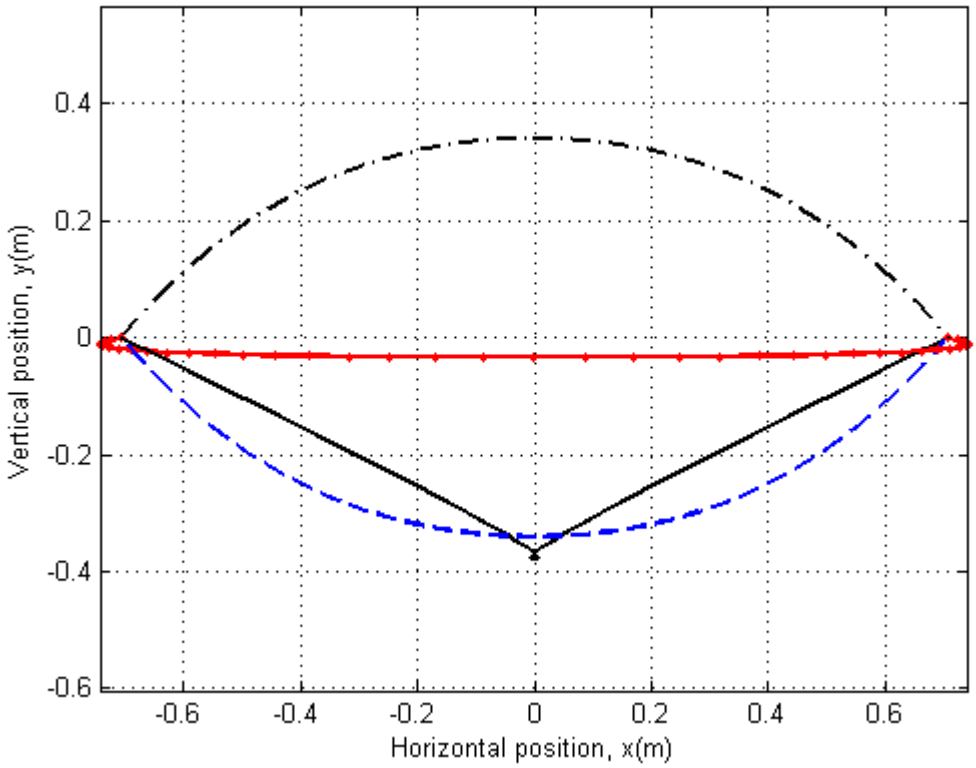

Figure 6.5. Multiple solutions for a single loading scenario

Additionally, parallel experimental analysis will yield better understanding of the problem, can be used in validation, and will lead to more realistic results. To this end, the

presented research in this dissertation is the first step towards dynamic Fluid Structure Interaction (FSI) analysis. In particular, since large displacements are of concern in many FSI problems, Isogeometric Analysis methods that introduced in this research can be effectively used as very powerful tools for more accurate analysis of this class of problems.

6.2. Comparison of the Described Methods

To investigate the strengths and shortcomings of the methods described in Chapter 4 and Chapter 5, the results of the analysis using these methods are compared. As an example, reconsider the problem investigated in Subsections 4.11.1 and 5.10.2. Figure 6.6 shows the results of the analysis using constant radius FE method with four elements and Bezier curve based analysis with six elements.

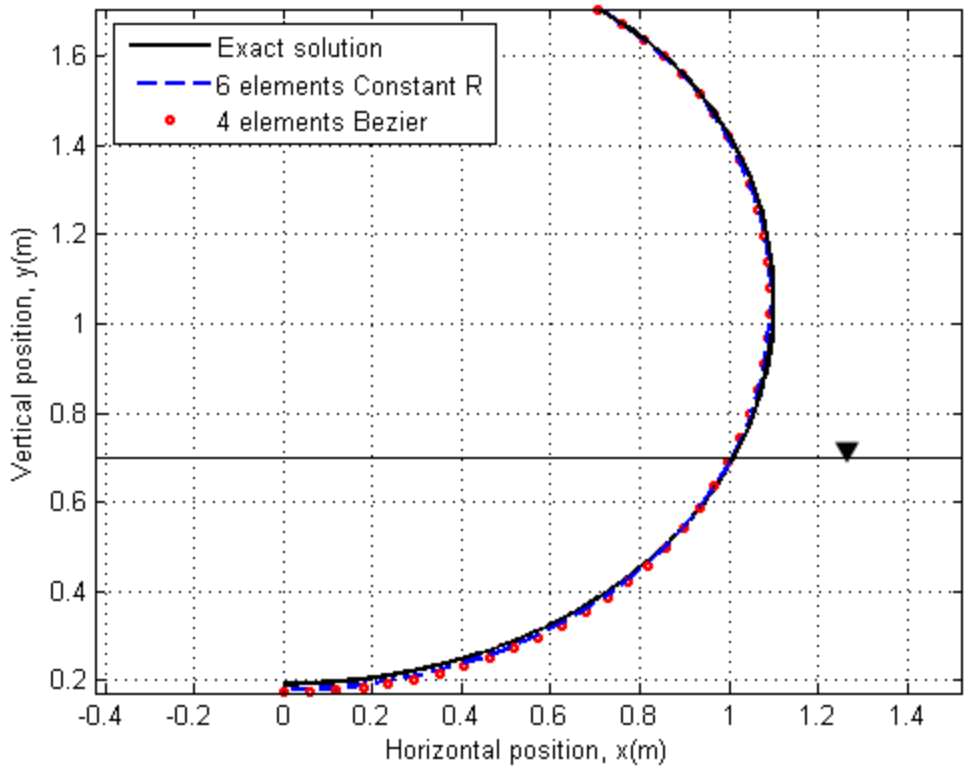

Figure 6.6. A comparison between the methods described in Chapters 4 and 5 applied to the semi-submerged membrane

This comparison shows very close results from the two methods. However, the number of DOFs should also be considered in this comparison. The six element constant radius FE model has seven nodes. Considering that the position of the last node and the horizontal position of the leftmost node is fixed, and all other nodes have two DOFs in terms of displacement in x and y direction, the model has $5\times 2+1=11$ DOFs. The four element quadratic Bezier curve based model has nine control points. Again, the constraints applied to the first and last control points are considered in calculating the DOFs. Also applying the C1 continuity condition at three control points at element joints and constant length constraint applied to four elements, DOFs of the model is equal to $(9-2)\times 2+1-4-3=8$. Therefore it can be concluded that in this example, with the

same number of DOFs, quadratic Bezier curve analysis gives more accurate results when compared with the analytical method.

As another example, reconsider the problem investigated in Subsections 4.11.3 and 5.10.4, a membrane under shear loading and internal pressure. Figure 6.7 shows the results of the analysis using a four element constant radius FE model and a three element quadratic Bezier curve model.

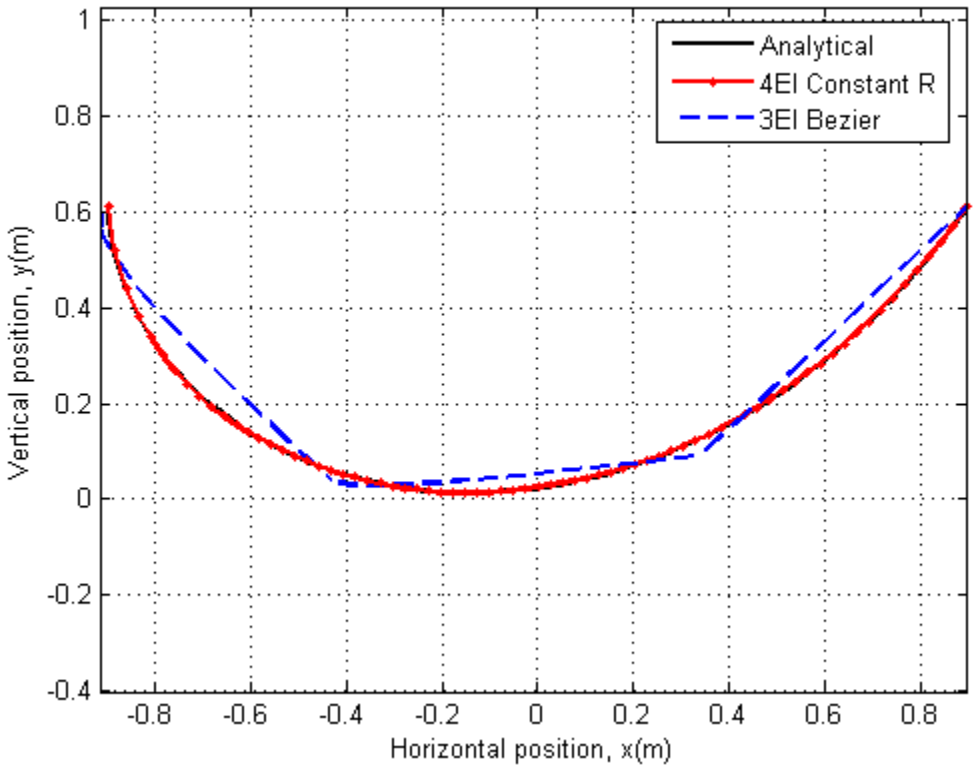

Figure 6.7. A comparison between the methods described in Chapters 4 and 5 applied to a membrane under shear loading and internal pressure

The constant radius FE model has $3\times 2=6$ DOFs and Bezier curve based model has $5\times 2-3-2=5$ DOFs considering constant length and C1 continuity constraints. In this

case, the constant radius FE method shows more accurate results when compared with the Bezier curve based analysis due to the issues discussed earlier in this Chapter.

The example described in Subsections 4.11.2 and 5.10.3 shows another aspect of the difference between the two methods. To investigate the deformation of a membrane under its own weight, the application of elements with constant radius along the length showed some limitations. The internal pressure of the membrane cannot be lowered that a certain value. This value grows with the number of elements. On the contrary, the application of the quadratic Bezier curve based analysis has no limitation in terms of the internal pressure. The catenary solution was obtained using the Bezier curve based method and the results were comparable to the analytical solution.

In conclusion, the method described in Chapter 5, exclusive of the issues regarding concentration of the energy in one side of the element and curvature discontinuity which happens in some cases and can be improved by increasing the number of elements or using higher degree base functions, is a very reliable method with wide range of applications suitable for complex geometries and where more accurate results are required. On the other hand, the method described in Chapter 4, despite some limitation, especially in cases of low curvature, is a simple method with less calculation when compared with the method described in Chapter 5 with very accurate results and more suitable for simple geometries where large number of elements is not necessary.

6.3. References

[1] Oden, J.T. and Sato, T. (1967), "Finite strains and displacements of elastic membranes by the finite element method," International Journal of Solids and Structures, 3, pp. 471-488.

[2] Verron E. and Marckmann G. (2001) "An Axisymmetric B-spline Model for the Non-Linear Inflation of Rubberlike Membranes", Computer Methods in Applied Mechanics and Engineering, 190, pp. 6271-6289.

[3] Bazilevs Y. et al. (2009) "Patient-specific isogeometric fluid–structure interaction analysis of thoracic aortic blood flow due to implantation of the Jarvik 2000 left ventricular assist device", Computer Methods in Applied Mechanics and Engineering, 198(45-46), pp. 3534-3550.

[4] Bazilevs Y. et al. (2010) "A fully-coupled fluid-structure interaction simulation of cerebral aneurysms", Computational Mechanics, 46(1), pp. 3-16.

[5] Zalek, S.F. et al. (2011), "Modeling of air cushion vehicle's flexible seals under steady state conditions", Ocean Systems Engineering, 1(1), 17-29.

[6] Demiroz, A (2005), "Prediction of large deformation behavior of fabric using galerkin finite element method," Textile Research Journal, 75(9), pp. 662-669.